博士論文

Study on Synthesis and Optical Properties of Conjugated Cyclic Imide Derivatives containing Donor and Acceptor

(ドナーとアクセプターを含む共役環状イミド誘導体の合成とその光学特性に関する研究)

2023 年 9 月

YANG XIAODONG

山口大学大学院創成科学研究科

Contents

Chapter 1 General Introduction

1.1 Luminescence 1

1.2 Aggregation Induced Emission (AIE) 1

1.3 Dual-State Emission (DSE) 5

1.4 Cyclic Imide 7

1.5 Research aims and significance 8

1.6 References 11

Chapter 2 Synthesis and optical properties of conjugated maleimide molecules containing amino with aggregation-induced emission enhancement (AIEE)

2.1 Introduction 16

2.2 Experimental 18

2.2.1 Materials 18

2.2.2 Measurements 19

2.2.3 Synthesis 20

2.2.3.A Synthesis of 2,3-dichloro-*N*-cyclohexylmaleimide (Compound **1**) 20

2.2.3.B Synthesis of 2-chloro-3-morpholino-*N*-cyclohexylmaleimide (Compound **2**) 21

2.2.3.C Synthesis of 2-biphenyl-3-morpholino-*N*-cyclohexylmaleimide by Suzuki-Miyaura coupling reaction (Compound **3**) 22

2.2.3.D Synthesis of 2-chloro-3-piperidino-*N*-cyclohexylmaleimide (Compound **4**) 23

2.2.3.E Synthesis of 2-biphenyl-3-piperidino-*N*-cyclohexylmaleimide by Suzuki-Miyaura coupling reaction (Compound **5**) 24

2.2.3.F Synthesis of 2-chloro-3-pyrrolidino-*N*-cyclohexylmaleimide (Compound **6**) 25

2.2.3.G Synthesis of 2-biphenyl-3-pyrrolidino-*N*-cyclohexylmaleimide by

Suzuki-Miyaura coupling reaction (Compound **7**) 26
2.2.4 Structure characterization 27
2.3 Results and discussion 32
2.3.1 Syntheses 32
2.3.2 UV/Vis absorption spectra and photoluminescence (PL) spectra 32
2.3.3 Aggregation-induced emission enhancement (AIEE) 35
2.3.4 Density functional theory (DFT) quantum calculations 38
2.4 Conclusions 39
2.5 References 41

Chapter 3 Synthesis and photophysical properties of a series of maleimide molecules with aggregation-induced emission enhancement (AIEE) effects

3.1 Introduction 44
3.2 Experimental 45
3.2.1 Materials 45
3.2.2 Structural analysis and measurements 46
3.2.3 Synthesis 47
3.2.3.A Synthesis of 4,4'-bis (2-morpholino-*N*-cyclohexylmaleimide-3-yl) -1,1'-biphenyl (Compound **1**) by Suzuki-Miyaura Coupling Reaction 47
3.2.3.B Synthesis of 4,4'-bis (2-piperidino-*N*-cyclohexylmaleimide-3-yl) -1,1'-biphenyl (Compound **2**) by Suzuki-Miyaura Coupling Reaction 48
3.2.3.C Synthesis of 4,4'-bis (2-pyrrolidino-*N*-cyclohexylmaleimide-3-yl) -1,1' biphenyl (Compound **3**) by Suzuki-Miyaura Coupling Reaction 49
3.2.3.D Synthesis of 4,4'-bis (2-chloro-*N*-cyclohexylmaleimide-3-yl) -1,1'-piperazino (compound **4**) by Suzuki-Miyaura Coupling Reaction 50
3.2.3.E Synthesis of 4,4'-bis (2-biphenyl-*N*-cyclohexylmaleimide-3-yl) -1,1'-piperazino (compound **5**) by Suzuki-Miyaura Coupling Reaction 51
3.2.4 Structure characterization 52

3.3 Results and discussion 55
3.3.1 Syntheses 55
3.3.2 UV/Vis absorption spectra and photoluminescence (PL) spectra 56
3.3.3 Aggregation-induced emission enhancement (AIEE) 58
3.4 Conclusions 62
3.5 References 63

Chapter 4 Synthesis and photophysical properties of blue emission maleimide molecules with Dual-State Emission (DSE) effects

4.1 Introduction 64
4.2 Experimental 67
4.2.1 Materials 67
4.2.2 Structural analysis and measurements 68
4.2.3 Synthesis 69
4.2.3.A Synthesis of 2-bromo-3-methyl-*N*-cyclohexylmaleimide (Compound **BMMI**) 69
4.2.3.B Synthesis of 2-methyl-3-biphenyl-*N*-cyclohexylmaleimide (Compound **1**) by Suzuki-Miyaura Coupling Reaction 70
4.2.3.C Synthesis of 4,4'-bis (2-methyl-*N*-cyclohexylmaleimide-3-yl) -1,1'-biphenyl (Compound **2**) by Suzuki-Miyaura Coupling Reaction 71
4.2.4 Structure characterization 72
4.3 Results and discussion 74
4.3.1 Syntheses and characterization 74
4.3.2 Dual-State Emission (DSE) effects 76
4.3.3 Density functional theory (DFT) quantum calculations 79
4.3.4 Solvatochromism 81
4.3.5 Acid/ alkali responsive properties 84
4.4 Conclusions 89
4.5 References 90

Chapter 5 Summary 94

Acknowledgments 96

Chapter 1

General Introduction

1.1 Luminescence

Luminescence is one of the beautiful and amazing phenomena in nature, such as the aurora created by nature. Simultaneously, the presence of luminophores is one of the most fundamental elements to life and society. The development and breakthrough of luminescent materials have promoted many high-tech applications and practical applications. Photoluminescence (abbreviated as PL) is light emission from any form of materials after the absorption of photons (electromagnetic radiation). In the mechanism of PL, the excited electrons generated by optical excitation, will return to the ground state, accompanied by emitting photons.[1] It is one of many forms of luminescence. It can be classified into two common forms, fluorescence and phosphorescence, according to the Jablonski diagram.[2,3] In this study, we mainly introduce the luminescence phenomenon in the field of fluorescence.

1.2 Aggregation Induced Emission (AIE)

Organic fluorescent materials have attracted extensive interest due to their advantages of flexible and adjustable structure, high fluorescence quantum yield, and wider application.[4-12] Therefore, the design and development of organic fluorescent materials are of great significance. However, some conjugated and rigid organic fluorescent compounds with strong emission in solution often encounter the aggregation caused quenching (ACQ) in aggregates or solid state. When the luminophores aggregate, the distance between the molecules becomes closer, and the aromatic rings of the adjoining luminophores experience intense intermolecular π-π stacking interactions. These interactions make the excited states decay or relax back to the ground state via non-radiative channels, resulting in the emission

quenching of the luminophores.

Perylene is a typical example illustrating the ACQ effect.[13] As shown in Figure 1.1(left), the fluorescence intensity of perylene was examined in the mixture of good solvent THF and poor solvent water. With the gradual increase of the fraction of water, the emission of perylene becomes weakened until quenching.[13] The planar polycyclic aromatic structure of perylene enables its molecules to pack in an ordered manner in the aggregates to prompt the formation of intermolecular π-π stacking interactions, resulting in the observed ACQ effect. To some extent, the ACQ effect limited the realistic application of luminophores in many fields.[13-16]

The emerge of aggregation-induced emission (AIE) molecules can solve this problem. In 1921, Schmidt published a paper titled "On the Luminescence of Solid Solutions" which showed that many compounds fluoresce in solidified solutions but are quenched in their respective fluid solvents.[17] After that, several papers about the luminescence of solids were reported, and the concept of aggregation-induced emission (AIE) was introduced by Tang in 2001.[18,19] Aromatic molecules have been the focus of AIE research due to their high emission efficiencies and high flexibilities. [20-21] However, aromatic molecules often encounter the intermolecular π-π stacking interactions in the solid state, which lead to aggregation-caused quenching. To prevent this interaction, aromatic AIE molecules have been designed with a bulky molecular size and a highly twisted conformation.[22-25] Among them, the hexaphenylsilole (HPS) molecules, which possess six phenyl rings, and tetraphenylethene (TPE) molecules, where the olefin stator is surrounded by four peripheral aromatic rotors, are typical examples illustrating the AIE effect.[19,25-27,]

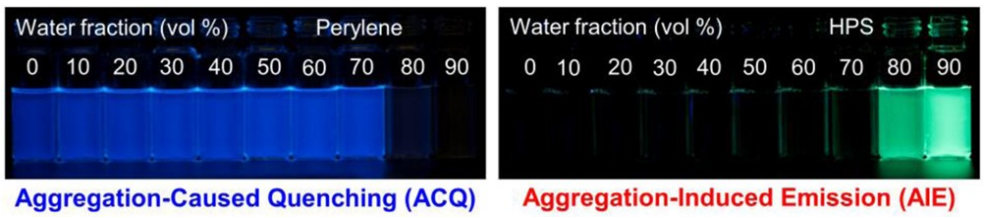

Figure 1.1. Fluorescence photographs of solutions or suspensions of (left) perylene (20 μM) and (right) hexaphenylsilole (HPS; 20 μM) in THF/ water mixtures with different fractions of water, with perylene and HPS showing typical ACQ and AIE effects, respectively.[13]

As shown in Figure 1.1 (right), the fluorescence intensity of HPS was examined in the mixture of good solvent THF and poor solvent water. With the gradual increase of fraction of water, the emission of HPS becomes stronger and has a bright emission when the fraction of water reaches ~80 %. Another typical AIEgens is tetraphenylethene (TPE).[13] Its structure is a propeller shape with a central olefin surrounded by four phenyl rings. The tetraphenylethene (TPE) is non-emissive when dissolved but becomes emissive when aggregated due to the restriction to the intramolecular rotations (RIR) of its phenyl rotors. Researchers have put forward various assumptions about the general mechanism behind aggregation-induced emission, including conformational planarization, J-aggregate formation, E/Z isomerization, twisted intramolecular charge transfer (TICT), and ESIPT.[13,25] Among them, the restriction of intramolecular motions (RIM) has been considered the main cause of AIE effects so far, including the restriction of intramolecular rotation (RIR) and the restriction of intramolecular vibration (RIV).[25,28] As shown in Figure 1.2, the RIM can reduce the nonradiative decay, thereby resulting in the emission.[25,29-31] Since then, as shown in Figure 1.3, a lot of AIEgens have been developed and reported.[32-36]

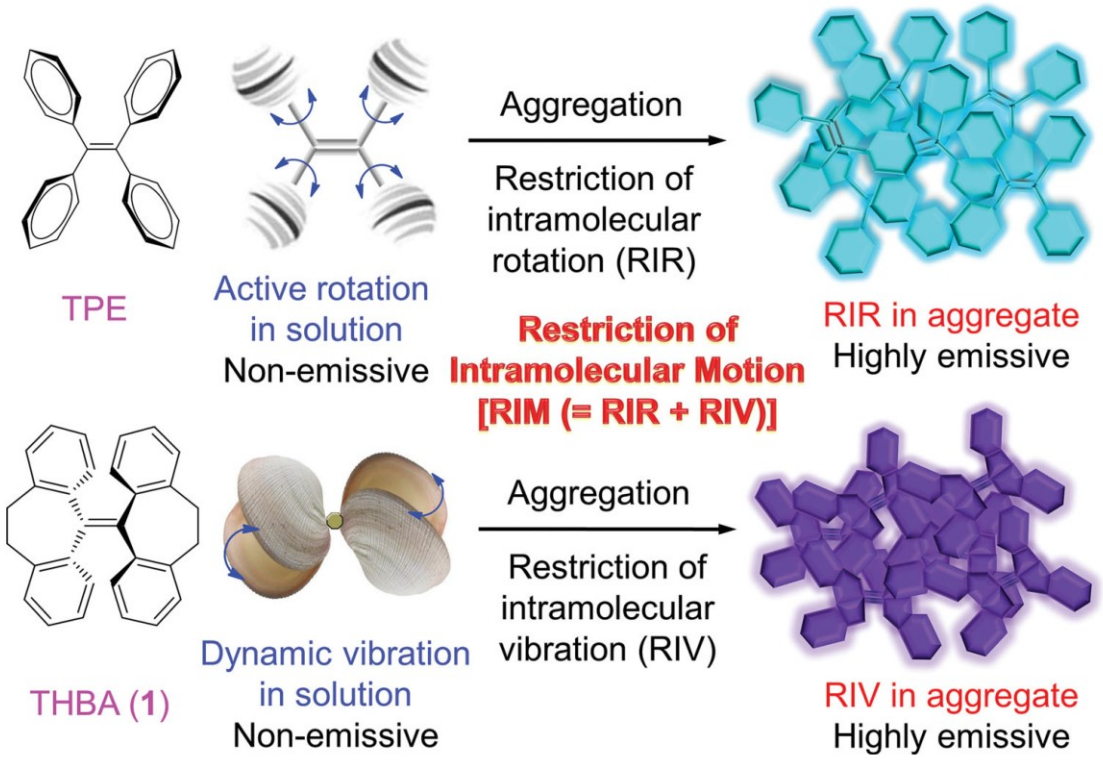

Figure 1.2. Propeller-shaped luminogen of tetraphenylethene (TPE) is non-luminescent in a dilute solution but becomes emissive when its molecules are aggregated, due to the restriction of intramolecular rotation (RIR) of its phenyl rotors against its ethylene stator in the aggregate state. Shell-like luminogen of THBA behaves similarly, due to the restriction of intramolecular vibration (RIV) of its bendable vibrators in the aggregates state. [25]

With the gradual deepening of research on AIEgens, the application of AIE gens has become abundant, ranging from bioimaging, chemosensing, optoelectronics to stimuli-responsive systems. [37-45] This indicates that the importance of their application in the solid state of molecules. However, many AIEgens exhibit single-state emission (none or weak emission in solution and stronger emission in aggregates or solid). To some extent, this single-state emission also can limit some high-tech applications in various fields. Based on this, if there are molecules that can be emissive in both solution and solid states, it will open up more possibilities for its application. Therefore, the development and design of the molecules that can possess strong emission both in solution and solid state is necessary.

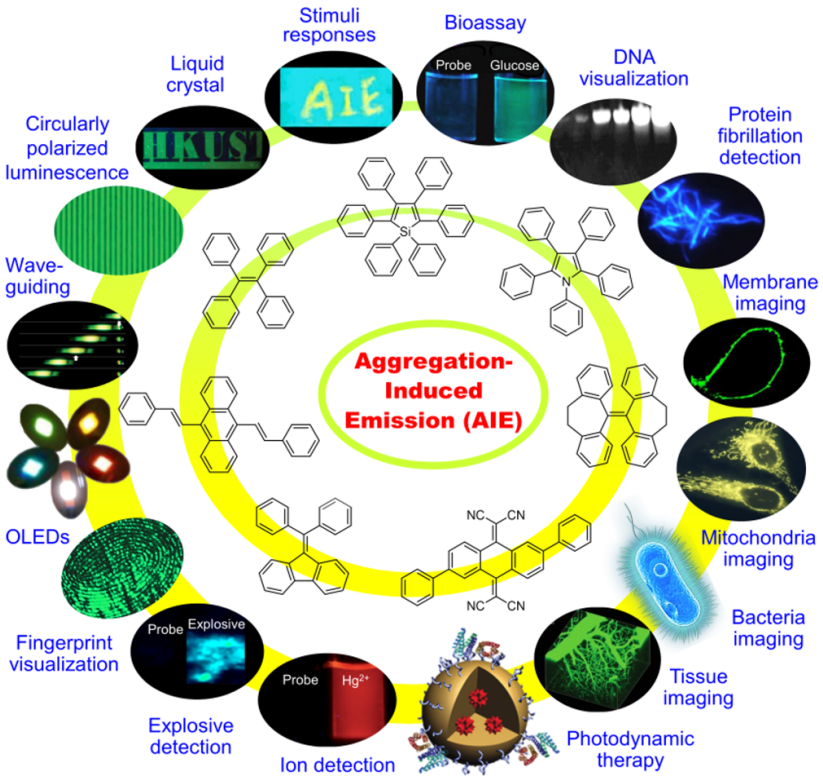

Figure 1.3. Typical examples of structural motifs of AIE gens and their technological applications. [13]

1.3 dual-state emission (DSE)

Dual-state emission (DSE) is a type of luminescence phenomenon that is emissive in both the solution and solid state. Dual-state emitter compounds are discrete molecular entities that exhibit fluorescence in solution and in the solid state. In comparison with traditional AIE molecules, DSE molecules have several advantages. The emergence of DSE molecules has overcome some of the disadvantages of AIE molecules.[46-48] It has attracted a wide range of concerns due to its excellent properties. [49-53] Additionally, conjugated molecules with DSE properties are often designed with conformational freedom to minimize intermolecular π-π stacking interactions and prevent fluorescence quenching in the solid. At the same time, these molecules should keep fast molecular motions at a minimum to eradicate nonradiative relaxation mechanisms in solution. Therefore, DSE compounds achieve a delicate compromise between multiple nonradiative aspects competing with the emissive mechanisms (Figure 1.4).[54]

The major strategy for constructing DSE molecules is as follows.

(1) The twisted Structures. The twisted structures can reduce the intermolecular π-π stacking interaction that caused by conjugated aromatic rings in aggregates, thereby avoiding fluorescence quenching. This has been demonstrated in previous studies.[46,53-55]

(2) Implementing donor (D)-acceptor (A) architectures. The regulation of emission can be achieved by employing donor (D)-acceptor (A) architectures.

(3) Appending long chains or voluminous peripheral. Another strategy to reduce intermolecular interactions within DSE compounds is to include alkyl chains or voluminous groups that promote the "self-isolation" of the fluorophores. The derivatives that containing tetraphenylethene (TPE) group are also frequently synthesized as DSE molecules (Figure 1.5).[56] Generally, it is used to generate emission in the solid state through the AIE phenomenon. In addition, triphenylamine (TPA) derivatives, carbazole derivatives, cyan stilbene derivatives, single benzene derivatives, coumarin derivatives and organoboron complexes and silicon derivatives are also used to synthesize DSE molecules.[57-62]

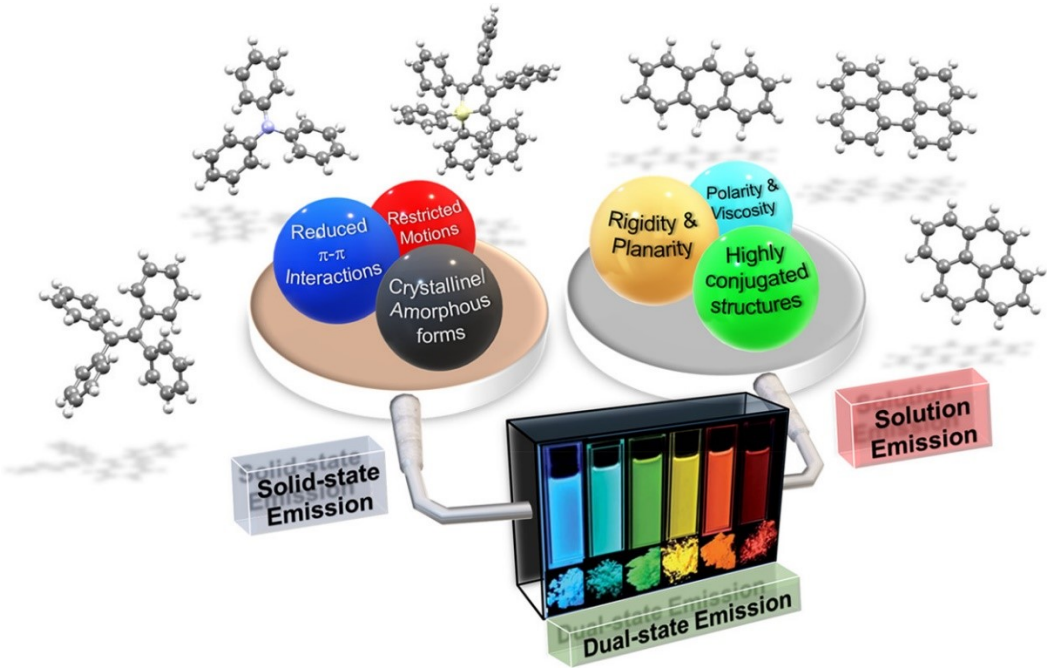

Figure 1.4. Delicate balance between solid state emission and solution emission to attain DSE.[54]

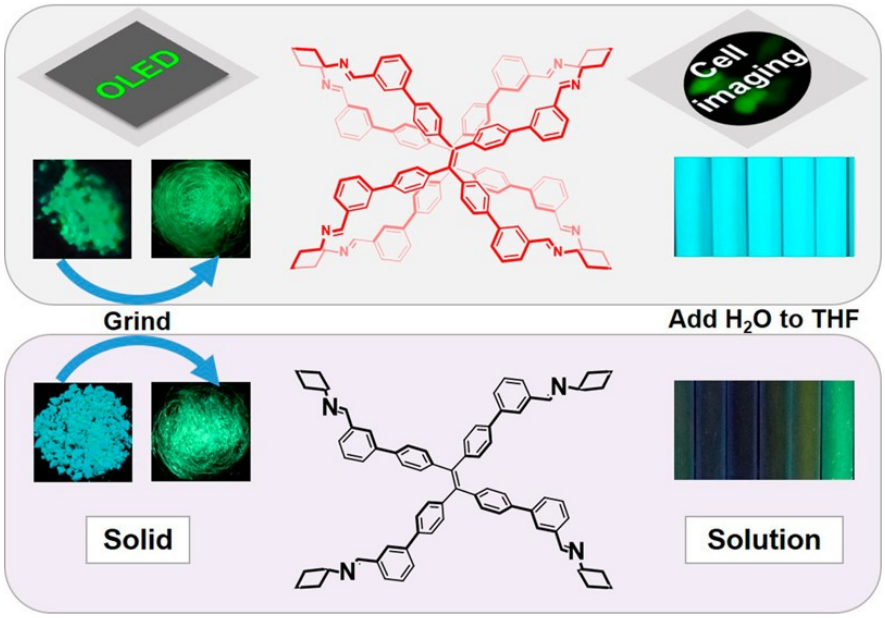

Figure 1.5. The luminophores with TPE as the skeleton.[56]

1.4 Cyclic Imide

Cyclic imides and their *N*-derivatives contain bisamide linkages with a general structure of [-CO-N(R)-CO-].[63] Cyclic imides are valuable for synthetic, biological and polymer chemistry as a kind of important organic compounds.[64-66] There are many types of cyclic imide, including maleimide, phthalimide, perylene diimide and naphthalene diimide et al. Among them, maleimide skeleton is an electron acceptor and has functionalized sites which can introduce three substituents. By introducing substituents with different electronic effects, the optical band gap can be effectively adjusted to achieve different color of luminescence.[66-68] As shown in Figure 1.6, in 2003, C.-T. Chen et al. obtained a full-color luminescent material from blue to red by introducing different donor or acceptor substituents at the 2- and 3-position of maleimide.[69] Moreover, it also has good chemical stability and high fluorescence intensity. Because of these advantages, as shown in Figure 1.7, in our previous works, maleimide fluorophores with fluorescence quantum efficiency is almost 100 % was synthesized by introducing two biphenyl groups on the maleimide ring.[68]

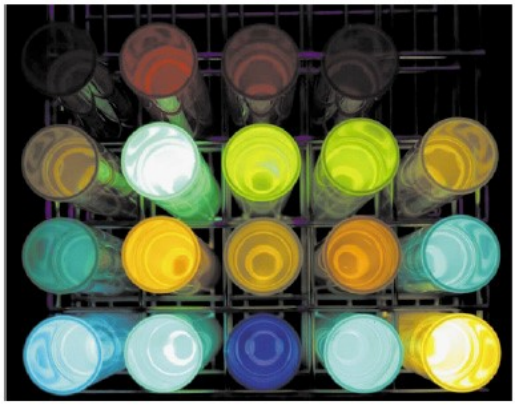

Figure 1.6. Fluorescence image of 3,4-diaryl-substituted maleimide derivatives in dichloromethane showing varied colors.[69]

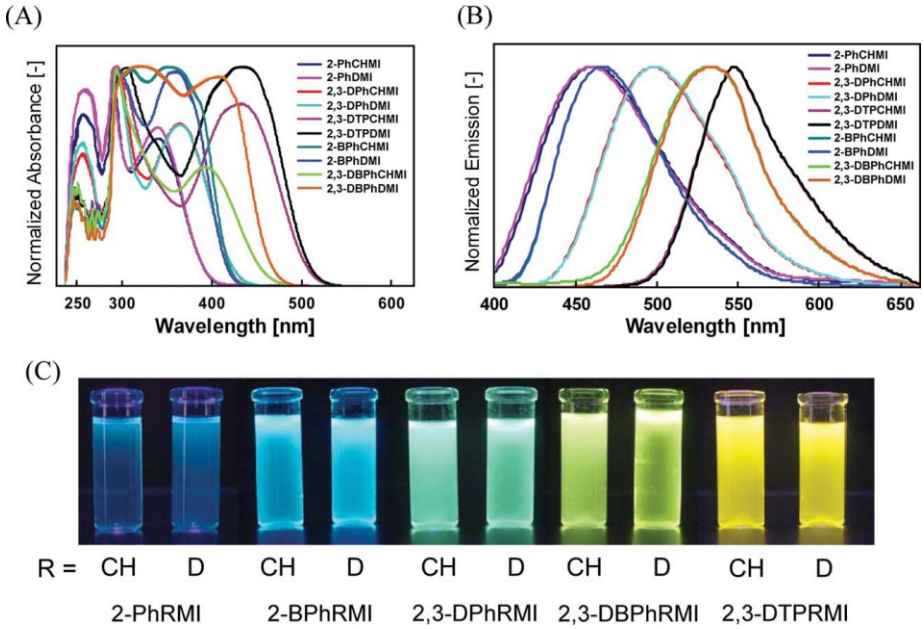

Figure 1.7. UV-vis spectra (A), fluorescence spectra (B), and fluorescence images (C) of model compounds in THF.[68]

1.5 Research Aims and significance

In this study, maleimides were used as a skeleton material to synthesize new D-A molecules with either AIE or DSE properties. Maleimides were chosen for their excellent properties as mentioned above, which made them a suitable skeleton material for the synthesis of molecules with these properties.

In Chapter 2, we synthesized a series of amino-aryl-maleimides was synthesized, in which

different non-planar electron-donating amino groups and a biphenyl group were introduced on the maleimide ring. , in which different non-planar electron-donating amino groups and a biphenyl group were introduced onto the maleimide ring. We examined their fluorescence behavior in a water-THF mixture to confirm emission in aggregates. The obtained luminophores exhibit yellowish-green emission both in solution and in the solid state. Furthermore, the emissive intensity in the solid state is stronger than that in solution, indicating aggregation-induced emission enhancement (AIEE) effects. We also examined their fluorescence behavior in solvents of varying polarity to confirm solvatochromic fluorescence. The results showed positive solvatochromic fluorescence with increasing solvents polarity. Subsequently, we performed the Density functional theory (DFT) quantum calculations to obtain the optimized conformation and positions of the HOMO and LUMO of all the molecules, providing more information about the photophysical properties at the molecular level.

In Chapter 3, based on chapter 2, a series of amino-aryl-maleimides was synthesized, in which varying the amounts of acceptors to confirm the influence of the acceptors amounts about optical properties. We through examined their fluorescence behavior in a water-THF mixture to confirm the emission in aggregates. The obtained luminophores show yellow fluorescence emission both in solution and solid state, show AIEE effects. Compared with the molecules in chapter 2, they have smaller red shift in different polarity solvents.

In Chapter 4, we synthesized two new dual-state emission (DSE) molecules that use maleimide as the skeleton and introduce different amounts of biphenyl-induced conjugation rigidity. We examined their fluorescence behavior in a water-THF mixture to confirm the emission in aggregates. The obtained luminophores showed bright blue fluorescence emission both in solution and solid state, displaying DSE effects. Furthermore, the luminophores also displayed positive solvatochromic effects in solvents of varying polarity. Additionally, we also examined their fluorescence behavior in the presence of trifluoroacetic acid (TFA) and triethylamine (TEA). The result indicated that they display the reversible acidchromic behaviour in response to the addition of trifluoroacetic acid (TFA) and triethylamine (TEA). And Density functional theory (DFT) quantum calculations were also performed to obtain the optimized conformation and the positions of HOMO and LUMO of

all the molecules, providing more information about the photophysical properties at the molecular level.

In chapter 5, summarized the conclusions of this research and discussed the potential applications of the molecules that synthesized in this research and described the direction in future work.

1.6 References

1 F.Wang, X.K.Liu, F. Gao, *Micro and Nano Technologies.*, 2019, 1-35.

2 D. Frackowiak, *J. Photochem. Photobiol., B* 1988, **2**, 399.

3 M. Tebyetekerwa, J. Zhang, Z. Xu, T. N. Truong, Z. Yin, Y. Lu, S. Ramakrishna, D. Macdonald and H. T. Nguyen., *ACS Nano*., 2020, **14**, 11, 14579-14604.

4 Z. Ma, S. Qiu, H-C. Chen, D. Zhang, Y-L. Lu and X-L. Chen, *J. Asian Nat. Prod. Res*., 2022, **24**, 1, 1-14.

5 Z. Li, J. R. Askim and K. S. Suslick, *Chem. Rev*., 2019, **119**, 231-292.

6 M. Gao, F. Yu, C. Lv, J. Choo and L. Chen, *Chem. Soc. Rev*., 2017, **46**, 2237-2271.

7 J. Liu, W. Zhu, H. Chen, Y. Lin and X. Li, *Sci. Adv. Mater.*, 2020, **12**, 1361-1370.

8 Z. Ma, S. Qiu, H-C. Chen, D. Zhang, Y-L. Lu and X-L. Chen, *J. Asian Nat. Prod. Res*., 2021, 1-15.

9 Q. Li, S. Liu, J. Li, X. Pan, J. Zhu and X. Zhu, *Macromol Rapid Commun*., 2021,**42**, 2, 2000517.

10 E. Lakay, S. Hermans, K. Koch and B. Klumperman, *Chem. Eng. J*., 2021, **414**, 128761.

11 N. Sharma, S. Kumar, Y. Chandrasekaran and S. Patil, *Org. Electron*., 2016, **38**, 180-185.

12 Y. Mise, K. Imato, T. Ogi, N. Tsunoji and Ooyama, *New J. Chem*., 2021, **45**, 4164-4173.

13 J. Mei, N. L. C. Leung, R. T. K. Kwok, J. W. Y. Lam and B. Z. Tang, 2015, **115**, 11718-11940.

14 T. Förster and K. Kasper, *Z. Phys. Chem. (Muenchen, Ger.)*, 1954, **1**, 275-277.

15 S. A. Jenekhe and J. A. Osaheni, *Science*, 1994, **265**, 765-768.

16 R. Bakalova, Z. Zhelev, I. Aoki, H. Ohba, Y. Imai and I. Kanno, *Anal. Chem*., 2006, **78**, 5925-5932.

17 G. C. Schmidt, *Ann. Phys*., 1921, **370**, 247-256.

18 F. Wurthner, *Angew. Chem. Int. Ed*., 2020, **59**, 14192-14196.

19 J. Luo, Z. Xie, J. W. Y. Lam, L. Cheng, H. Chen, C. Qiu, H. S. Kwok, X. Zhan, Y. Liu, D. Zhu and B. Z. Tang, *Chem. Commun*., 2001, 1740-1741.

20 B. Z. Tang, X. Zhan, G. Yu, P. P. Sze Lee, Y. Liu, D. Zhu, *J. Mater. Chem.*, 2001, **11**, 2974-2978

21 X. Li, D. Wang, Y. Zhang, W. Lu, S. Yang, G. Hou, Z. Zhao, H. Qin, Y. Zhang, M. Li a) and G. Qing, *Chem. Sci.,* 2021, **12**, 12437-12444.

22 Z. Zhao, H. Zhang, J. W. Y. Lam and B. Z. Tang, *Angew. Chem., Int. Ed*., 2020, **59**, 9888-9907.

23 J. Li, J. Wang, H. Li, N. Song, D. Wang and B. Z. Tang, *Chem. Soc. Rev.*, 2020, **49**, 1144-1172.

24 T. Wu, J. Huang and Y. Yan, *Chem.-Asian J*., 2019, **14**, 730-750.

25 J. Mei, Y. Hong, J. W. Y. Lam, A. Qin, Y. Tang, B. Z. Tang, *Adv. Mater*., 2014, **26**, 5429-5479.

26 Z. Zhao, B. He and B. Z. Tang, *Chem. Sci*., 2015, **6**, 5347-5365.

27 Z. Zhao, J. W. Y. Lam and B. Z. Tang, *J. Mater. Chem*., 2012, **22**, 23726-23740.

28 N. L. C. Leung, N. Xie, W. Yuan, Y. Liu, Q. Wu, Q. Peng, Q. Miao, J. W. Y. Lam and B. Z. Tang, *Chem. Eur. J*., 2014, **20**, 15349-15353.

29 S. Xu, T. Liu, Y. Mu, Y. F. Wang, Z. Chi, C. C. Lo, S. Liu, Y. Zhang, A. Lien and J. Xu, *Angew. Chem., Int. Ed*., 2015, **54**, 874-878.

30 H. Qu, X. Tang, X. Wang, Z. Li, Z. Huang, H. Zhang, Z. Tian and X. Cao, *Chem. Sci*., 2018, **9**, 8814-8818.

31 E. P. J. Parrott, N. Y. Tan, R. Hu, J. A. Zeitler, B. Z. Tang and E. Pickwell-MacPherson, *Mater. Horiz*., 2014, **1**, 251-258.

32 J. Shi, N. Chang, C. Li, J. Mei, C. Deng, X. Luo, Z. Liu, Z. Bo, Q. Dong Yong and Z.

Tang Ben, *Chem. Commun*., 2012, **48**, 10675-10677.

33 H. Nie, K. Hu, Y. Cai, Q. Peng, Z. Zhao, R. Hu, J. Chen, S.J. Su, A. Qin and B. Z. Tang, *Mater. Chem. Front*., 2017, **1**, 1125-1129.

34 Y. Hu, X. Liang, D. Wu, B. Yu, Y. Wang, Y. Mi, Z. Cao and Z. Zhao, *J. Mater. Chem. C*, 2020, **8**, 734-741.

35 H. Sun, X.X. Tang, R. Zhang, W.H. Sun, B.X. Miao, Y. Zhao, Z.H. Ni, *Dyes Pigm*., 2020, **174**, 108051.

36 M. Kaur, H. Kaur, M. Kumar and V. Bhalla, *Chem. Rec*., 2021, **21**, 240-256.

37 J. Mei, Y. Hong, J. W. Y. Lam, A. Qin, Y. Tang, B. Z. Tang, *Adv. Mater.*, 2014, **26**, 5429-5479.

38 F. Yu, Q. Yan, K. Liang, Z. Cong, Q. Shao, Y. Wanga, L. Hong, L. Jiang, G. Ye, H. Wang, B. Chi, G. Xia, *J. Lumin*., 2021, **233**, 117882.

39 Y. Hong, J. W. Y. Lam, B. Z. Tang, Chem. *Soc. Rev.*, 2011, **40**, 5361-5388.

40 Z. Chi, X. Zhang, B. Xu, X. Zhou, C. Ma, Y. Zhang, S. Liu, J. Xu, *Chem. Soc. Rev*., 2012, **41**, 3878-3896.

41 Li, K. D. Ding, B. Liu, B. Z. Tang, *Acc. Chem. Res*. 2013, **46**, 2441-2453.

42 J. Liu, J. W. Y. Lam, B. Z. Tang, *J. Inorg. Organomet. Polym. Mater*., 2009, **19**, 249-258.

43 Z. Zhao, J. W. Y. Lam, Tang, B. Z. *J. Mater. Chem*. 2012, **22**, 23726-23740.

44 R. T. K. Kwok, C. W. T. Leung, J. W. Y. Lam, B. Z. Tang, *Chem. Soc. Rev*. 2015, **44**, 4228-4238.

45 M. Wang, G. Zhang, D. Zhang, D. Zhu, B. Z. Tang, *J. Mater. Chem*., 2010, **20**, 1858-1867.

46 G. Chen, W.B. Li, T.R. Zhou, Q. Peng, D. Zhai, H.X. Li, W.Z. Yuan, Y.M. Zhang and B. Z. Tang, *Adv. Mater*., 2015, **27**, 4496-4501.

47 S. Kumar, P. Singh, P. Kumar, R. Srivastava, S.K. Pal and S. Ghosh, *J. Phys. Chem. C.,*

2016, **120**, 12723-12733.

48 Y. Li, Y. Lei, L. Dong, L. Zhang, J. Zhi, J. Shi, B. Tong and Y. Dong, *Chem. Eur. J*., 2019, **25**, 573-581.

49 M. N. Huang, R. N. Yu, K. Xu, S. X. Ye, S. Kuang, X. H. Zhu and Y. Q. Wan, *Chem. Sci*., 2016, **7**, 4485-4491.

50 Y. Y. Zhang, J. T. Pan, C. Y. Zhang, H. W. Wang, G. B. Zhang, L. Kong, Y. P. Tian and J. X. Yang, *Dyes Pigm*., 2015, **123**, 257-266.

51 T. T. Jing and L. F. Yan, *Sci China Chem*., 2018, **61**, 863-870.

52 W. J. Li, D. D. Liu, F. Z. Shen, D. G. Ma, Z. M. Wang, T. Feng, Y. X. Xu, B. Yang and Y. G. Ma, *Adv. Funct. Mater*., 2012, **22**, 2797-2803.

53 Q. Qiu, P. Xu, Y. Zhu, J. Yu, M. Wei, W. Xi, H. Feng, J. Chen and Z. Qian, *Chem. Eur. J*., 2019, **25**, 15983-15987.

54 J. L. Belmonte-Vázquez, Y. A. Amador-Sánchez, L. A. Rodríguez-Cortés and B.Rodríguez-Molina, *Chem. Mater*., 2021, **33**, 7160-7184.

55 X. Zhang, Y. Zhou, M. Wang, Y. Chen, Y. Zhou, W. Gao, M. Liu, X. Huang, H. Wu, *Chem. -Asian J*., 2020, **15**, 1692-1700.

56 X. Zheng, W. Zhu, C. Zhang, Y. Zhang, C. Zhong, H. Li, G. Xie, X. Wang, C. Yang, *J. Am. Chem. Soc.*, 2019, **141**, 11 4704-4710.

57 Q. Qiu, P. Xu, Y. Zhu, J. Yu, M. Wei, W. Xi, H. Feng, J. Chen, Z. Qian, *Chem. -Eur. J*. 2019, **25**, 15983-15987.

58 15 N. Venkatramaiah, G. D. Kumar, Y. Chandrasekaran, R. Ganduri and S. Patil, *ACS Appl. Mater. Interfaces*, 2018, **10**, 3838-3847.

59 M. Martínez-Abadía, R. Giménez, M. B. Ros, *Adv. Mater*., 2018, **30**, 1704161.

60 H. Liu, S. Zhang, L. Ding, Y. Fang, *Chem. Commun*. 2021, **57**, 4011-4014.

61 D. Cappello, D. A. B. Therien, V. N. Staroverov, F. LagugneLabarthet, J. B. Gilroy,

Optoelectronic, *Chem. -Eur. J.*, 2019, **25**, 5994-6006.

62 M. Shimizu, R. Shigitani, T. Kinoshita, H. Sakaguchi, *Chem.-Asian J.* 2019, **14**, 1792-1800.

63 F. Hassanzadeh and E. Jafari, *J Res Med Sci*., 2018, **23**: 53.

64 N. A. Espinosa-Jalapa, A. Kumar, G. Leitus, Y. Diskin-Posner and D. Milstein, *J. Am. Chem. Soc*., 2017, **139**, 11722-11725.

65 K. Rad-Moghadam, L. Kheyrkhah, *Commun*., 2009, **39**, 2108-2115.

66 J. Wang, R. Zheng, H. Chen, H. Yao, L. Yan, J. Wei, Z. Lin and Q. Ling, *Org. Biomol. Chem*., 2018, **16**, 130-139.

67 M. Nakamura, K. Yamabuki and T. Oishi, K. Onimura, *J. Polym. Sci. Part A: Polym. Chem*., 2013, **51**, 4945-4956.

68 K. Onimura, M. Matsushima, M. Nakamura, T. Tominaga, K. Yamabuki and T. Oishi, *J. Polym. Sci. Part A: Polym. Chem*., 2011, **49**, 3550-3558.

69 H-C. Yeh, W-C. Wu and C-T. Chen, *Chem. Commun*., 2003, 404-405.

Chapter 2

Synthesis and optical properties of conjugated maleimide molecules containing amino with aggregation-induced emission enhancement (AIEE)

2.1 Introduction

Maleimide-type luminophores, which have been utilized for organic luminescence, have a simple chemical structure and are easy to synthesize. Their emission colours and properties can be widely adjusted by modifying the substituents on the 3- and 4-positions of the maleimide ring. They can be applied in various fields, such as fluorescent probes, wavelength-conversion luminophores, OLEDs, etc.[1-4]

However, most luminophores often encounter severe concentration- or aggregation-caused quenching (ACQ), which can limit their high-tech applications. In response to this problem, aggregation-induced emission (AIE) luminophores, which are highly emissive as aggregates are formed, were reported in 2001 by Tang.[5] The restriction of intramolecular motions (RIM) has been considered to be the main cause of AIE effects so far, including the restriction of intramolecular rotation (RIR) and the restriction of intramolecular vibration (RIV).[6] Intramolecular motion is inhibited when the molecules are aggregated, thereby suppressing the non-radiative decay, and the molecules emit mainly through the radiative transition.

Additionally, AIE molecules generally have non-planar molecular conformations to suppress π-π accumulation in aggregates, and thereby enhance the emission. AIE molecules have been attracting increasing attention and have been applied in various fields.[7-11] As the classical AIE molecule, tetraphenyl ethylene (TPE) has been extensively researched. By modifying maleimide (MI) to tetraphenyl ethylene (TPE), a probe for thiol detection was developed in 2010 by Tang.[12] However, it was not emissive in both solution aggregates.

Later, Naka reported amino-aryl-maleimides that are emissive in aggregates.[2] In comparison with the AIE molecules with a TPE unit, amino-maleimides with AIE effects have simple structures and are easy to synthesize.[2] Therefore, as new AIE molecules, amino-maleimides enrich the types of AIE molecules available and are expected to bring more possibilities to the AIE field. We reasoned that a series of luminophores with different fluorescence performances might be obtained by varying the type of amino group. In our previous works, luminophores with fluorescence quantum efficiency of almost 100% were synthesized by introducing two biphenyl groups on the maleimide ring.[13] Therefore, in this article, we designed a series of amino-aryl-maleimides, in which different non-planar electron-donating amino groups and a biphenyl group were introduced on the maleimide ring. Compared with the luminophores that are only emissive in solution or in the solid state, the obtained luminophores show yellowish-green emission both in solution and in the solid state. Moreover, the emissive intensity in the solid state is stronger than that in solution, showing aggregation-induced emission enhancement (AIEE) effects.[14] This is beneficial to the applications of AIE molecules in OLED, probes, and other fields.[15-22] We are currently considering application to OLED. The results were reported at the 12th SPSJ International Polymer Conference (IPC2018).

2.2 Experimental

2.2.1 Materials

All commercially obtained chemicals in this study were used without any further purification. Magnesium sulfate (anhydrous), zinc chloride and cyclohexylamine were purchased from Kishida Reagents Chemicals. Dichloromaleic anhydride, palladium (II) acetate, piperidine, pyrrolidine and silica gel 60N (63-213 mm), which was used for column chromatography, were purchased from Wako Pure Chemical Industries. Moreover, 60F 254 silica gel plates for analytical thin-layer chromatography were purchased from Merck. 1,1,1,3,3,3-Hexamethyl-disilazane (HMDS) was purchased from TCI, and morpholine was available from Ishizu Seiyaku. Triphenylphosphine was purchased from Kanto Chemical, and 4-biphenylboronic acid was available from Combi-Blocks. Commercially available products (1st grade) were used for all solvents.

2.2.2 Measurements

The ^{1}H (500 MHz) and ^{13}C (125 MHz) nuclear magnetic resonance (NMR) spectra were recorded using a JNM-LA500 spectrometer with $CDCl_3$ as the solvent and TMS as an internal standard. The abbreviations for the NMR spectroscopy data are as follows: s, singlet; d, doublet; t, triplet; m, multiplet. The ultraviolet-visible (UV-vis) spectra were recorded using a UV-1650PC (Shimadzu Corporation) spectrometer, and the photoluminescence (PL) spectra were recorded using a FP-6300(JASCO Corporation) spectrophotometer.

2.2.3 Synthesis

2.2.3.A Synthesis of 2,3-dichloro-*N*-cyclohexylmaleimide (Compound **1**)

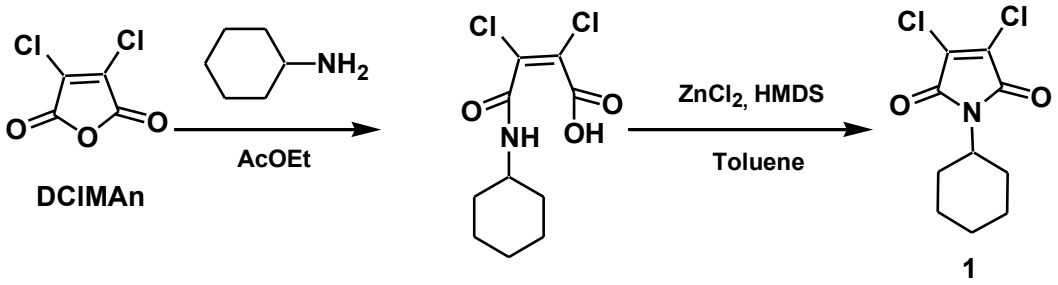

Scheme 2.1

Dichloromaleic anhydride (4.00 g, 24.0 mmol) was dissolved in ethyl acetate (50 mL) in a 100 mL flask, and cyclohexylamine (1.98 g, 20.0 mmol) was added to the solution in ethyl acetate (20 mL) was added dropwise at 0 ºC, and then return to room temperature and stirred overnight. After that, the solution was concentrated in vacuo. Then a solution of hexamethyldisilazane (2.62 mL, 12.5 mmol) in toluene (160 mL) was slowly added dropwise at 60 ºC. When the temperature was raised to 110°C, zinc chloride (3.43 g, 25.2 mmol) and hexamethyldisilazane (7.90 mL, 37.8 mmol) was slowly added dropwise, and the mixture was refluxed for 20 hrs. The reaction mixture was diluted with additional ethyl acetate, and then washed using distilled water. The combined organic layer was dried over $MgSO_4$, and the filtrate was concentrated in vacuo. The residue was purified on a silica gel column using n-hexane/EtOAc (30/1: v/v) to obtain a white powder (melting point: 141-143°C, 4.60 g, 18.6 mmol, 77 %).

^{1}H-NMR ($CDCl_3$) δ (ppm from TMS) : 3.96 - 4.02 (1H, m, cyclohexyl), 1.99 - 2.08 (2H, m, cyclohexyl),1.17 - 1.37 (3H, m, cyclohexyl), 1.82 - 1.89 (2H, m, cyclohexyl), 1.64 - 1.74 (3H, m, cyclohexyl).

2.2.3.B Synthesis of 2-chloro-3-morpholino-*N*-cyclohexylmaleimide (Compound **2**)

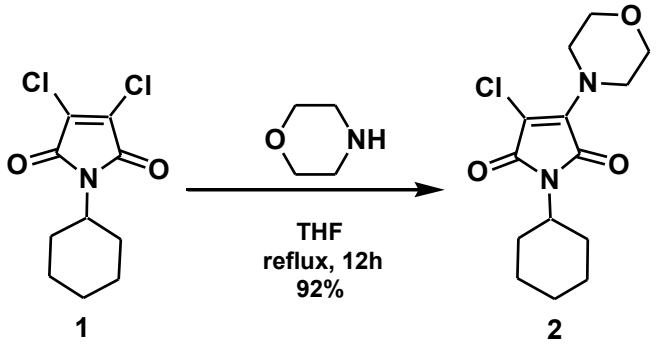

Scheme 2.2

A THF solution of 2,3-dichloro-*N*-cyclohexylmaleimide (0.40 g, 1.61 mmol) and morpholine (0.15 g, 1.77 mmol) was heated under reflux for 12 hrs under a nitrogen atmosphere. The reaction mixture was diluted with additional ethyl acetate, and then washed using distilled water. The combined organic layer was dried over $MgSO_4$, and the filtrate was concentrated in vacuo. The residue was purified on a silica gel column using n-hexane/EtOAc (4/1: v/v) to obtain a yellow powder (melting point: 142-144 °C, 0.440 g, 1.48 mmol, 92%).

^{1}H-NMR ($CDCl_3$) δ (ppm from TMS): 1.17-1.34 (3H, m, cyclohexyl), 1.62-1.68 (3H, m, cyclohexyl), 1.80-1.83 (2H, m, cyclohexyl), 1.97-2.06 (2H, m, cyclohexyl), 3.78-3.80 (4H, m, morpholine unit), 3.87-3.92 (1H, m, -N-CH-), 3.93-3.96 (4H, m, morpholine unit).

^{13}C-NMR ($CDCl_3$) δ (ppm from TMS): 40.11, 40.82, 44.03, 58.62, 60.99, 73.66, 96.40, 132.47, 152.50, 153.16.

Elemental analysis: Calculated for $C_{14}H_{19}N_2O_3Cl$: C, 56.28; H, 6.41; N, 9.38. Found: C, 56.29; H, 6.49; N, 9.33.

2.2.3.C Synthesis of 2-biphenyl-3-morpholino-*N*-cyclohexylmaleimide by Suzuki-Miyaura coupling reaction (Compound **3**)

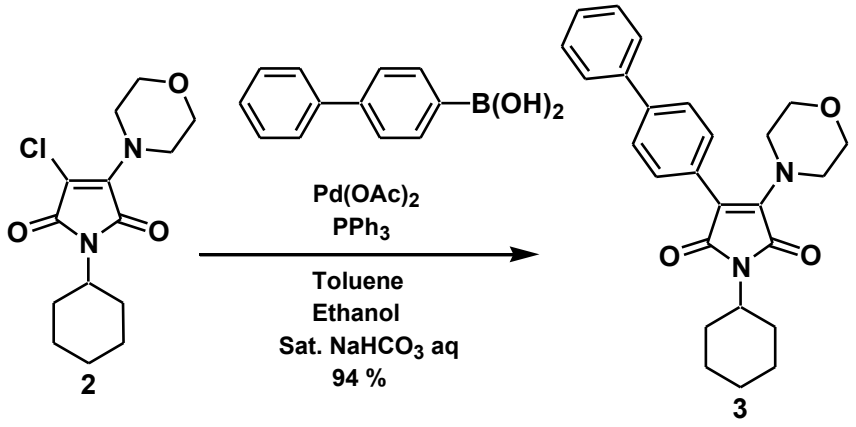

Scheme 2.3

A mixture of **2** (0.20 g, 0.67 mmol) and 4-biphenylboronic acid (0.160 g, 0.800 mmol) was added to a flask. Then, toluene (4 mL), ethanol (2 mL) and sat. $NaHCO_3$ aqueous solution (4 mL) were added successively, and the mixture was stirred at room temperature for 20 min. $Pd(OAc)_2$ (0.0150 g, 0.0670 mmol) and PPh_3 (0.0180 g, 0.0670 mmol) were added to the flask. The mixture was heated under reflux for 5 hrs under a nitrogen atmosphere. After that, the reaction mixture was diluted with additional ethyl acetate and then washed using distilled water. The combined organic layer was dried over $MgSO_4$, and the filtrate was concentrated in vacuo. The residue was purified on a silica gel column using n-hexane/EtOAc (9/1: v/v) to obtain a yellow powder (melting point: 180-182 °C, 0.26 g, 0.64 mmol, 94%).

^{1}H-NMR ($CDCl_3$) δ (ppm from TMS): 1.18-1.37 (3H, m, cyclohexyl), 1.66-1.72 (3H, m, cyclohexyl), 1.82-1.85 (2H, m, cyclohexyl), 2.06-2.14 (2H, m, cyclohexyl), 3.55-3.57 (4H, m, morpholine unit), 3.71-3.73 (4H, m, morpholine unit), 3.93-4.00 (1H, m, cyclohexyl), 7.35-7.39 (3H, m, -BPh), 7.43-7.47 (2H, m, -BPh), 7.59-7.63 (4H, m,-BPh).

^{13}C-NMR ($CDCl_3$) δ (ppm from TMS): 40.27, 40.94, 44.10, 59.42, 60.55, 73.54, 104.26, 121.41, 121.70, 122.08, 123.15, 123.86, 124.54, 132.33, 132.48, 134.37, 154.36, 156.91. Elemental analysis: Calculated for $C_{26}H_{28}N_2O_3$: C, 74.98; H, 6.78; N, 6.72. Found: C, 74.71; H, 6.88; N, 6.38.

2.2.3.D Synthesis of 2-chloro-3-piperidino-*N*-cyclohexylmaleimide (Compound **4**)

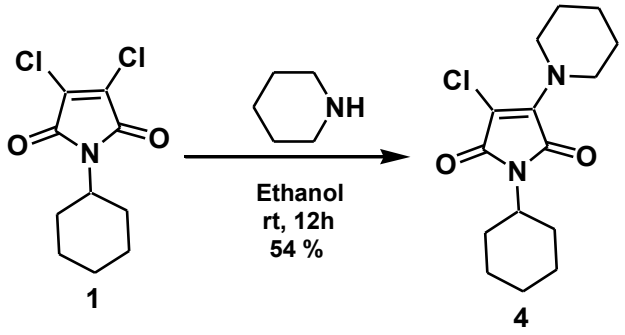

Scheme 2.4

An ethanol solution (35 mL) of 2,3-dichloro-*N*-cyclohexylmaleimide (1.50 g, 6.05 mmol) and piperidine (0.500 g, 5.50 mmol) was stirred at room temperature for 12 hrs under a nitrogen atmosphere. The reaction mixture was diluted with additional ethyl acetate, and then washed using distilled water. The combined organic layer was dried over $MgSO_4$, and the filtrate was concentrated in vacuo. The residue was purified on a silica gel column using n-hexane/EtOAc (9/1: v/v) to obtain a yellow powder (melting point: 165-168 °C, 0.880 g, 2.97 mmol, 54%).

^{1}H-NMR ($CDCl_3$) d (ppm from TMS): 1.15-1.34 (3H, m, -CH_2-), 1.63-1.70 (9H, m, -CH_2-), 1.80-1.82 (2H, m, -CH_2-), 1.98-2.07 (2H, m, -CH_2 -), 3.85-3.93 (5H, m, -N-CH- and -N-CH_2-).

^{13}C-NMR ($CDCl_3$) d (ppm from TMS): 39.38, 40.17, 40.87, 41.41, 44.06, 59.66, 60.88, 94.87, 133.24, 152.62, 153.51.

Elemental analysis: Calculated for $C_{15}H_{21}N_2O_2Cl$: C, 60.70; H, 7.13; N, 9.44. Found: C, 59.69; H, 7.16; N, 9.12.

2.2.3.E Synthesis of 2-biphenyl-3-piperidino-*N*-cyclohexylmaleimide by Suzuki-Miyaura coupling reaction (Compound **5**)

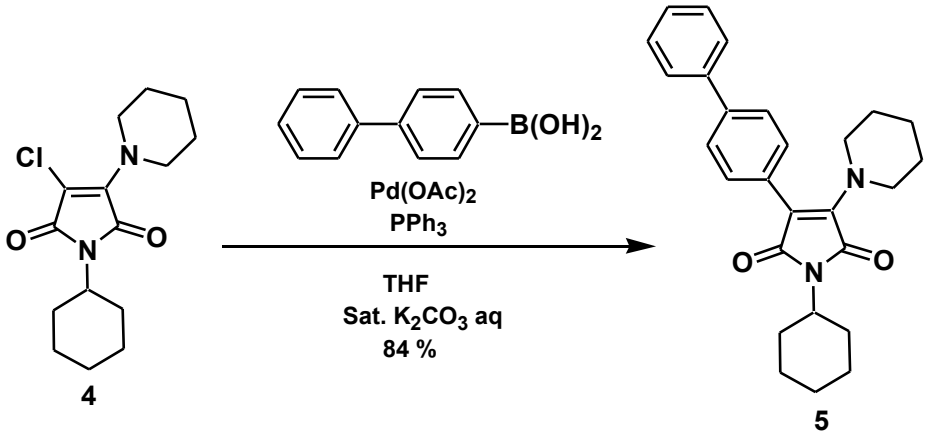

Scheme 2.5

A mixture of **4** (0.200 g, 0.670 mmol) and 4-biphenylboronic acid (0.170 g, 0.870 mmol) was added to a flask. Then, THF (6 mL) and sat. K_2CO_3 aqueous solution (3 mL) were added successively, and the mixture was stirred at room temperature for 20 min. $Pd(OAc)_2$ (0.030 g, 0.130 mmol) and PPh_3 (0.100 g, 0.390 mmol) were added to the flask, and the mixture was heated under reflux for 14 hrs under a nitrogen atmosphere. After that, the reaction mixture was diluted with additional ethyl acetate and then washed using distilled water. The combined organic layer was dried over $MgSO_4$, and the filtrate was concentrated in vacuo. The residue was purified on a silica gel column using n-hexane/EtOAc (9/1: v/v) to obtain a yellowish-green powder (melting point: 119-124 °C, 0.23 g, 0.56 mmol, 84%).

^{1}H-NMR ($CDCl_3$) δ (ppm from TMS): 1.20-1.37 (4H, m, -CH 2-), 1.63-1.72 (8H, m, -CH 2-), 1.82-1.84 (2H, m,-CH 2-), 2.08-2.15 (2H, m, -CH 2-), 3.46 (4H, s, -N-CH_2-), 3.93-4.00 (1H, m, -N-CH-), 7.33-7.39 (3H, m, -BPh), 7.42-7.46 (2H, m, -BPh), 7.58-7.62 (4H, m, -BPh).

^{13}C-NMR ($CDCl_3$) δ (ppm from TMS): 39.24, 40.30, 40.97, 40.99, 44.11, 60.43, 60.46, 102.96, 121.28, 121.67, 121.94, 123.11, 124.40, 124.53, 131.88, 132.66, 135.33, 154.40, 157.14.

Elemental analysis: Calculated for $C_{27}H_{30}N_2O_2$: C, 78.23; H, 7.29; N, 6.76. Found: C, 77.12; H, 7.31; N, 6.30.

2.2.3.F Synthesis of 2-chloro-3-pyrrolidino-*N*-cyclohexylmaleimide (Compound **6**)

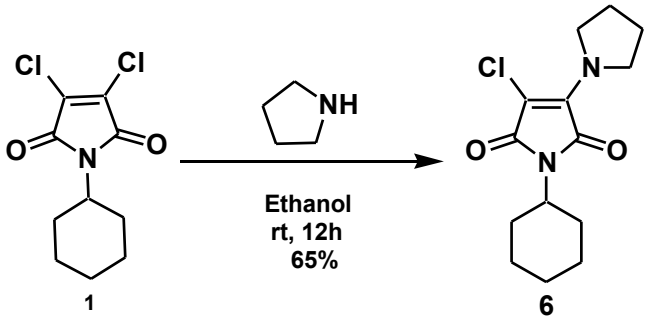

Scheme 2.6

An ethanol solution (35 mL) of 2,3-dichloro-*N*-cyclohexylmaleimide (1.50 g, 6.05 mmol) and pyrrolidine (0.600 g, 7.26 mmol) was stirred at room temperature for 12 hrs under a nitrogen atmosphere. The reaction mixture was diluted with additional ethyl acetate and then washed using distilled water. The combined organic layer was dried over $MgSO_4$, and the filtrate was concentrated in vacuo. The residue was purified on a silica gel column using n-hexane/EtOAc (9/1: v/v) to obtain a yellow powder (melting point: 140-144 °C, 1.11 g, 2.88 mmol, 65%).

^{1}H-NMR ($CDCl_3$) δ (ppm from TMS): 1.18-1.34 (3H, m, -CH_2-), 1.63-1.65 (3H, m, -CH_2 -), 1.79-1.82 (2H, m, -CH_2-), 1.91-1.93 (4H, m, -CH 2-), 1.99-2.07 (2H, m, -CH_2-), 3.88-3.93 (5H, m, N-CH_2-).

^{13}C-NMR ($CDCl_3$) δ (ppm from TMS): 40.18, 40.87, 44.10, 60.25, 60.76, 91.89, 132.16, 152.11, 154.02.

Elemental analysis: Calculated for $C_{14}H_{19}N_2O_2Cl$: C, 59.47; H, 6.77; N, 9.91. Found: C, 59.38; H, 6.79; N, 9.85.

2.2.3.G Synthesis of 2-biphenyl-3-pyrrolidino-*N*-cyclohexylmaleimide by Suzuki-Miyaura coupling reaction (Compound **7**)

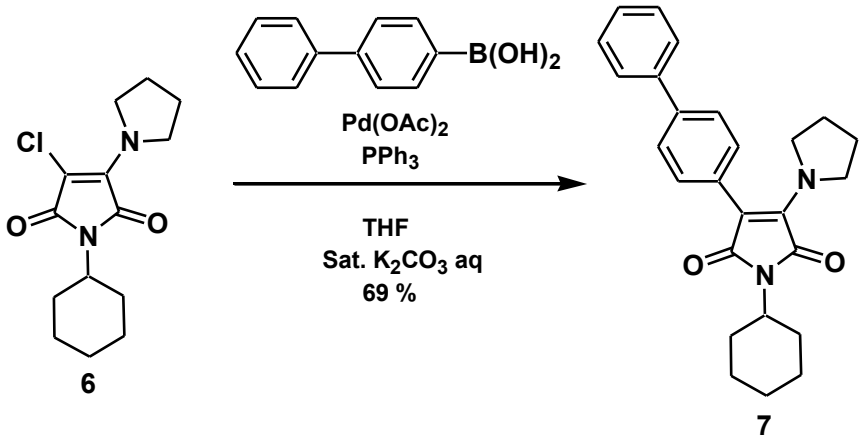

Scheme 2.7

A mixture of **6** (0.200 g, 0.670 mmol) and 4-biphenyl-boronic acid (0.170 g, 0.870 mmol) was added to a flask. Then, THF (6 mL) and sat. K_2CO_3 aqueous solution (3 mL) were added successively, and the mixture was stirred at room temperature for 20 min. Pd $(OAc)_2$ (0.030 g, 0.130 mmol) and PPh_3 (0.100 g, 0.390 mmol) were added to the flask, and the mixture was heated under reflux for 14 hrs under a nitrogen atmosphere. After that, the reaction mixture was diluted with additional ethyl acetate and then washed using distilled water. The combined organic layer was dried over $MgSO_4$, and the filtrate was concentrated in vacuo. The residue was purified on a silica gel column using n-hexane/EtOAc (7/1: v/v) to obtain yellow powder (melting point: 195-198 °C, 0.18 g, 0.46 mmol, 69%).

^{1}H-NMR ($CDCl_3$) δ (ppm from TMS): 1.20-1.35 (3H, m, cyclohexyl), 1.65-1.72 (3H, m, cyclohexyl), 1.82-1.86 (6H, m, -CH 2-), 2.09-2.16 (2H, m, cyclohexyl), 3.52 (4H, s, -N-CH_2-), 3.94-4.00 (1H, m, cyclohexyl), 7.55-7.56 (3H, m, -BPh), 7.56-7.57 (2H, m, -BPh), 7.60-7.62 (4H, m, -BPh).

^{13}C-NMR ($CDCl_3$) d (ppm from TMS): 40.36, 40.97, 44.14, 60.36, 61.31, 100.33, 120.87, 121.70, 121.86, 123.09, 124.63, 125.34, 131.65, 132.75, 133.71, 153.82, 157.62.

Elemental analysis: Calculated for $C_{26}H_{28}N_2O_2$: C, 77.97; H, 7.05; N, 6.99. Found: C, 77.51; H, 7.25; N, 6.37.

2.2.4 Structure characterization

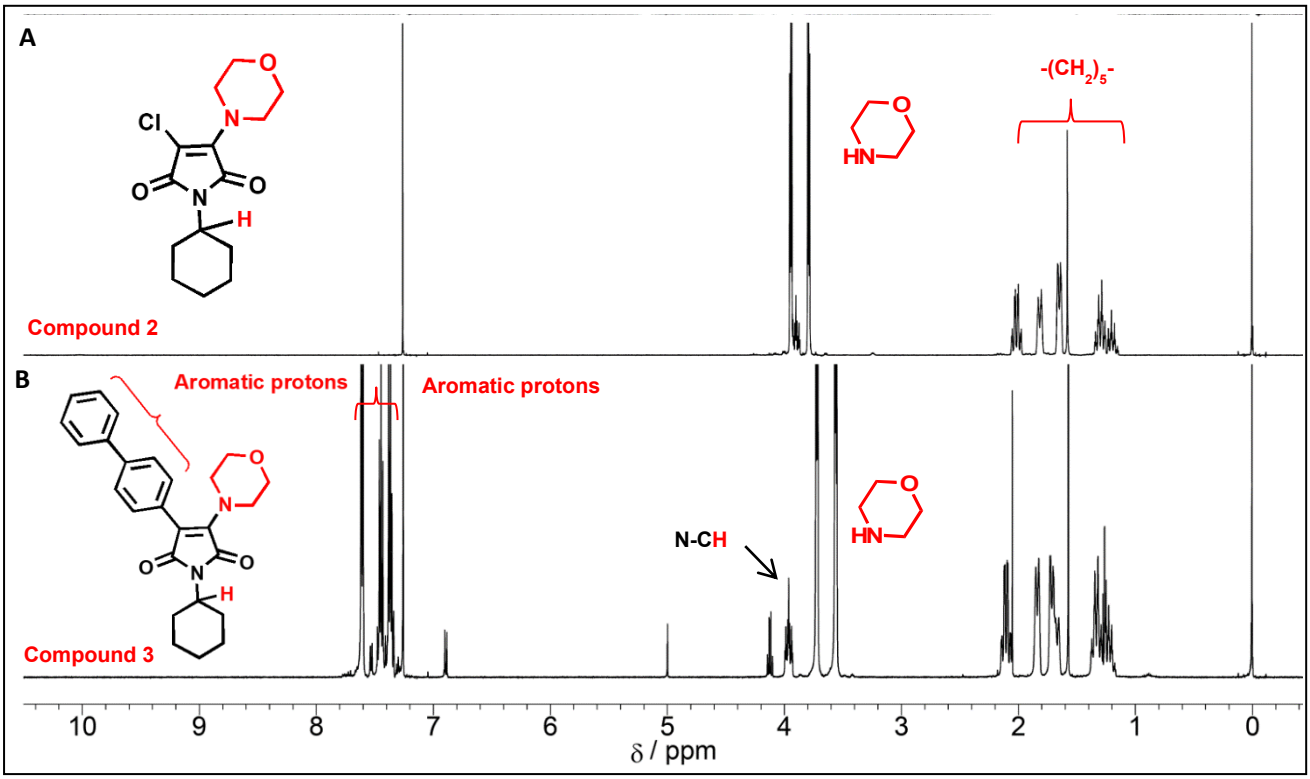

Figure 2.1. ^{1}H NMR Spectra of (A) **2** and (B) **3** in $CDCl_3$.

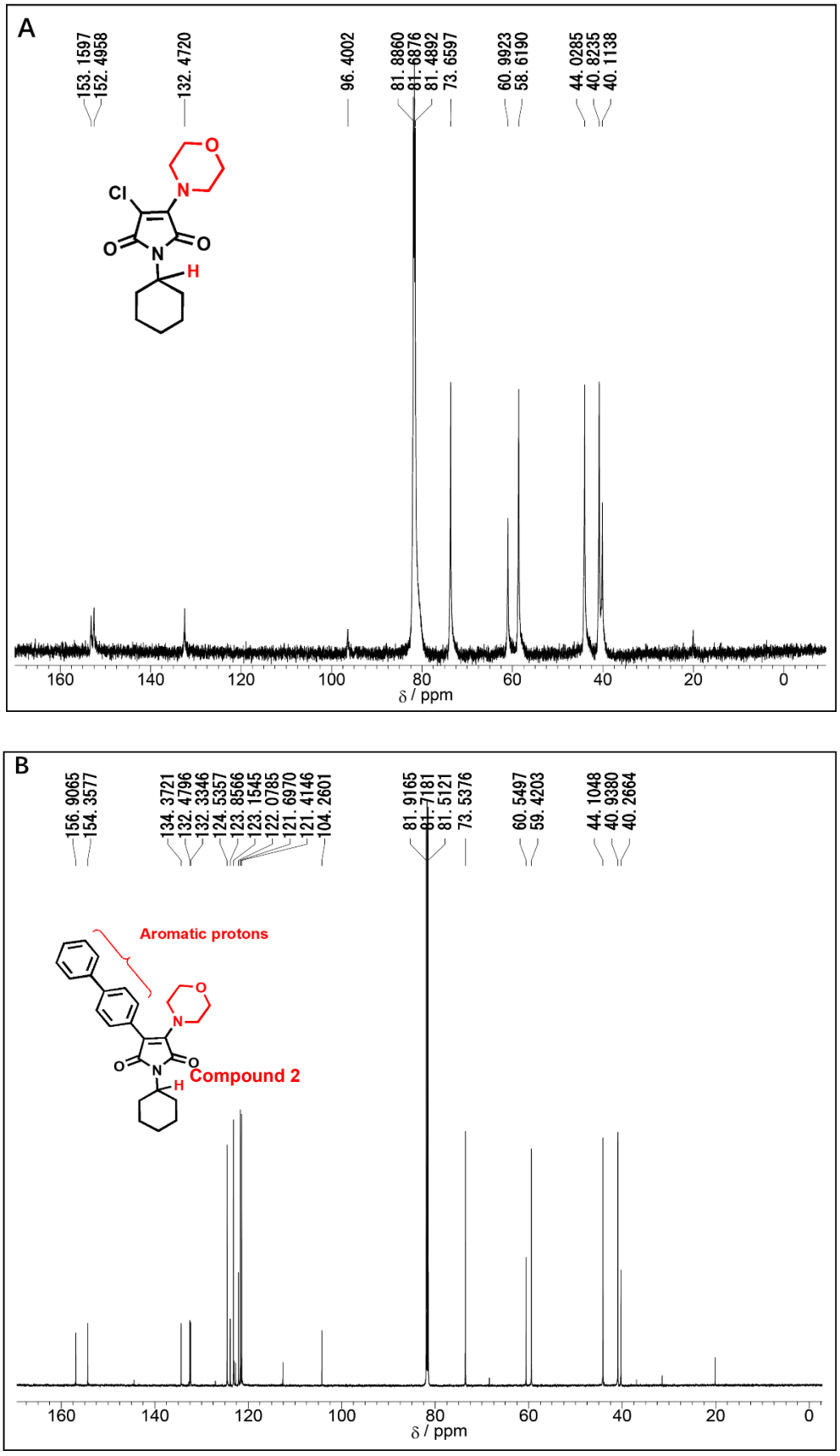

Figure 2.2. ^{13}C NMR Spectra of (A) **2** and (B) **3** in $CDCl_3$.

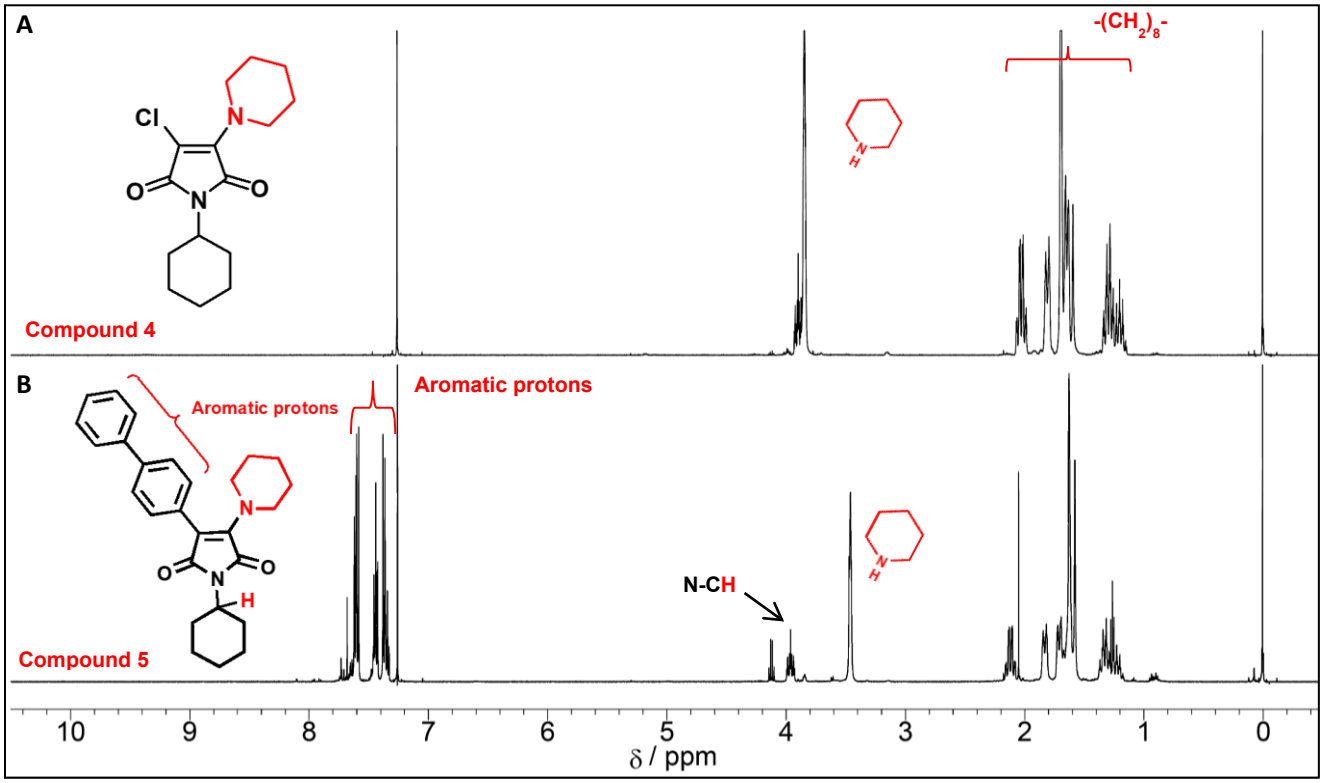

Figure 2.3. ^{1}H NMR Spectra of (A) **4** and (B) **5** in $CDCl_3$.

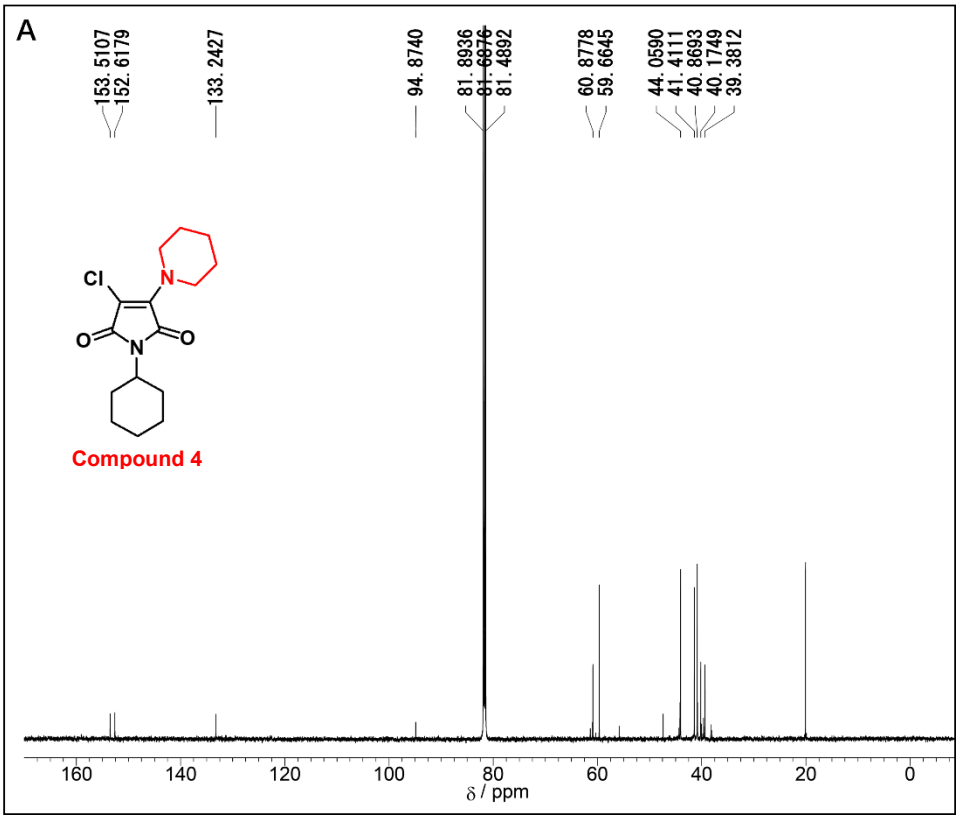

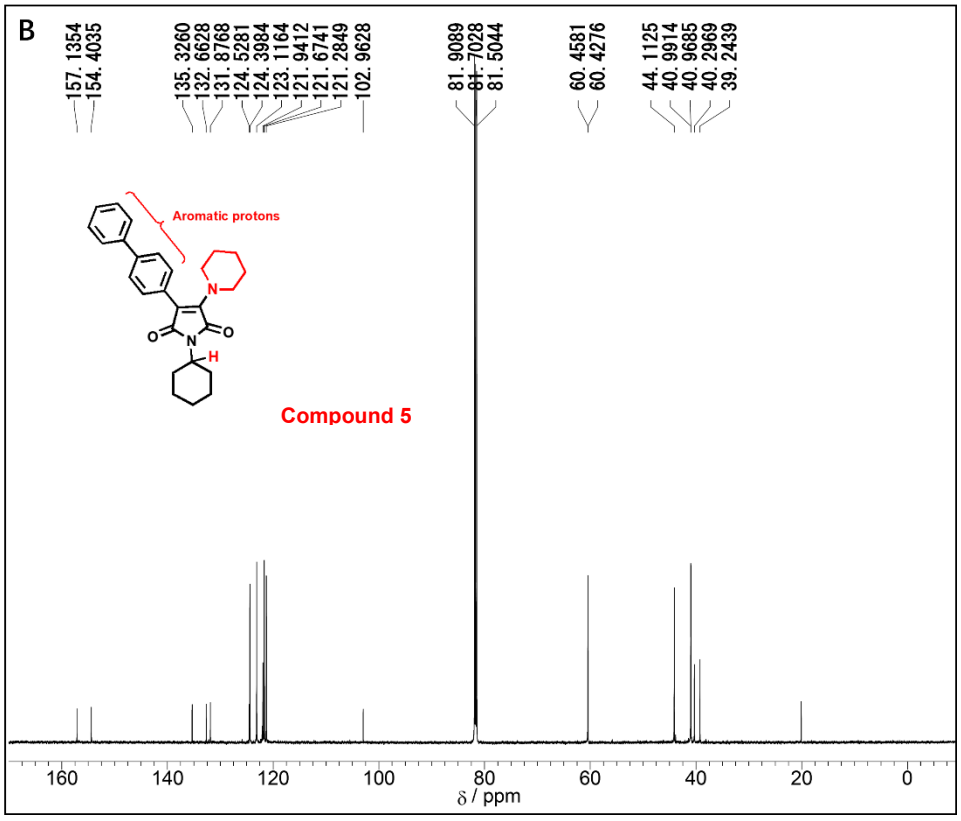

Figure 2.4. ^{13}C NMR Spectra of (A) **4** and (B) **5** in $CDCl_3$.

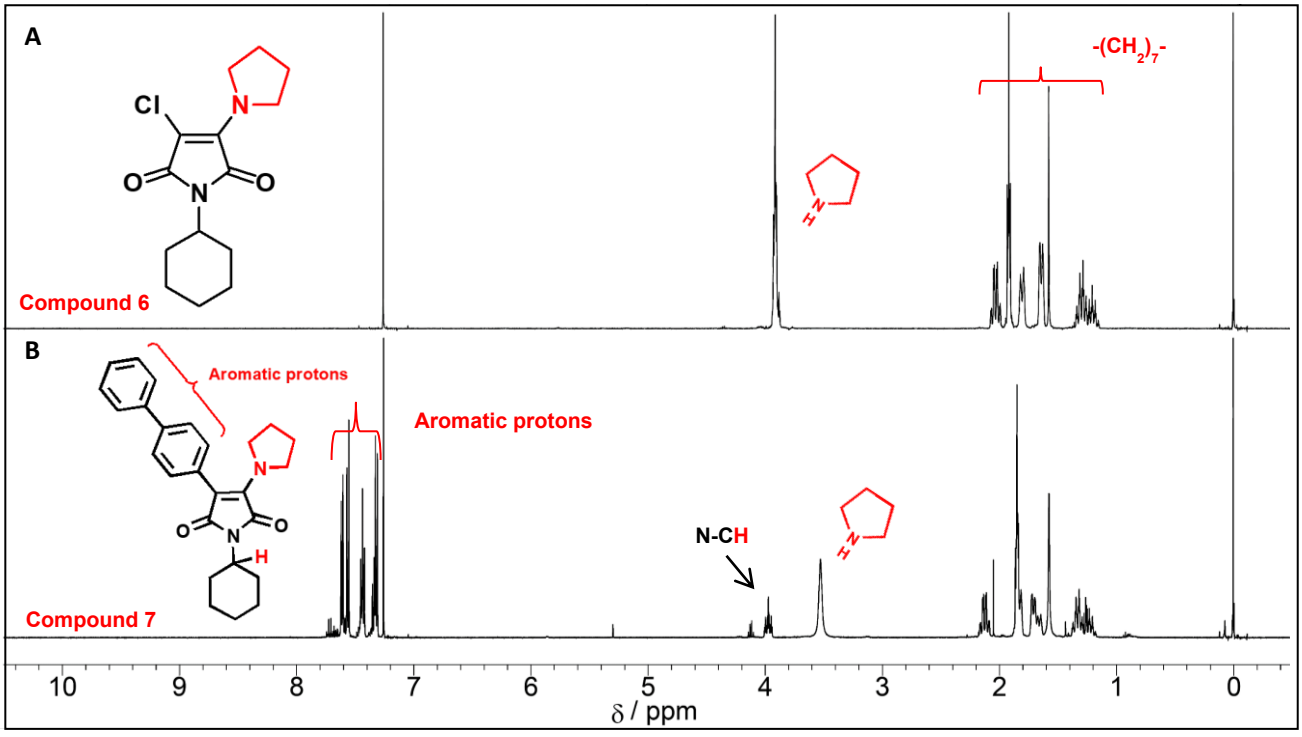

Figure 2.5. ^{1}H NMR Spectra of (A) **6** and (B) **7** in $CDCl_3$.

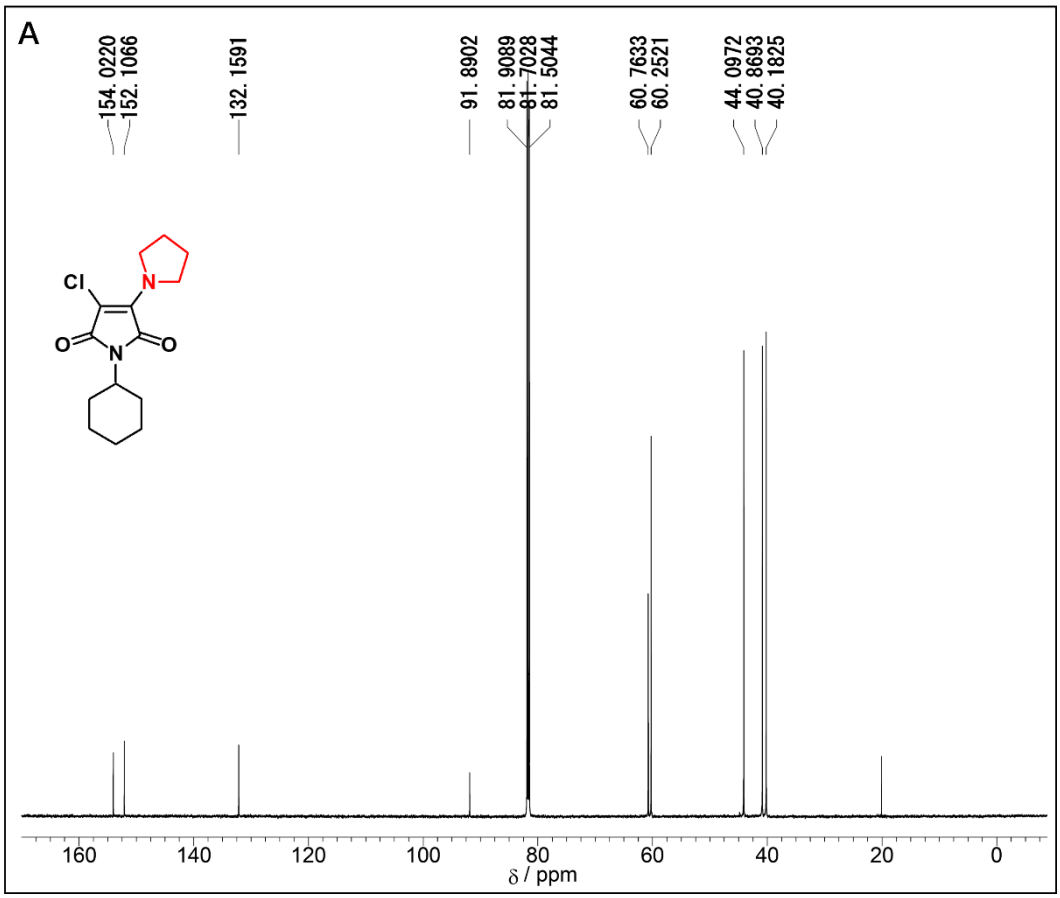

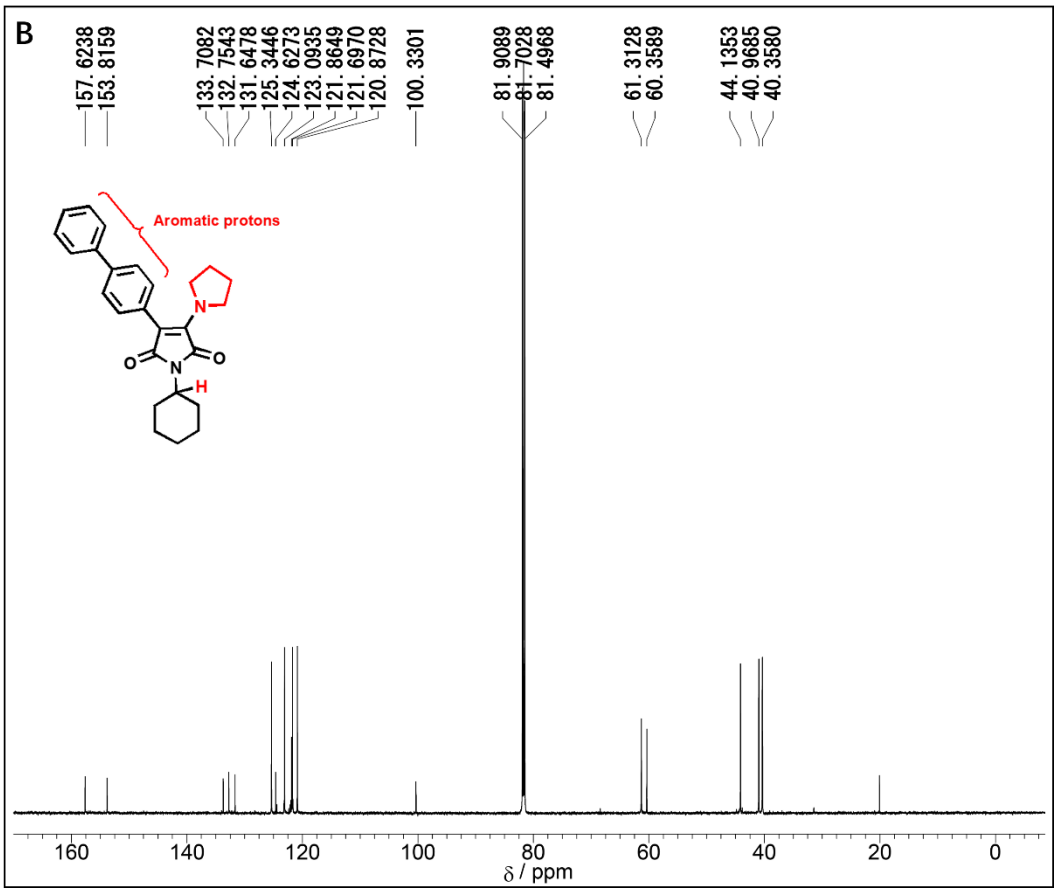

Figure 2.6. ^{13}C NMR Spectra of (A) **6** and (B) **7** in $CDCl_3$.

2.3 Results and discussion

2.3.1 Syntheses

As shown in Scheme 2.1, we synthesized dichloro-*N*-cyclohexyl-maleimide **1** from dichloromaleic anhydride and cyclohexylamine, and 2-chloro-3-amino-*N*-cyclohexylmaleimides (**2**, **4**, **6**) were synthesized by reacting **1** with different amino groups (morpholinyl, piperidinyl, pyrrolidinyl). Then, amino-biphenyl-*N*-cyclohexyl-maleimides **3**, **5** and **7** containing different amino groups were synthesized by reaction with 4-biphenylboronic acid through the Suzuki-Miyaura coupling reaction, respectively. Their structures were confirmed by NMR (^{1}H and ^{13}C), and the structure characterization is described in the Figure 2.1-2.6. The yields of amino-biphenyl-*N*-cyclohexyl maleimides **3**, **5** and **7** are 94%, 84% and 69% as a yellow powder, respectively.

2.3.2 UV/Vis absorption spectra and photoluminescence (PL) spectra

The maleimide luminophores **3**, **5** and **7** were investigated through UV/vis absorption spectra (Figure 2.7.A), photoluminescence (PL) spectra (Figure 2.7.B) and the fluorescence quantum yields (Φ_F) in dilute THF solutions and the solid state. The results of the optical measurements are summarized in Table 2.1. Similar absorption peaks can be observed for these maleimide luminophores (Figure 2.7.A); the absorption maximum wavelengths of luminophore **3** (λ_{max} = 410 nm) and **5** (λ_{max} = 413 nm) were red-shifted relative to that of **7** (λ_{max} = 401 nm). It is indicated that the red-shift of absorption was due to the difference in the electron-donating ability of the amino groups. The luminophores, with CIE coordinates of (0.38, 0.57) for **3**, (0.29, 0.58) for **5** and (0.30, 0.60) for **7**, show yellowish-green emission in dilute THF (Table 2.1). Figure 2.7.B shows that the maximum emission wavelength of luminophore **3** is 548 nm, which is red shifted by 13 nm and 14 nm relative to those of **5** (535 nm) and **7** (534 nm). Moreover, we found that all the luminophores have a good spectral separation of absorption and emission with large Stokes shifts (>100 nm) (Table 2.1). Overall, compared with the other luminophores, luminophore **3** (with morpholinyl) possessed the longest wavelength and largest Stokes shift in the fluorescence emission spectra.

Correspondingly, compared to piperidinyl and pyrrolidinyl, morpholinyl is more helpful to the expansion of the Stokes shift of the compound. Large Stokes shifts (>100 nm) (Table 2.1) can prevent interference from the excitation light and scattered light, as well as the influence caused by reabsorption.[23-25] This is important for potential applications in biological fields.[23-28]

Table 2.1. Optical properties of luminophore **1**, **2** and **3**.

Compound	λ_{abs} [a)] (nm)	λ_{em} [a] (nm)	Δs (nm)	CIE (x, y) [a)]	Φ (%) [b)]	
					solution	solid
1	410	547	137	0.38，0.57	1.8	27.2
2	413	535	122	0.29，0.58	10.1	14.2
3	401	534	133	0.30，0.30	6.1	11.2

a) 1.0 x 10^{-4} mol/L in THF. b) Φ is the fluorescence quantum yield.

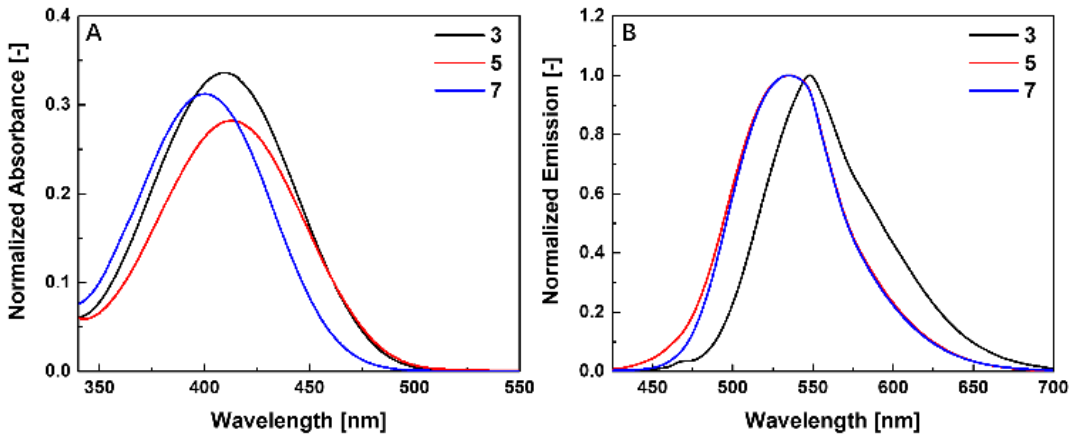

Figure 2.7. (A) UV spectra and (B) PL spectra of maleimides luminophores in THF (*conc.*: 1.0 x 10^{-4} mol/L).

We reasoned that the emission properties of the maleimide luminophores would be related to the polarity of the solvent. Therefore, their UV/vis absorption spectra and photoluminescence (PL) spectra were measured in solvents with different polarity to determine whether the maleimide luminophores show solvatochromism effects (Figure. 2.8-2.10). The absorption spectra of these luminophores exhibited little change with various

solvents of increasing polarity, such as toluene < THF < acetone < acetonitrile < DMF, indicating that the ground state of the luminophores is little influenced by the solvent polarity. However, an obvious red shift of the maximum emission wavelength of luminophores **5** and **7** was observed with increasing polarity of the solvents. Intramolecular charge transfer (ICT) was considered to be the main reason, and the presence of intramolecular charge transfer (ICT) was subsequently verified using density functional theory (DFT) quantum calculations.

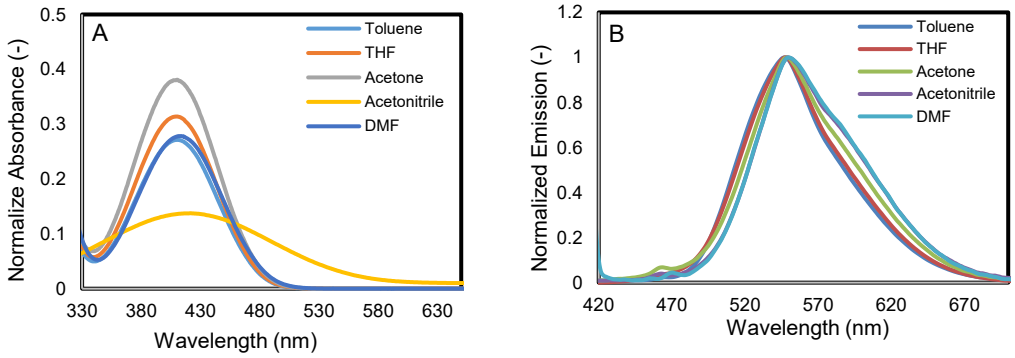

Figure 2.8. (A) UV spectra and (B) PL spectra of compound **3** in different solvents (*conc*.: 1.0 x 10^{-4} mol/L).

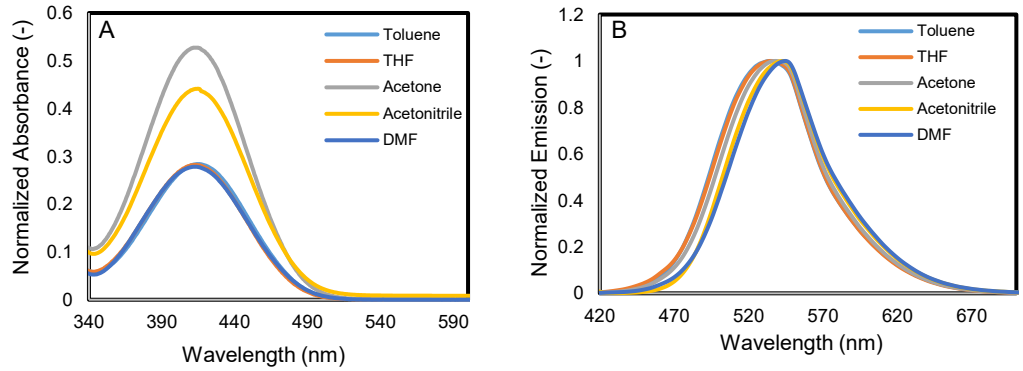

Figure 2.9. (A) UV spectra and (B) PL spectra of compound **5** in different solvents (*conc*.: 1.0 x 10^{-4} mol/L).

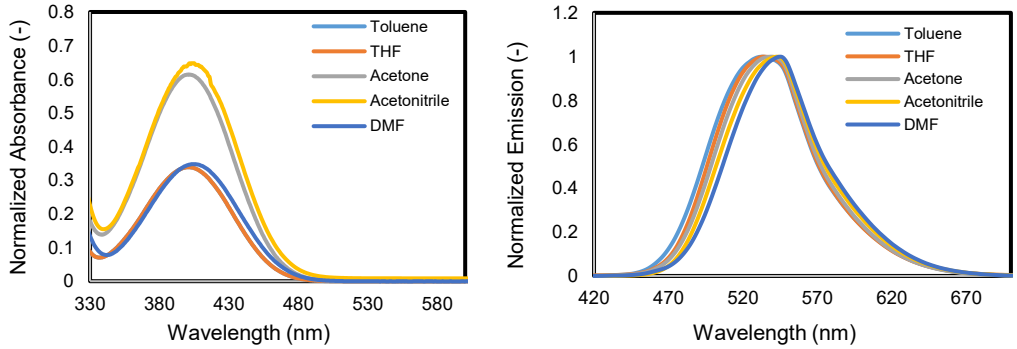

Figure 2.10. (A) UV spectra and (B) PL spectra of compound **7** in different solvents (*conc*.: 1.0 x 10^{-4} mol/L)

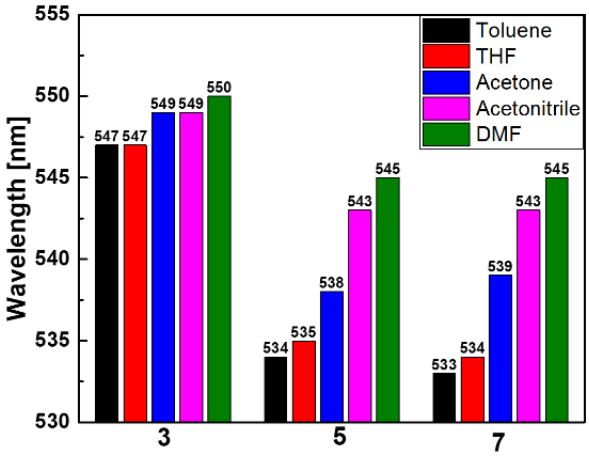

Figure 2.11. The change of maximum emission wavelength of maleimides luminophores in different solvents (*conc*.: 1.0 x 10^{-4} mol/L).

The changes in the maximum emission wavelength of the maleimide luminophores in different polarity solvents are shown in Figure 2.11. In toluene, the maximum emission wavelengths for luminophores **3**, **5** and **7** are 547 nm, 534 nm, and 533 nm, respectively, while in DMF, they are 550 nm, 545 nm, and 545 nm respectively, corresponding to red shifts of 3 nm, 11 nm, and 12 nm. The luminophores **5** and **7** have a larger red shift (11 nm, 12 nm) than the luminophore **3**, indicating that the piperidinyl and pyrrolidinyl give rise to an obvious change with varying solvent polarity. This is consistent with the mentioned results of the change of fluorescence intensity in mixed solvents (THF-water). Therefore, positive solvatochromic fluorescence was observed for all the maleimide luminophores. This is beneficial for extensive applications as good dyes in fibers. [29,30]

2.3.3 Aggregation-induced emission enhancement (AIEE)

In addition, the fluorescence quantum yields of luminophores **3** (Φ_F = 27.2%), 5 (Φ_F = 14.2%) and 7 (Φ_F = 11.2%) in the solid state are significantly higher than those in dilute THF solutions (Table 2.1), revealing aggregation-induced emission enhancement (AIEE) effects. This is because the molecular motion is restricted in the solid state, which can reduce the nonradiative decay and result in enhanced emission. [31,32] On the other hand, planar molecules may undergo stacking, resulting in relatively strong intermolecular interactions and leading to concentration quenching in the solid state. However, we observed non-planar conformations for luminophores **3**, **5** and **7** in the optimized molecular geometries obtained using density

functional theory (DFT) quantum calculations (Figure 2.13.). They inhibited aggregation caused quenching (ACQ) via the intermolecular π-π stacking interaction. Consequently, the emission of luminophores **3**, **5** and **7** can be observed in the solid state. In particular, the fluorescence quantum yield (Φ_F) of 3 in the solid state (Φ_F =27.2%) is more than 15 times as high as that in dilute THF (Φ_F = 1.8%). This indicates that the participation of the morpholinyl group is more conducive to aggregation-induced emission (AIEE) effects than the participation of piperidinyl and pyrrolidinyl.

To further confirm their AIEE characteristics, their fluorescence behaviors was examined in a water-THF mixture with different water ratios. As the maleimide luminophores are insoluble in water, increasing the water ratio in the mixed solvent can change their form from solvated to aggregated gradually.

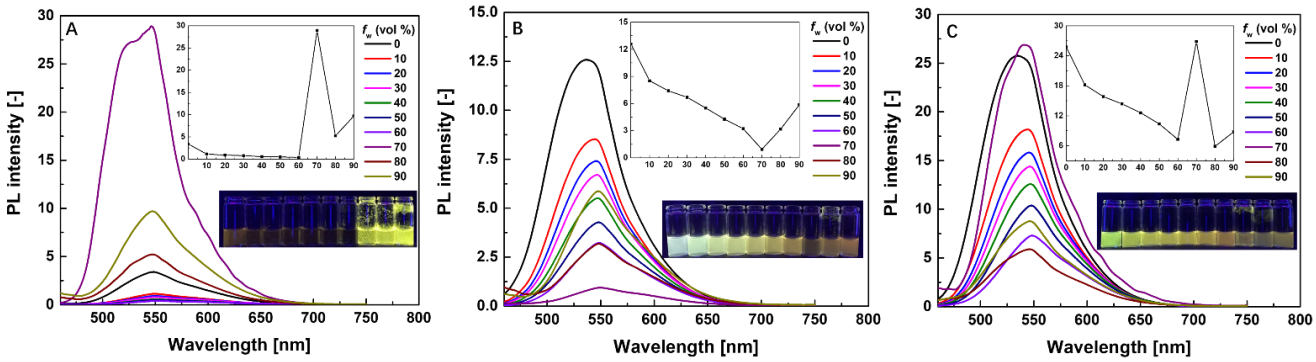

Figure 2.12. PL spectra and change of fluorescence intensity of (A) **3**, (B) **5** and (C) **7** in mixing ratio THF and water (conc.: 1.0 x 10^{-4} mol/L).

Figure 2.12 depicts the PL spectra and photographs of the maleimide luminophores. The maleimide luminophores **3** and **7** have similar fluorescence performance when the water ratio is changed in the mixed solvent (Figure. 2.12.A and C). However, when the water ratio is less than 60%, luminophore **3** shows little change, while the maximum emission wavelength of luminophore **7** shows a red-shift and its fluorescence intensity is decreased. As the luminophores contain donor and acceptor units in their molecular structures, we believe that intramolecular charge transfer (ICT) caused by them is the main reason for this change,[33-36] which we subsequently verified using density functional theory (DFT) quantum calculations. For both luminophores **3** and **7**, the fluorescence intensity reaches its highest value when the

water ratio increases to 70%, whereas it decreases when the water ratio is more than 70%. The main reason is that the aggregates are formed gradually, restricting the intramolecular motion and reducing nonradiative transition when the water ratio is greater than 60%, showing AIEE effects. However, in mixtures with higher water ratios (more than 70%), the dye molecules may quickly aggregate in a random way to form less-emissive amorphous particles, leading to a decrease in fluorescence intensity.[37] Moreover, for the same reason, luminophore **5** also has a similar change in fluorescence intensity when the water ratio is less than 60%, whereas the fluorescence intensity increases gradually when the water ratio is greater than 70% (Figure 2.12.B), showing obvious AIEE effects. This phenomenon is often observed for some compounds with AIE or AIEE properties. By comparing the maximum emission wavelength when water was added, we found that luminophores **5** and **7** show a color change and have a small red shift when water is added to the mixed solvent (Figure 2.12.B and C). They can be used as fluorescence probes, especially for the detection of the content of water in Refer.

2.3.4 Density functional theory (DFT) quantum calculations

To further comprehend the AIE effects and verify the intramolecular charge transfer (ICT), density functional theory (DFT) quantum calculations were performed at the B3LYP/6-31G (d, p) level of theory with the Gaussian 09W class of programs to obtain the optimized conformation of the molecules. The highest occupied molecular orbital (HOMO) plots, the lowest unoccupied molecular orbital (LUMO) plots and optimized conformations of luminophores **3**, **5** and **7** are illustrated in Figure 2.13. As shown in Figure 2.13, all the luminophores have non-planar conformations, which can hinder the strong intermolecular π-π stacking interaction and allow them to be emissive in the aggregated state and to show AIE effects. On the other hand, in the structure of the luminophores, the biphenyl and amino groups are connected to the maleimide ring by a rotatable C-C single bond and C-N bond, respectively, which can rotate freely in the single-molecule state and but are inhibited in the aggregated state. This restriction of intramolecular rotation (RIR) in the aggregated state can also lead to the emission in the aggregated state and AIE effects. Furthermore, we confirmed the positions of the HOMO and LUMO of all the luminophores from the theoretical calculation results, and we found that they showed similar results (Figure 2.13). As an example, the electron density of the LUMO of luminophore **7** is mainly located on the maleimide group, while that of the HOMO is distributed on the maleimide group and the biphenyl and pyrrolidinyl, which are connected to the maleimide (Figure 2.13.C). This indicates that luminophore **7** has a donor and acceptor, enabling the molecule to exhibit an ICT process in the excited state.[38,39]

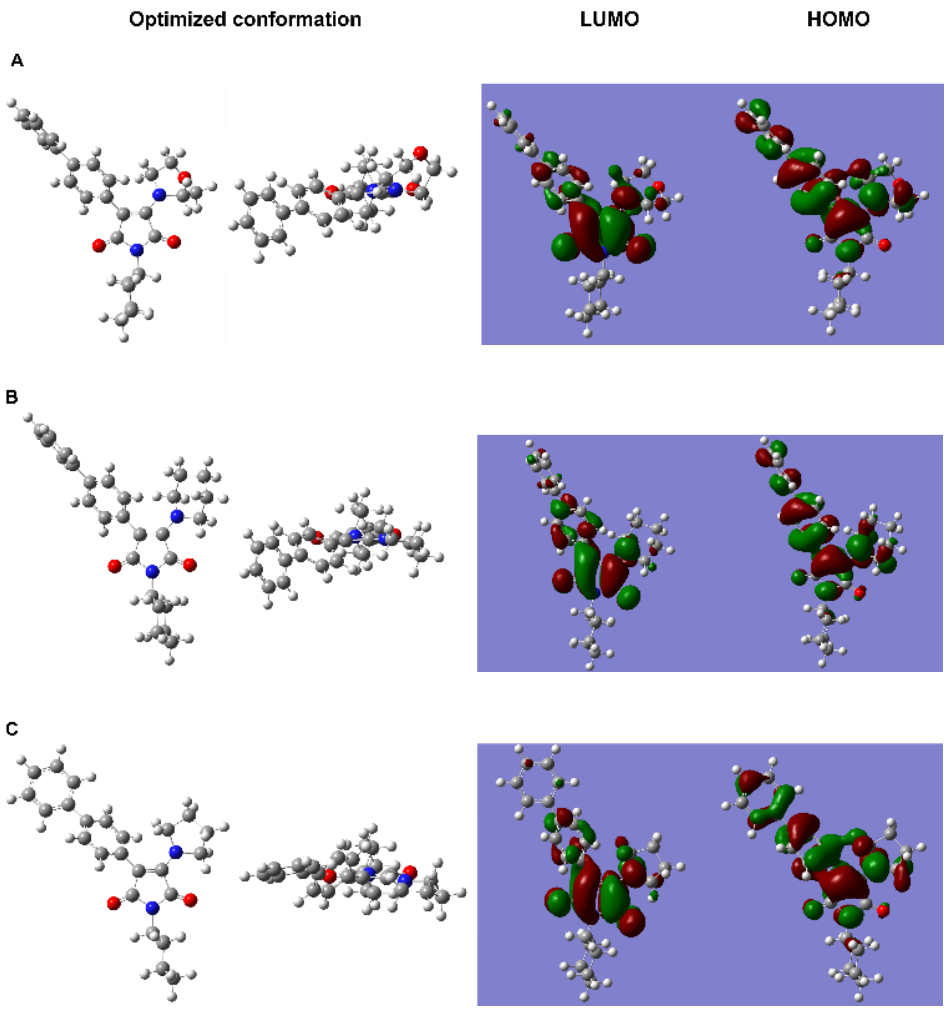

Figure 2.13 Optimized conformation of (A) **3**, (B) **5** and (C) **7** from different orientation and calculated spatial distributions of HOMO and LUMO at the B3LYP/6-31G(d) level in Gaussian 09.

2.4 Conclusions

A series of AIEE conjugated maleimide molecules with simple structures containing different amino groups were synthesized and characterized. Because the intramolecular rotation is restricted in the solid state, which reduces the nonradiative decay, these molecules show AIEE characteristics. Additionally, their non-planar conformations are also helpful to inhibit intermolecular π-π stacking and enhance the emission. These AIEE molecules can

solve the ACQ problems of general molecules in the solid state, and unlike common AIE molecules, they can also show emission in both solution and the solid state. In addition, the molecules respond to differences in the polarity of various solvents and show positive solvatochromism. Therefore, as new AIEE molecules, conjugated amino-maleimides can enrich the types of AIEE molecules, and they are expected to provide a new strategy for the development of the AIE field.

2.5 References

1 B. K. Kaletas -, R. M. Williams, B. Konig and L. D. Cola, *Chem. Commun*., 2002, 776-777.

2 T. Kato and K. Naka, *Chem. Lett*., 2012, **41**, 1445-1447.

3 Z. Mahmood and J. Zhao, *J. Org. Chem*., 2016, **81**, 587-594.

4 Y. Qin, G. Li, T. Qi and H. Huang, *Mater. Chem. Front*., 2020, **4**, 1554-1568.

5 5 J. Luo, Z. Xie, J. W. Y. Lam, L. Cheng, H. Chen, C. Qiu, H. S. Kwok, X. Zhan, Y. Liu, D. Zhu and B. Z. Tang, *Chem. Commun*., 2001, 1740-1741.

6 N. L. C. Leung, N. Xie, W. Yuan, Y. Liu, Q. Wu, Q. Peng, Q. Miao, J. W. Y. Lam and B. Z. Tang, *Chem. - Eur. J*., 2014, **20**, 15349-15353.

7 Y. Liu, Y. Tang, N. N. Barashkov, I. S. Irgibaeva, J. W. Y. Lam, R. Hu, D. Birimzhanova, Y. Yu and B. Z. Tang, *J. Am. Chem. Soc*., 2010, **132**, 13951-13953.

8 J. Liu, Y. Zhong, P. Lu, Y. Hong, J. W. Y. Lam, M. Faisal, Y. Yu, K. S. Wong and B. Z. Tang, *Polym. Chem*., 2010, **1**, 426-429.

9 Y. Liu, C. Deng, L. Tang, A. Qin, R. Hu, J. Z. Sun and B. Z. Tang, J. *Am. Chem. Soc*., 2011, **133**, 660-663.

10 Y. Yu, C. Feng, Y. Hong, J. Liu, S. Chen, K. M. Ng, K. Q. Luo and B. Z. Tang, *Adv. Mater*., 2011, **23**, 3298-3302.

11 Y. Hong, C. Feng, Y. Yu, J. Liu, J. W. Y. Lam, K. Q. Luo and B. Z. Tang, *Anal. Chem*., 2010, **82**, 7035-7043

12 12 Y. Liu, Y. Yu, J. W. Y. Lam, Y. Hong, M. Faisal, W. Z. Yuan and B. Z. Tang, *Chem. - Eur. J*., 2010, **16**, 8433-8438.

13 K. Onimura, M. Matsushima, M. Nakamura, T. Tominaga, K. Yamabuki and T. Oishi, *J. Polym. Sci., Part A: Polym. Chem*., 2011, **49**, 3550-3558.

14 J. Mei, N. L. C. Leung, R. T. K. Kwok, J. W. Y. Lam and B. Z. Tang, Chem. Rev., 2015, **115**, 11718-11940.

15 N. Venkatramaiah, G. D. Kumar, Y. Chandrasekaran, R. Ganduri and S. Patil, *ACS Appl. Mater. Interfaces*., 2018, **10**, 3838-3847.

16 G. M. Farinola and R. Ragni, *Chem. Soc. Rev*., 2011, **40**, 3467–3482.

17 Y. Yang, Q. Zhao, W. Feng and F. Li, *Chem. Rev.*, 2013, **113**, 192–270.

18 Z. Guo, S. Park, J. Yoon and I. Shin, *Chem. Soc. Rev*., 2014, **43**, 16-29.

19 Y. Qin, G. Li, T. Qi and H. Huang, *Mater. Chem. Front*., 2020, **4**, 1554.

20 R. Wang, T. Hu, Y. Liu, X. Wei, J. Liu, Z. Li, X. Hu, H. Gao, G. Liu, Y. Y. Takamura, C. S. Lee, P. Wang, Y. Yi and Y. Wang, *J. Phys. Chem. C*, 2020, **124**, 20816-20826.

21 S. V. Kunz, C. M. Cole, A. Welle, P. E. Shaw, P. Sonar, N. P. Thoebes, T. Baumann, S. D. Yambem, E. Blasco, J. P. Blinco and C. B. Kowollik, *Macromolecules*, 2019, **52**, 9105-9113.

22 Y. Hu, Y. Zhang, W. Han, J. Li, X. Pu, D. Wu, Z. Bin and J. You, *Chem. Eng. J*., 2021, **428**, 131186.

23 X. Wang, L. Zhang, Q. Li and Y. Gao, *Dyes Pigm*., 2020, **181**, 108614.

24 Y. Yu, X. Li, Y. Yuan and H. Zhang, *Polymer*, 2021, **217**, 123477.

25 Z. E. Chen, Q. L. Qi and H. Zhang, Spectrochim. *Acta, Part A*, 2020, **238**, 118384.

26 L. D. Lavis and R. T. Raines, *ACS Chem. Biol*., 2014, **9**, 855–866.

27 Z. Gao, Y. Hao, M. Zheng and Y. Chen, *RSC Adv*., 2017, **7**, 7604-7609.

28 D. Li, Q. Wang, N. Rao, Y. Zhang, Y. Lea, L. Liua, L. Li, L. Huang and L. Yana, *J. Mol. Struct*., 2021, **1239**, 130521.

29 A. Jabbar, Ambreen, S. Riaz, F. A. Navaid and M. I. Choudhary, *J. Mol. Struct*., 2019, **1195**, 161-167.

30 S. Riaz, Ambreen, F. A. Navaid, M. I. Choudhary and A. Jabbar, *J. Mol. Liq*., 2019, **287**, 110917.

31 Y. Hong, J. W. Y. Lam and B. Z. Tang, *Chem. Soc. Rev*., 2011, **40**, 5361-5388.

32 Y. Hong, J. W. Y. Lam and B. Z. Tang, *Chem. Commun*., 2009, 4332-4353.

33 H. M. Fahmy, H. M. Kandel, H. A. S. Al-shamiri, N. A. Negm, A. H. M. Elwahy and M. T. H. A. Kana, *J. Fluoresc*., 2018, **28**, 1421-1430.

34 M. Nakamura, K. Yamabuki, T. Oishi and K. Onimura, *J. Polym. Sci., Part A: Polym. Chem*., 2013, **51**, 4945-4956.

35 J. Li, C. Hou, C. Huang, S. Xu, X. Peng, Q. Qi, W. Y. Lai and W. Huang, *Research*, 2020, 3839160.

36 W. Rettig, Angew. *Chem., Int. Ed. Engl*., 1986, **25**, 971-988.

37 X. Luo, J. Li, C. Li, L. Heng, Y. Q. Dong, Z. Liu, Z. Bo and B. Z. Tang, *Adv. Mater*., 2011, **23**, 3261-3265.

38 J. Li, C. Yang, X. Peng, Y. Chen, Q. Qi, X. Luo, W.-Y. Lai and W. Huang, *J. Mater. Chem. C*, 2018, **6**, 19-28.

39 X. Liu, M. Sang, H. Lin, C. Liu, J. Zhang, J. Yi, K. Gao, W.-Y. Lai and W. Huang, *Chem. - Eur. J.*, 2020, **26**, 3103-3112.

Chapter 3

Synthesis and photophysical properties of a series of maleimide molecules with aggregation-induced emission enhancement (AIEE) effects

3.1 Introduction

Based on chapter 2, a series of amino-aryl-maleimides was synthesized, in which varying the amounts of acceptors to confirm the influence of the acceptor amounts about optical properties. In addition, we also varying the amino group and the molecule structures to obtain more information. Though introducing biphenyl group to the molecules that containing piperazine, we compared the difference of the photophysical properties of two molecules with whether it is contained biphenyl. We through examined the fluorescence behavior of all molecules in a water-THF mixture to confirm the emission in aggregates. The obtained luminophores all show fluorescence emission both in solution and solid state, show AIEE effects. Furthermore, we also examined their solvatochromism effects in different polarity solvents. In comparison with the molecules in chapter 2, they have smaller red shift in different polarity solvents.

3.2 Experimental

3.2.1 Materials

All commercially chemicals in this study were used without any further purification. Magnesium sulfate (anhydrous) and zinc chloride were purchased from Kishida Reagents Chemicals. Citraconic anhydride, palladium (II) acetate and the silica gel 60N (63-213 mm) which used as column chromatography were purchased from Wako Pure Chemical Industries. Moreover, the silica gel plate $60F_{254}$ for analytical thin-layer chromatography were purchased from Merck. Bromine, Piperazine, 1,1,1,3,3,3-hexamethydisilazane (HMDS), 4-biphenyl-boronic acid and 4,4'-biphenyl-diboronic acid were purchased from Tokyo Chemical Industry (TCI). Triphenylphosphine was purchased from Kanto Chemical. Commercially available products (1st grade) were used as all solvents.

3.2.2 Structural analysis and measurements

The ^{1}H (500 MHz) and ^{13}C (125 MHz) nuclear magnetic resonance (NMR) spectra were recorded on a JNM-LA500 spectrometer, using $CDCl_3$ as solvents and tetramethylsilane (TMS) as an internal standard ($\delta = 0.00$). The melting points were recorded on Buchi M-560. The abbreviations for the NMR spectroscopy data are as follows: s, singlet; m, multiplet. The ultraviolet-visible (UV-vis) spectra were recorded on UV-1650PC (Shimadzu Corporation) spectrometer, and the photoluminescence (PL) spectra were recorded on FP-6300 (JASCO Corporation) spectrophotometer at room temperature.

3.2.3 Synthesis

3.2.3.A Synthesis of 4,4'-bis (2-morpholino-*N*-cyclohexylmaleimide-3-yl)-1,1'-biphenyl by Suzuki-Miyaura Coupling Reaction (compound **1**)

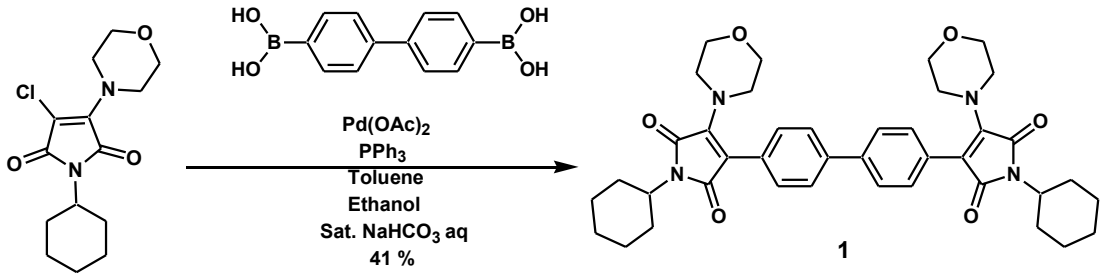

Scheme 3.1

A mixture of 2-chloro-3-morpholino-*N*-cyclohexylmaleimide (0.31 g, 1.00 mmol) and 4,4'-biphenyl-diboronic acid (0.130 g, 0.500 mmol) was added to a flask. Then, toluene (6 mL), ethanol (3 mL) and sat. $NaHCO_3$ aqueous solution (6 mL) were added successively, and the mixture was stirred at room temperature for 20 min. $Pd(OAc)_2$ (0.0450 g, 0.200 mmol) and PPh_3 (0.0160 g, 0.600 mmol) were added to the flask. The mixture was heated under reflux for 24 hrs under a nitrogen atmosphere. After that, the reaction mixture was diluted with additional ethyl acetate and then washed using distilled water. The combined organic layer was dried over $MgSO_4$, and the filtrate was concentrated in vacuo. The residue was purified on a silica gel column using dichloromethane / *n*-hexane (25/1: v/v) to obtain an orange-yellow powder (0.14 g, 0.21 mmol, 41 %).

^{1}H-NMR ($CDCl_3$) δ (ppm from TMS): 7.62-7.63 (4H, d, *J*=1.75, -BPh), 7.37-7.39 (4H, d, *J*=8.6, -BPh), 3.93-3.99 (2H, m, -N-CH-), 3.71-3.73 (8H, m, morpholine unit), 3.55-3.57 (8H, m, morpholine unit), 2.07-2.14 (4H, m, $-CH_2-$), 1.83-1.85 (4H, m, $-CH_2-$), 1.66-1.72 (6H, m, $-CH_2-$), 1.20-1.35 (6H, m, $-CH_2-$).

3.2.3.B Synthesis of 4,4'-bis (2-piperidino-*N*-cyclohexylmaleimide-3-yl)-1,1'-biphenyl by Suzuki-Miyaura Coupling Reaction (compound **2**).

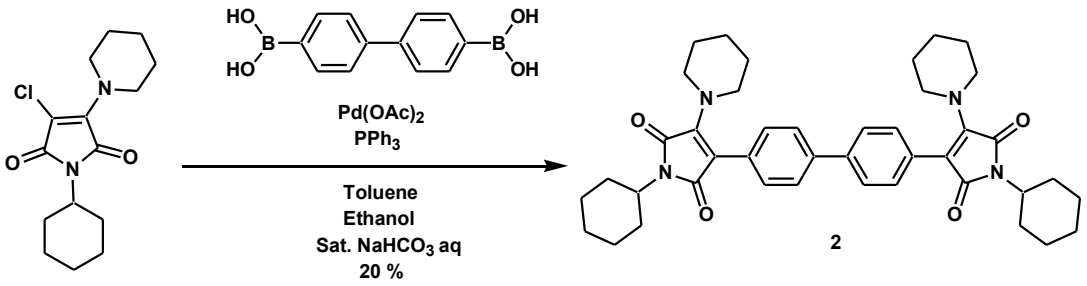

Scheme 3.2

A mixture of 2-chloro-3-piperidino-*N*-cyclohexylmaleimide (0.21 g, 0.67 mmol) and 4,4'-biphenyl-diboronic acid (0.120 g, 0.470 mmol) was added to a flask. Then, toluene (6 mL), ethanol (3 mL) and sat. $NaHCO_3$ aqueous solution (6 mL) were added successively, and the mixture was stirred at room temperature for 20 min. $Pd(OAc)_2$ (0.0210 g, 0.094 mmol) and PPh_3 (0.0740 g, 0.280 mmol) were added to the flask. The mixture was heated under reflux for 24 hrs under a nitrogen atmosphere. After that, the reaction mixture was diluted with additional ethyl acetate and then washed using distilled water. The combined organic layer was dried over $MgSO_4$, and the filtrate was concentrated in vacuo. The residue was purified on a silica gel column using *n*-hexane / EtOAc (9/1: v/v) to obtain an orange-yellow powder (0.062 g, 0.092 mmol, 20 %).

^{1}H-NMR ($CDCl_3$) δ (ppm from TMS): 7.60-7.62 (4H, d, *J*=8, -BPh), 7.36-7.38 (4H, d, *J*=8, -BPh), 3.94-3.99 (2H, m, -N-CH-), 3.46 (8H, s, -N-CH_2-), 2.09-2.18 (6H, m, -CH_2-), 1.82-1.85 (6H, m,-CH_2-), 1.58-1.72 (14H, m, -CH_2-), 1.20-1.32 (6H, m, -CH_2-).

3.2.3.C Synthesis of 4,4'-bis (2-pyrrolidino-*N*-cyclohexylmaleimide-3-yl)-1,1'-biphenyl by Suzuki-Miyaura Coupling Reaction (compound **3**)

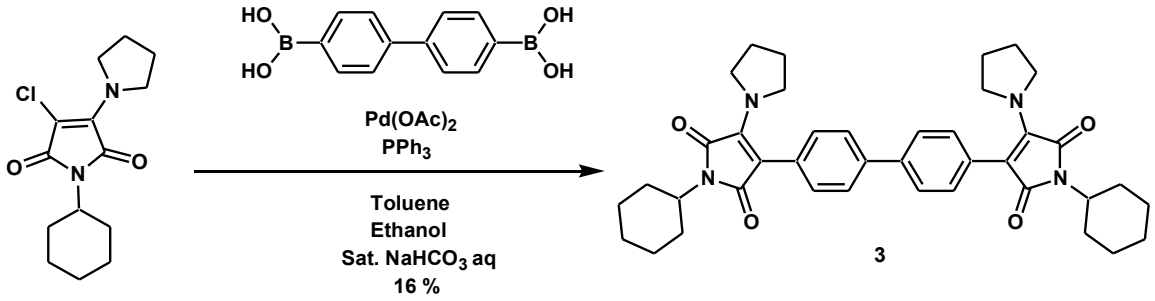

Scheme 3.3

A mixture of 2-chloro-3-pyrrolidino-*N*-cyclohexylmaleimide (0.210 g, 0.710 mmol) and 4,4'-biphenyl-diboronic acid (0.120 g, 0.500 mmol) was added to a flask. Then, THF (6 mL) and sat. K_2CO_3 aqueous solution (3 mL) were added successively, and the mixture was stirred at room temperature for 20 min. $Pd(OAc)_2$ (0.024 g, 0.099 mmol) and PPh_3 (0.078 g, 0.300 mmol) were added to the flask, and the mixture was heated under reflux for 24 hrs under a nitrogen atmosphere. After that, the reaction mixture was diluted with additional ethyl acetate and then washed using distilled water. The combined organic layer was dried over $MgSO_4$, and the filtrate was concentrated in vacuo. The residue was purified on a silica gel column using dichloromethane / *n*-hexane (1/35: v/v) to obtain orange-yellow powder (0.05 g, 0.076 mmol, 16 %).

^{1}H-NMR ($CDCl_3$) δ (ppm from TMS): 7.57-7.70 (4H, m, -BPh), 7.26-7.32 (4H, m, -BPh), 3.96-4.01 (2H, m, -N-CH-), 3.53 (8H, s, -N-CH_2-), 2.05-2.13 (6H, m, -CH_2-), 1.84-1.87 (10H, m,-CH_2-), 1.69-1.72 (6H, m, -CH_2-), 1.23-1.34 (6H, m, -CH_2-).

3.2.3.D Synthesis of 4,4'-bis (2-chloro-*N*-cyclohexylmaleimide-3-yl)-1,1'-piperazino by Suzuki-Miyaura Coupling Reaction (compound **4**)

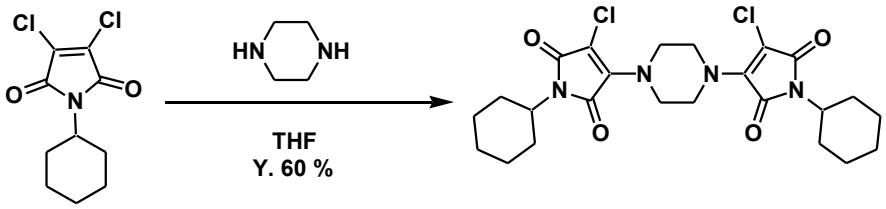

Scheme 3.4

2,3-dichloro-*N*-cyclohexylmaleimide (1.20 g, 4.84 mmol) was dissolved in THF (30 mL) in a flask, and piperazine (0.25 g, 2.90 mmol) was added to the flask. Then the mixture was heated under reflux for 40 hrs under a nitrogen atmosphere at 60 ℃. After that, the reaction mixture was diluted with additional ethyl acetate and then washed using distilled water. The combined organic layer was dried over $MgSO_4$, and the filtrate was concentrated in vacuo. The residue was purified on a silica gel column using dichloromethane / *n*-hexane (4/1: v/v) to obtain yellow powder (0.83 g, 0.74 mmol, 60 %).

^{1}H-NMR ($CDCl_3$) δ (ppm from TMS): 4.02 (8H, s, -N-CH_2-), 3.88-3.94 (2H, m, -N-CH-), 1.98-2.05 (4H, m, -CH_2-), 1.81-1.84 (4H, m,-CH_2-), 1.62-1.67 (6H, m, -CH_2-), 1.18-1.35 (6H, m, -CH_2-).

3.2.3.E Synthesis of 4,4'-bis (2-biphenyl-*N*-cyclohexylmaleimide-3-yl)-1,1'-piperazino by Suzuki-Miyaura Coupling Reaction (compound **5**).

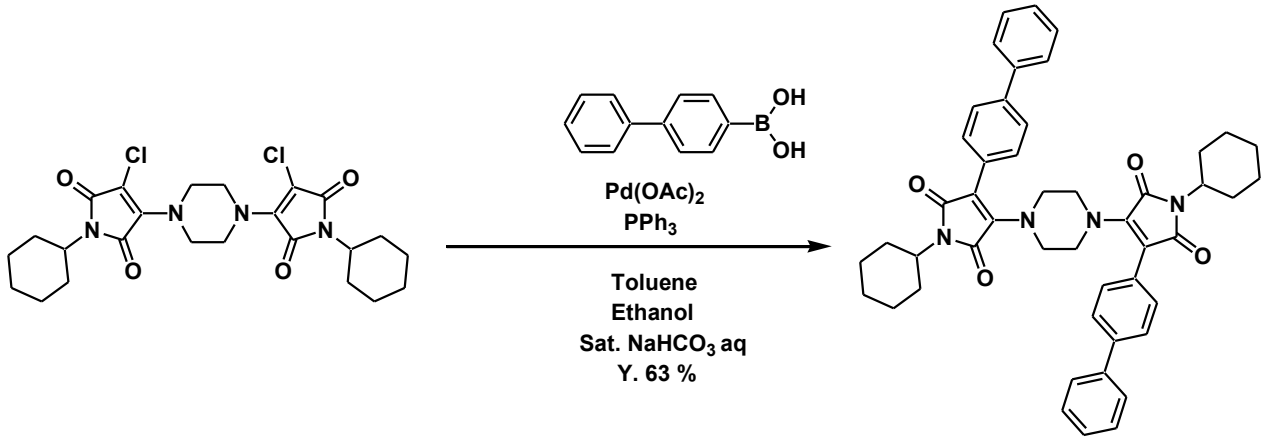

Scheme 3.5

A mixture of 4,4'-bis (2-chloro-*N*-cyclohexylmaleimide-3-yl)-1,1'-piperazino (0.30 g, 0.59 mmol) and 4-biphenyl-boronic acid (0.26 g, 1.30 mmol) was added to a flask. Then, toluene (8 mL), ethanol (4 mL) and sat. $NaHCO_3$ aqueous solution (8 mL) were added successively, and the mixture was stirred at room temperature for 20 min. $Pd(OAc)_2$ (0.026 g, 0.118 mmol) and PPh_3 (0.093 g, 0.353 mmol) were added to the flask. The mixture was heated under reflux for 24 hrs under a nitrogen atmosphere at 130 ℃. After that, the reaction mixture was diluted with additional ethyl acetate and then washed using distilled water. The combined organic layer was dried over $MgSO_4$, and the filtrate was concentrated in vacuo. The residue was purified on a silica gel column using dichloromethane / *n*-hexane (2/1: v/v) to obtain an orange-yellow powder (0.28 g, 0.37 mmol, 63 %).

^{1}H-NMR ($CDCl_3$) δ (ppm from TMS): 7.56-7.59 (8H, m, -BPh), 7.41-7.44 (4H, m, -BPh), 6.91-7.36 (6H, m, -BPh), 3.95-4.13 (2H, m, -N-CH-), 3.57 (8H, s, -N-CH_2-), 2.05-2.09 (4H, m, -CH_2-), 1.82-1.84 (4H, m,-CH_2-), 1.68-1.71 (6H, m, -CH_2-), 1.27-1.34 (6H, m, -CH_2-).

3.2.4 Structure characterization

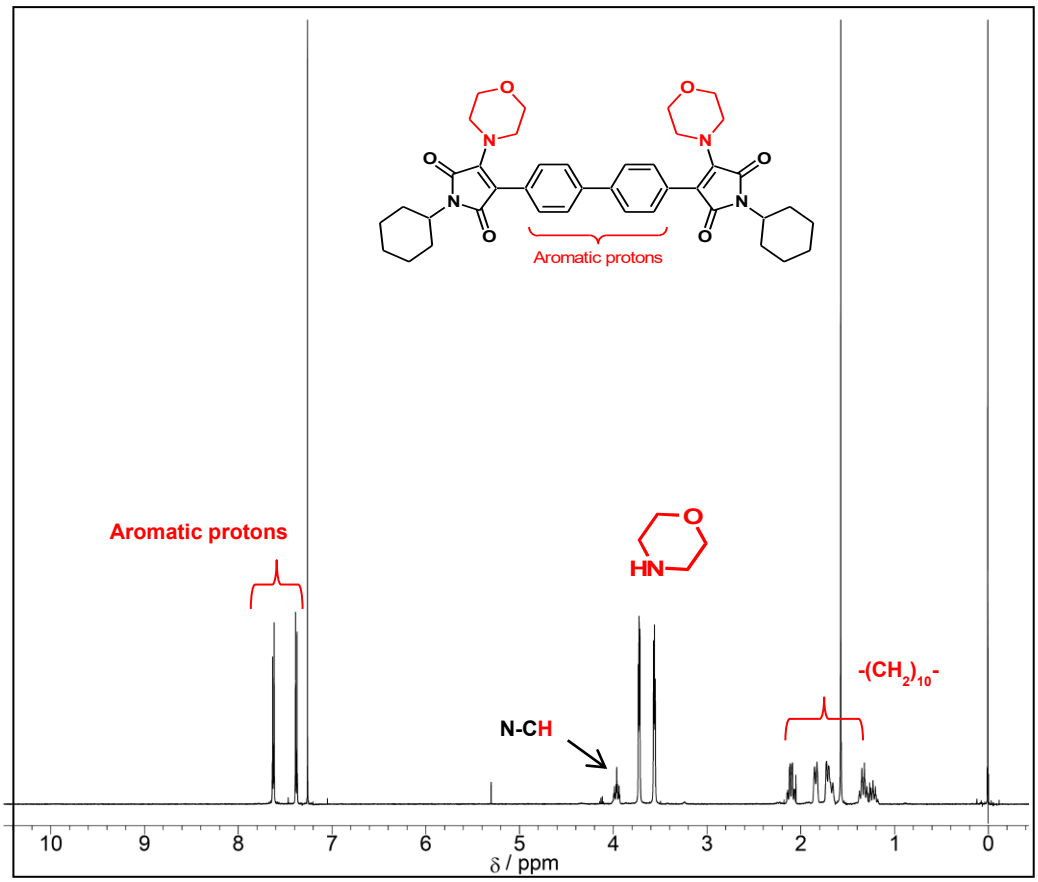

Figure 3.1. ^{1}H NMR Spectra of compound **1** in $CDCl_3$.

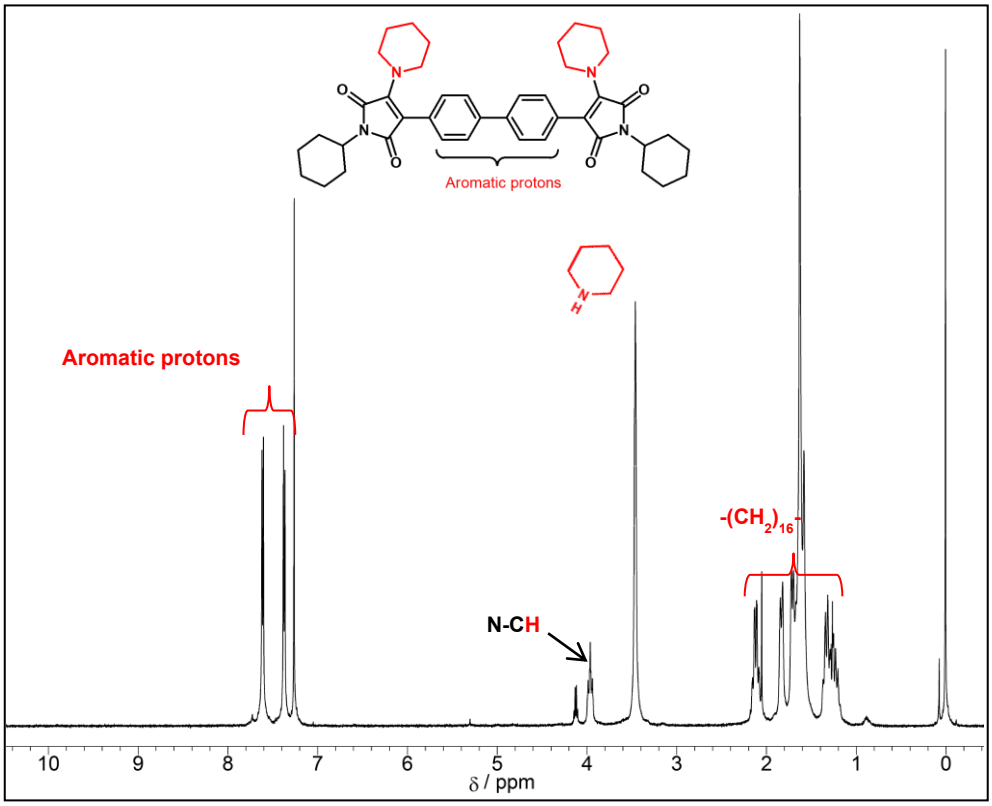

Figure 3.2. ^{1}H NMR Spectra of compound **2** in $CDCl_3$.

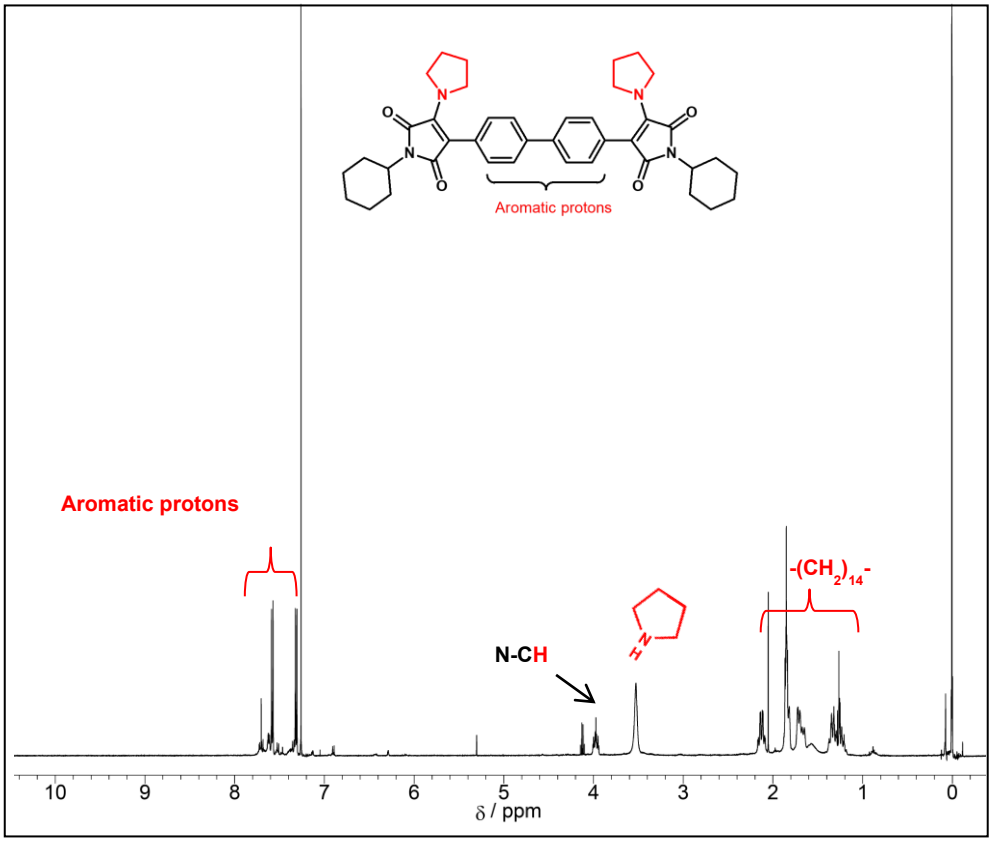

Figure 3.3. ^{1}H NMR Spectra of compound **3** in $CDCl_3$.

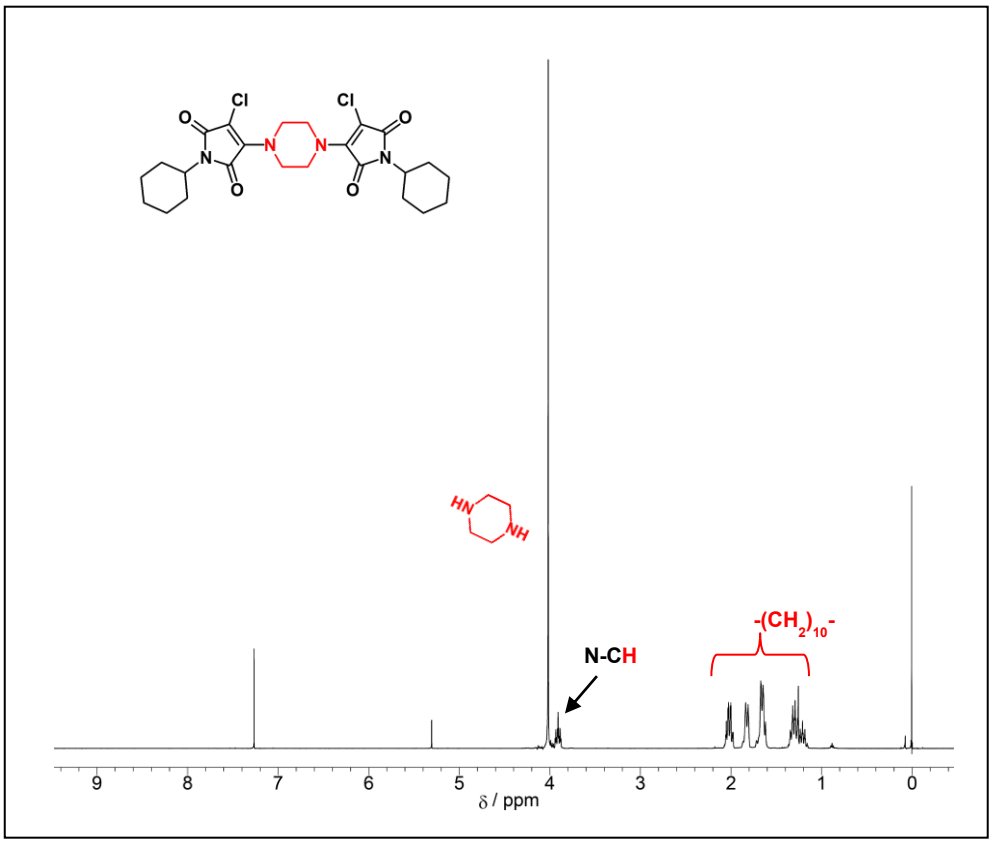

Figure 3.4. ^{1}H NMR Spectra of compound **4** in $CDCl_3$.

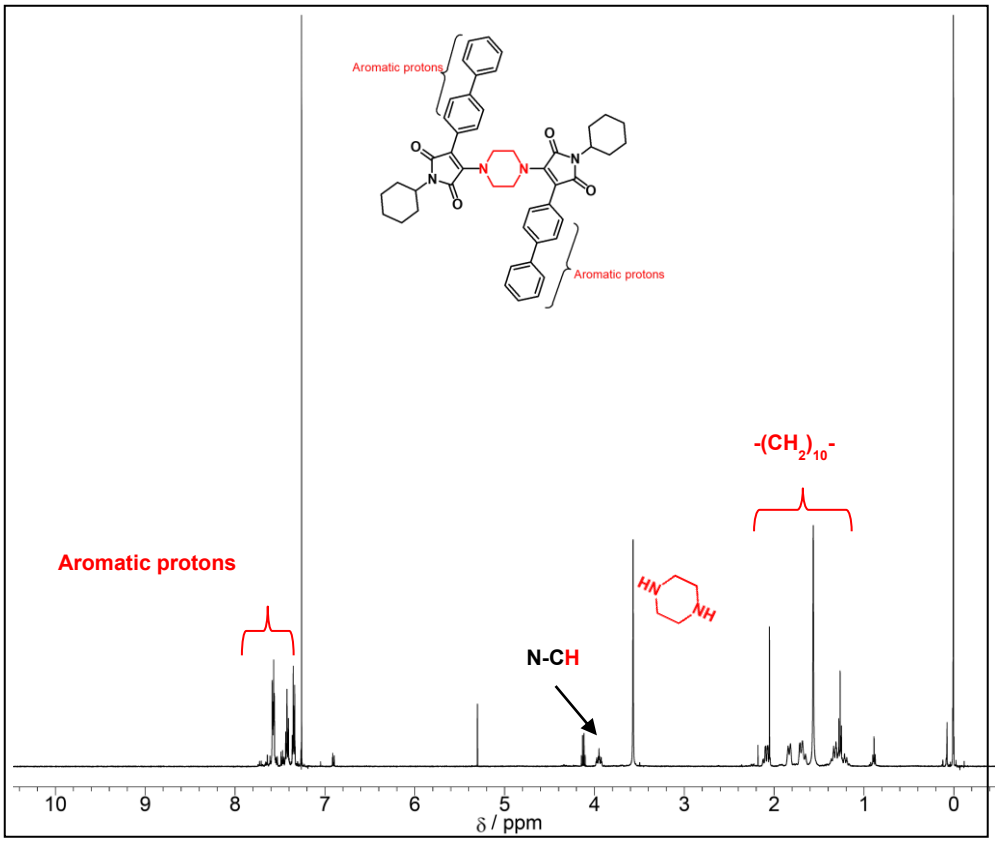

Figure 3.5. ^{1}H NMR Spectra of compound **5** in $CDCl_3$.

3.3 Results and discussion

3.3.1 Syntheses

As shown in Scheme 3.1-3.5, 4,4'-bis (2-amino-*N*-cyclohexylmaleimide-3-yl)-1,1'-biphenyl **1**, **2** and **3** containing different amino groups (morpholinyl, piperidinyl, pyrrolidinyl) were synthesized by reaction with 4,4'-biphenyl-diboronic acid through the Suzuki-Miyaura coupling reaction, respectively. And 4,4'-bis (2-chloro-*N*-cyclohexylmaleimide-3-yl)-1,1'-piperazino (compound **4**) and 4,4'-bis (2-biphenyl-*N*-cyclohexylmaleimide-3-yl)-1,1'-piperazino (compound **5**) were synthesized. Their structures were confirmed by NMR (^{1}H). The spectra characterization is described in Figure 3.1-Figure 3.5. The maleimide fluorophores are air-stable solids that are soluble in common organic solvents but insoluble in water. The yields of amino-biphenyl-*N*-cyclohexyl maleimides **1**, **2** and **3** are 41 %, 20 % and 16 % as an orange-yellow powder, respectively. And the yields of compounds **4** and **5** are 60 % and 63 %.

3.3.2 UV/Vis absorption spectra and photoluminescence (PL) spectra

The maleimide luminophores **1**, **2**, **3, 4** and **5** were investigated through UV/vis absorption spectra, photoluminescence (PL) spectra, and the fluorescence quantum yields (Φ_F) in dilute THF solutions (Figure 3.6). The results of the optical measurements are summarized in Table 3.1. Similar absorption peaks can be observed for amino maleimide luminophores **1**, **2** and **3** (Figure 3. 6. A). The absorption maximum wavelengths by of luminophore **1** (λ_{max} = 416 nm) and **2** (λ_{max} = 420 nm) were red-shifted relative to that of **3** (λ_{max} = 404 nm). It is indicated that the red-shift of absorption was due to the difference in the electron-donating ability of the amino groups. Luminophore **5** (λ_{max} = 419 nm) was red-shifted relative to that of **4** (λ_{max} = 402 nm). This is owing to the induction of the biphenyl. In addition, the luminophores, with CIE coordinates of (0.40, 0.58) for **1**, (0.40, 0.57) for **2** and (0.39, 0.58) for **3**, show yellow emission in dilute THF (Table 3.1). The luminophores, with CIE coordinates of (0.18, 0.45) for **4**, and (0.37, 0.60) for **5**, show blue emission (**4**) and yellow emission (**5**) in dilute THF (Table 3.1). Figure 3.6.B shows that the maximum emission wavelength of luminophore **1**, **2**, **3, 4** and **5** are 548 nm, 549 nm, and 548 nm, 498 nm and 547 nm, respectively.

We found that there is little impact in excited state for the luminophores with the change of amino groups. This is different from the compounds that synthesized in chapter 2, indicating the amount of acceptor maybe have some influence in optical properties. In addition, we found that all the luminophores have a good spectral separation of absorption and emission with large Stokes shifts (＞100 nm) (Table 3.1). Overall, in comparison with the other luminophores, luminophore **3** (with pyrrolidinyl) possessed the largest Stokes shift. Correspondingly, compared to morpholinyl and piperidinyl, pyrrolidinyl is more helpful to the expansion of the Stokes shift of the compound. Large Stokes shifts (＞100 nm) (Table 3.1) can prevent interference from the excitation light and scattered light, as well as the influence caused by reabsorption.[1-3] This is important for potential applications in biological fields.[1-6]

Table 3.1. Optical properties of all luminophores.

Compound	λ_{abs} [a)] (nm)	λ_{em} [a] (nm)	Δs (nm)	CIE (x, y) [a)]
1	416	548	132	0.40，0.58
2	420	549	129	0.40，0.57
3	404	548	144	0.39，0.58
4	402	498	96	0.18，0.45
5	419	547	128	0.37，0.60

a) 1.0 x 10^{-4} mol/L in THF.

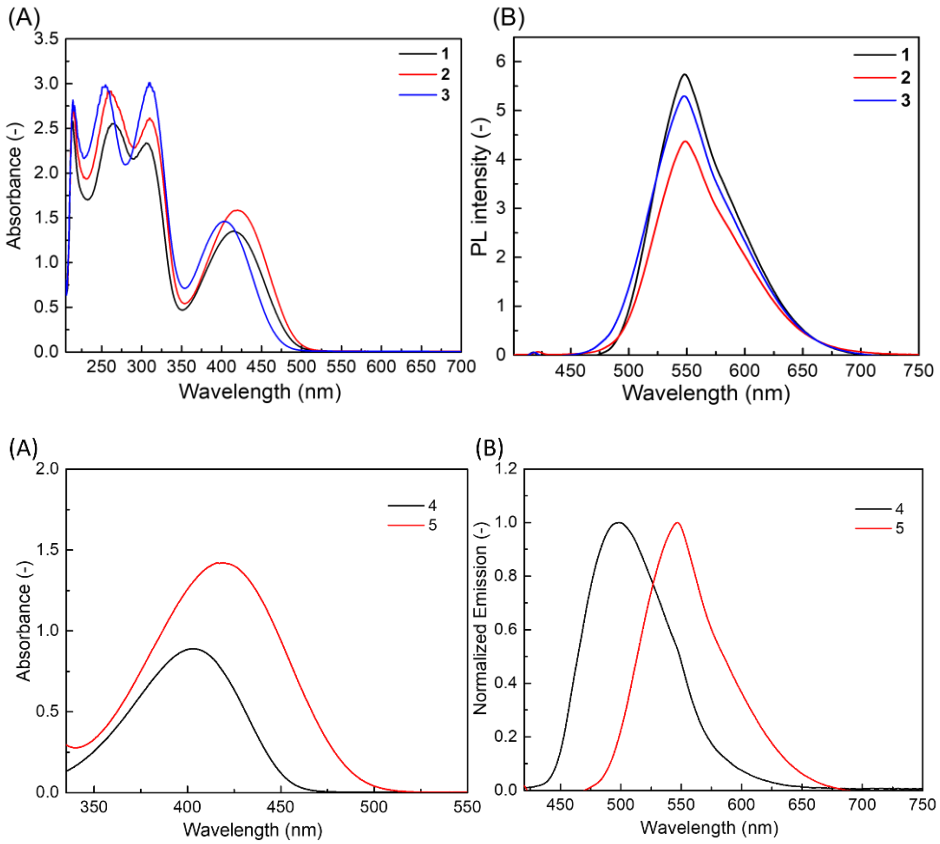

Figure 3.6. (A) UV spectra and (B) PL spectra of maleimides luminophores in THF (*conc.*: 1.0 x 10^{-4} mol/L).

We reasoned that the emission properties of the maleimide luminophores would be related to the polarity of the solvent. Therefore, their UV/vis absorption spectra and

photoluminescence (PL) spectra were measured in solvents with different polarity to determine whether the maleimide luminophores show solvatochromism effects. The changes in the maximum absorption wavelength and maximum emission of the maleimide luminophores in different polarity solvents are shown in Figure 3.7. The absorption spectra and PL spectra of these luminophores exhibited a small change with various solvents of increasing polarity, such as toluene < THF < acetone < acetonitrile < DMF, indicating that these luminophores is little influenced by the solvent polarity. This is different from the molecules that possess one acceptor (synthesized in chapter 2).

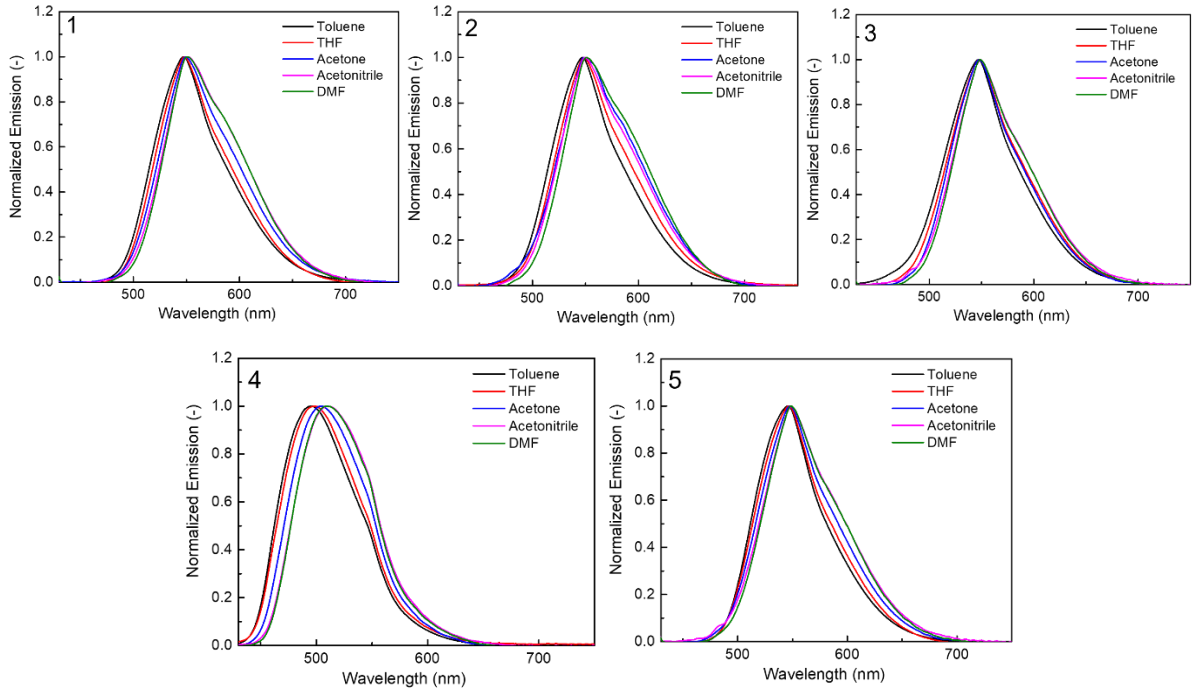

Figure 3.7. The change of maximum emission wavelength of maleimides luminophores in different solvents (*conc.*: 1.0 x 10^{-4} mol/L).

3.3.3 Aggregation-induced emission enhancement (AIEE)

In addition, as shown in Figure 3.8, we observed the yellow emission both in solution and solid, revealing aggregation-induced emission enhancement (AIEE) effects. This is because the molecular motion is restricted in the solid state, which can reduce the nonradiative decay and result in enhanced emission.[7-8] On the other hand, planar molecules may undergo

stacking, resulting in relatively strong intermolecular interactions and leading to concentration quenching in the solid state. They inhibited aggregation caused quenching (ACQ) via the intermolecular π-π stacking interaction. Consequently, the emission of luminophores **1**, **2**, **3**, **4** and **5** can be observed in the solid state.

To further confirm their AIEE characteristics, their fluorescence behaviors was examined in a water-THF mixture with different water ratios. As the maleimide luminophores are insoluble in water, increasing the water ratio in the mixed solvent can change their form from solvated to aggregated gradually.

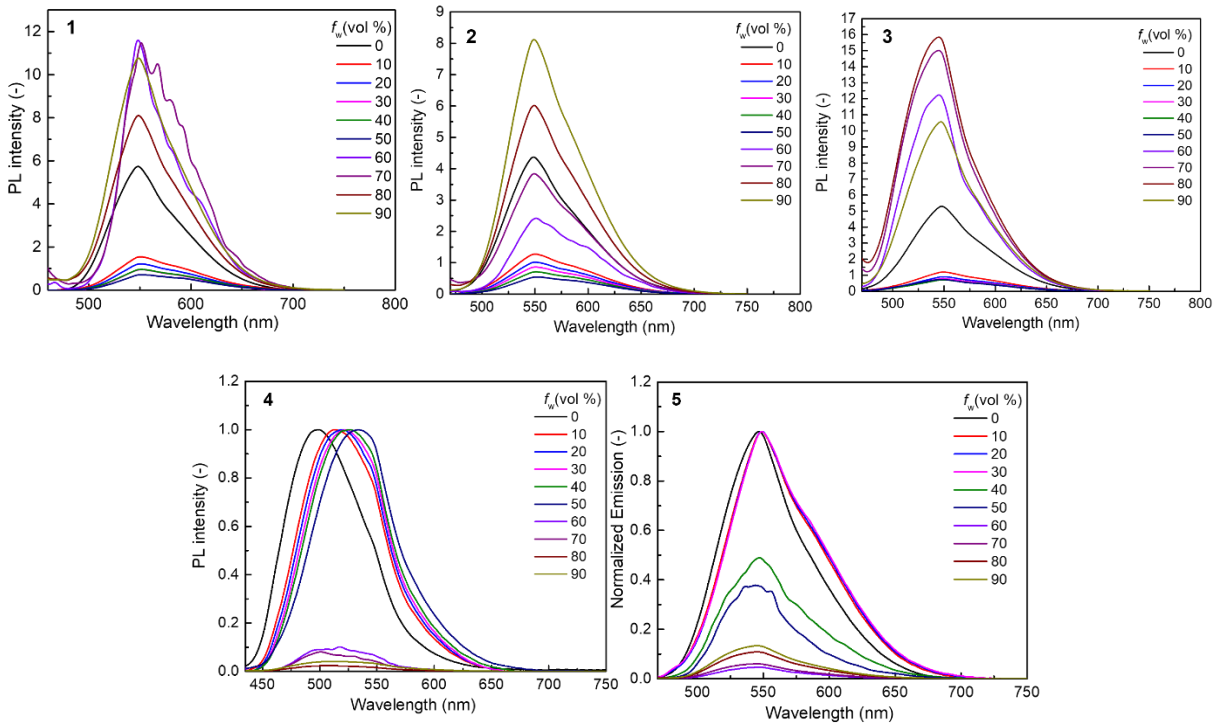

Figure 3.8. PL spectra and change of fluorescence intensity of maleimides luminophores in mixing ratio THF and water (*conc.*: 1.0 x 10^{-4} mol/L).

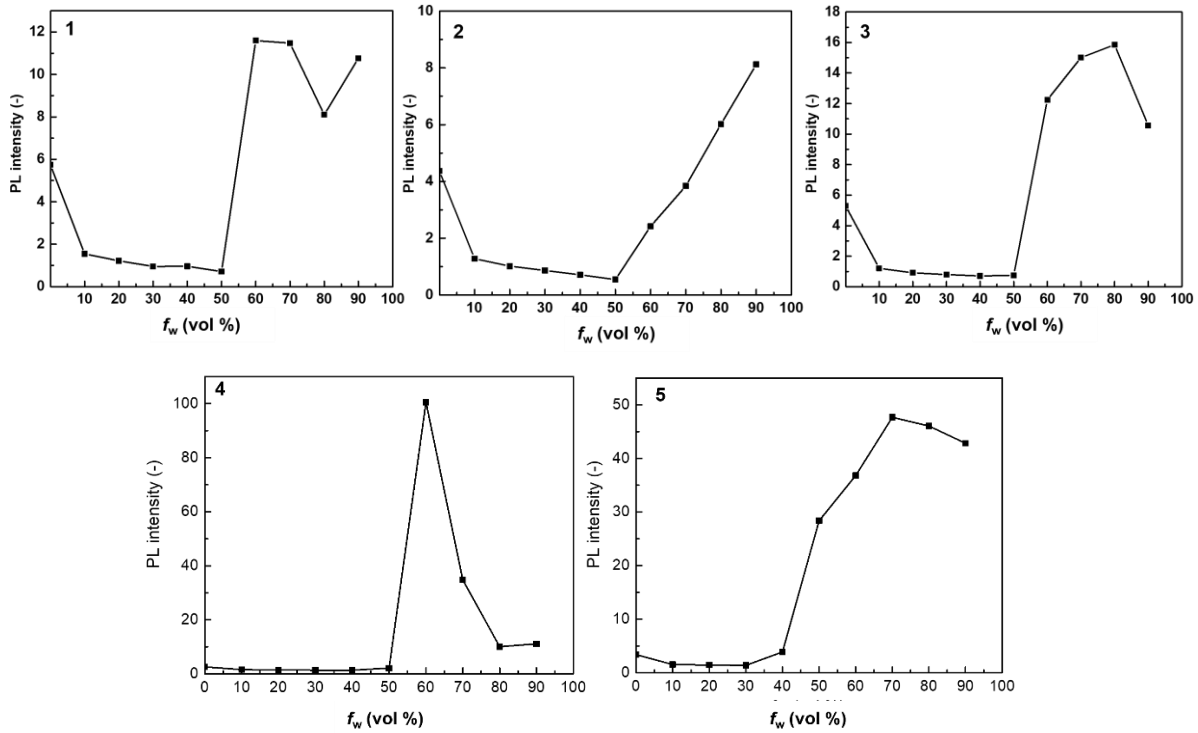

Figure 3.9. The change of fluorescence intensity of **1**, **2**, **3**, **4** and **5** in mixing ratio THF and water (*conc*.: 1.0 x 10^{-4} mol/L).

Figure 3.8 and Figure 3.9 depicts the PL spectra and the change of fluorescence intensity of the maleimide luminophores. The maleimide luminophores have similar fluorescence performance (the reduce of fluorescence intensity with the increase of water ratio in the mixture solution) when the water ratio less than 50 % (Figure.3.8 and Figure 3.9). As the luminophores contain donor and acceptor units in their molecular structures, probably the intramolecular charge transfer (ICT) caused by them is the main reason for this change. In addition, the fluorescence intensity of all luminophores is gradually increased when the water ratio is more than 50%. The main reason is that the aggregates are formed gradually, restricting the intramolecular motion, and reducing nonradiative transition, showing AIEE effects. For the luminophores **2,** the fluorescence intensity is increased with the increase of water ratio, showing obvious AIEE effects. However, for luminophores **1**, **3**, **4** and **5**, after the fluorescence intensity reaching the highest value, it begins to decline. The main reason is that in the mixtures with higher water ratios, the dye molecules may quickly aggregate in a random way to form less-emissive amorphous particles, leading to a decrease in fluorescence

intensity. This phenomenon is often observed for some compounds with AIE or AIEE properties. [9]

3.4 Conclusions

Based on the molecules that synthesized in chapter 2, a series of AIEE conjugated maleimide molecules with simple structures containing different amino groups were synthesized and characterized. Because the intramolecular rotation is restricted in the solid state, which reduces the nonradiative decay, these molecules show AIEE characteristics. Additionally, we speculate that the molecules that synthesized in this chapter also have non-planar conformations which can be helpful to inhibit intermolecular π-π stacking and enhance the emission in solid state. The highest occupied molecular orbital (HOMO), the lowest unoccupied molecular orbital (LUMO) and optimized conformation will be verified in future study by density functional theory (DFT) quantum calculations. As new AIEE molecules, conjugated amino-maleimides with different number of acceptors are expected to provide a new strategy for the development of the AIE field.

3.5 References

1 X. Wang, L. Zhang, Q. Li and Y. Gao, *Dyes Pigm*., 2020, **181**, 108614.

2 Y. Yu, X. Li, Y. Yuan and H. Zhang, *Polymer*, 2021, **217**, 123477.

3 Z. E. Chen, Q. L. Qi and H. Zhang, *Spectrochim*. *Acta, Part A*, 2020, **238**, 118384.

4 L. D. Lavis and R. T. Raines, *ACS Chem. Biol*., 2014, **9**, 855–866.

5 Z. Gao, Y. Hao, M. Zheng and Y. Chen, *RSC Adv*., 2017, **7**, 7604-7609.

6 D. Li, Q. Wang, N. Rao, Y. Zhang, Y. Lea, L. Liua, L. Li, L. Huang and L. Yana, *J. Mol. Struct*., 2021, **1239**, 130521.

7 Y. Hong, J. W. Y. Lam and B. Z. Tang, *Chem. Soc. Rev*., 2011, **40**, 5361-5388.

8 Y. Hong, J. W. Y. Lam and B. Z. Tang, *Chem. Commun*., 2009, 4332-4353.

9 X. Luo, J. Li, C. Li, L. Heng, Y. Q. Dong, Z. Liu, Z. Bo and B. Z. Tang, *Adv. Mater*., 2011, **23**, 3261-3265.

Chapter 4

Synthesis and photophysical properties of blue emission maleimide molecules with Dual-State Emission (DSE) effects

4.1 Introduction

Organic fluorescent materials have attracted extensive interest due to their advantages of flexible and adjustable structure, high fluorescence quantum yield and wider application.[1-8] Therefore, the design and development of organic fluorescent materials is of great significance. However, most conjugated and rigid organic fluorescent compounds with strong emission in solution often encounter aggregation caused quenching (ACQ) in aggregates or the solid state. This limits their realistic application in many fields.[9-12] The emergence of aggregation induced emission (AIE) molecules can solve this problem. In 1921, Schmidt published a paper titled "On the Luminescence of Solid Solutions" that discussed how many compounds fluoresce in solidified solutions but are quenched in the respective fluid solvents.[13] After that, several papers about the luminescence of solids were reported, and the concept of AIE was introduced in 2001 by Tang.[14-15] The AIE phenomenon is mainly caused by the restriction of intramolecular motion (RIM) mechanism, which includes the restriction of intramolecular rotation (RIR) and the restriction of intramolecular vibration (RIV). The RIM can reduce nonradiative decay, thereby resulting in the emission.[16-20] Since then, many AIE molecules have been developed and reported.[21-23] However, some high-tech applications of many AIE molecules that emit strongly only in a single state and AIEE molecules that emit weakly in solution but exhibit enhanced emission upon aggregation may be limited in certain fields.

Dual-state emission (DSE) is a type of luminescence phenomenon that emits in both the solution and solid state. The emergence of DSE molecules compensates for the disadvantage of many AIE molecules that only emit in a single state.[24-27] It has attracted a wide range of concerns due to its excellent properties.[28-32] Among them, fewer blue emission DSE molecules have been reported. Therefore, designing and developing blue-emitting DSE molecules is important for covering entire visible region and promoting practical applications. One major strategy to design DSE molecules is to construct a twisted molecule that has a conjugation-induced rigidity unit. The conjugation-induced rigidity unit facilitates emission in solution, and the twisted structure avoids the fluorescence quenching that caused by intermolecular π-π stacking interaction in the solid state, thereby achieving dual-state emission (DSE).[24, 32-33]

On the other hand, maleimide is a highly reactive organic compound with unsaturated cyclic imides and electron-poor dienophile properties, which can affect its fluorescence properties.[34] The presence of double bonds in the maleimide can lead to the formation of a rigid, planar structure, which can enhance the fluorescence properties of the fluorophore by increasing its conjugation and reducing its flexibility. However, the double bonds in maleimide can also lead to the change of fluorescence by electron transfer mechanisms. Additionally, the maleimide skeleton acts as an electron acceptor and features functionalized sites that can accommodate up to three substituents. The introduction of substituents with varying electronic effects enables effective tuning of the optical band gap, resulting in different luminescent colors.[35-38] Moreover, it also boasts good chemical stability and high fluorescence intensity. Due to these advantages, maleimide-based dyes are extensively utilized in various domains.[39-44] And in our previous works, we synthesized maleimide fluorophores with almost 100% fluorescence quantum efficiency by introducing two biphenyl groups on the maleimide ring.[38] In addition, we also designed and synthesized a series of conjugated maleimide molecules that contain different amino groups, displaying AIEE effects in the solid state.[45]

Based on our previous work, in this article, we synthesized new DSE molecules by replacing the amino group of the conjugated maleimide molecule with a methyl group. Specifically, we designed and synthesized new DSE molecules using maleimide as the

skeleton and introducing a different number of conjugation-induced rigidity biphenyl by Suzuki-Miyaura coupling. They show bright blue fluorescence emission both in solution and in solid state, displaying DSE effects. Moreover, they also display positive solvatochromic effects in solvent of different polarity. In response to the addition of trifluoroacetic acid (TFA) and triethylamine (TEA), they display the reversible acidochromic behaviour. Compared to the conjugated maleimide molecules containing amino that were synthesized in our previous work, these molecules exhibit higher fluorescence quantum yields both in solution and in the solid state. This is because the electron-donating ability of the amino group is helpful for intramolecular charge transfer (ICT) effect, resulting in a reduction of fluorescence quantum yields. However, the replacement of the methyl group can to some degree avoid some twist activity and increase the fluorescence quantum yield. At the same time, the non-planar structure of methyl can also increase the steric hindrance, preventing the intermolecular π-π stacking interactions that are caused by molecules compactly packing together. Thus, the introduction of a methyl group with a simple structure may provide new ideas for the construction of new DSE molecules.

4.2 Experimental

4.2.1 Materials

All commercially chemicals in this study were used without any further purification. Magnesium sulfate (anhydrous) and zinc chloride were purchased from Kishida Reagents Chemicals. Citraconic anhydride, palladium (II) acetate and the silica gel 60N (63-213 mm) which used as column chromatography were purchased from Wako Pure Chemical Industries. Moreover, the silica gel plate $60F_{254}$ for analytical thin-layer chromatography were purchased from Merck. Bromine, 1,1,1,3,3,3-hexamethydisilazane (HMDS) and 4,4'-biphenyl-diboronic acid bis(pinacol) Ester were purchased from Tokyo Chemical Industry (TCI). Triphenylphosphine was purchased from Kanto Chemical. 4-Biphenylboronic acid was available from Combi-Blocks. Commercially available products (1st grade) were used as all solvents.

4.2.2 Structural analysis and measurements

The ^{1}H (500 MHz) and ^{13}C (125 MHz) nuclear magnetic resonance (NMR) spectra were recorded using a JNM-LA500 spectrometer and $CDCl_3$ as solvent, with tetramethylsilane (TMS) as an internal standard ($\delta = 0.00$). The melting points were measured using a Buchi M-560. The NMR spectroscopy data abbreviations are defined as follows: "s" for singlet and "m" for multiplet. The ultraviolet-visible (UV-vis) spectra were recorded using a UV-1650PC (Shimadzu Corporation) spectrometer, while the photoluminescence (PL) spectra were recorded on an FP-6300 (JASCO Corporation) spectrophotometer at room temperature. The fluorescence quantum yields were determined using a C11347 Quantaurus-QY (Hamamatsu photonics K. K). The density functional theory (DFT) was conducted using the B3LYP/6-31G (d) level of theory with the Gaussian 09 program. The graphical outputs of the computational results were then generated using Multiwfn software[68] and VMD - Visual Molecular Dynamics software.

4.2.3 Synthesis

4.2.3.A Synthesis of 2-bromo-3-methyl-*N*-cyclohexylmaleimide (compound **BMMI**)

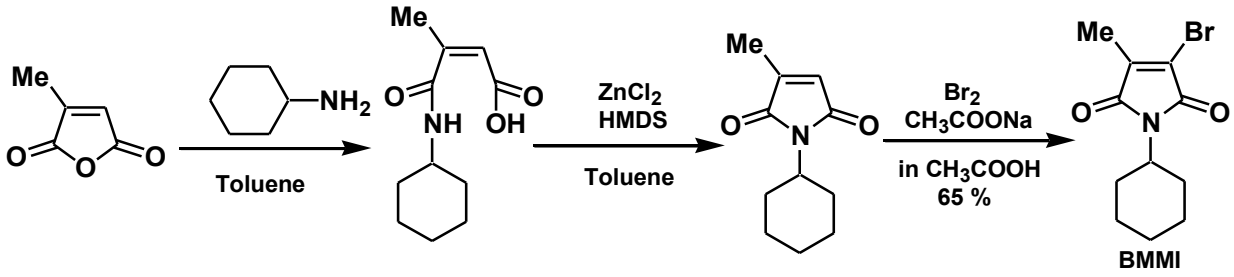

Scheme 4.1

A solution of cyclohexylamine (2.05 mL, 17.8 mmol) in toluene (50 mL) was dropwise to a solution of citraconic anhydride (1.60 mL, 17.8 mmol) in toluene (150 mL), and the mixture was stirred at room temperature for 1 hr. Then, added the $ZnCl_2$ (2.43 g, 17.8 mmol) and during the temperature was raised to 80 ºC, a solution of HMDS (5.68 mL, 26.8 mmol) was dropped. The mixture was stirred at 80 ºC for 5 hrs under nitrogen atmosphere. Then, the solvent was removed and extract with ethyl acetate. The residue was purified on a silica gel column using *n*-hexane / EtOAc (30/1: v/v) to obtain 2-methyl-*N*-cyclohexylmaleimide (2.70 g, 14.0 mmol). Then, 2-methyl-*N*-cyclohexylmaleimide (2.70 g, 14.0 mmol) in acetic acid (25 mL), bromine (Br_2) (1.07, 20.9 mmol) in acetic acid (5 mL) and sodium acetate (anhydrous) (1.15 g, 14.0 mmol) were added into the flask. The mixture was heated in under reflux for 3 hrs under a nitrogen atmosphere. Then, removal of the acetic acid and extract with ethyl acetate to give the crude product, which was purified by recrystallization from ethyl acetate/*n*-hexane to obtain white solid (2.45 g, 9.01 mmol, 65 %).

^{1}H-NMR (500 MHz, $CDCl_3$) δ (ppm from TMS): 3.90 - 3.97 (m, 1H), 1.99 - 2.07 (m, 5H), 1.82 - 1.85 (m, 2H), 1.57 - 1.68 (m, 3H), 1.20 - 1.33 (m, 3H).

^{13}C-NMR (125 MHz, $CDCl_3$) δ (ppm from TMS): 155.6, 152.4, 133.5, 120.0, 61.4, 44.1, 40.80, 40.1, 28.6.

4.2.3.B Synthesis of 2-methyl-3-biphenyl-*N*-cyclohexylmaleimide (Compound **1**) by Suzuki-Miyaura Coupling Reaction

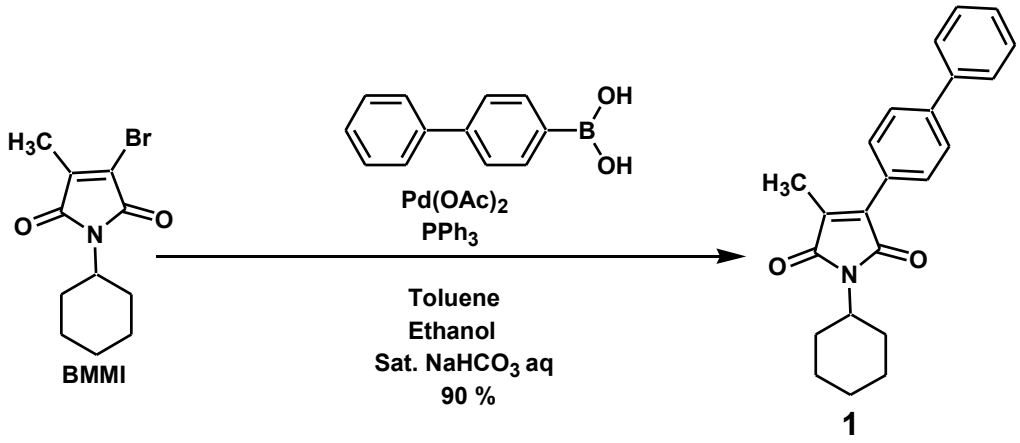

Scheme 4.2

A mixture of obtained 2-bromo-3-methyl-*N*-cyclohexylmaleimide (0.360 g, 1.33 mmol) and 4-biphenylboronic acid (0.310 g, 1.57 mmol) was added into the flask. Then, toluene (2 mL), ethanol (1 mL) and sat. $NaHCO_3$ aqueous solution (2 mL) was added, successively and the mixture was stirred at room temperature for 20 min. Added $Pd(OAc)_2$ (0.0300 g, 0.130 mmol) and PPh_3 (0.0300 g, 0.110 mmol) into the flask. The mixture was heated under reflux for 5 hrs under a nitrogen atmosphere. After that the reaction mixture was extract with ethyl acetate. The residue was purified on a silica gel column using *n*-hexane / EtOAc (7/1: v/v) to obtain pale-yellow solid (m.p. 103 - 109 ºC, 0.41 g 1.20 mmol, 90 %).

^{1}H-NMR (500 MHz, $CDCl_3$) δ (ppm from TMS): 7.62 - 7.70 (m, 6H), 7.45 - 7.48 (m, 2H), 7.36 - 7.39 (m, 1H), 3.96 - 4.02 (m, 1H), 2.22 (s, 3H), 2.09 - 2.16 (m, 2H), 1.84 - 1.87 (m, 2H), 1.59 - 1.73 (m, 3H), 1.24 - 1.38 (m, 3H).

^{13}C-NMR (125 MHz, $CDCl_3$) δ (ppm from TMS): 157.7, 157.0, 133.8, 132.3, 129.1, 129.0, 124.1, 123.2, 122.6, 122.4, 121.9, 121.8, 60.8, 44.1, 40.9, 40.2, 28.1.

Elemental analysis: Calcd for $C_{23}H_{23}NO_2$: C, 79.97; H, 6.71; N, 4.05. Found: C, 79.69; H, 7.04; N, 3.77.

4.2.3.C Synthesis of 4,4'-bis (2-methyl-*N*-cyclohexylmaleimide-3-yl)-1,1'-biphenyl (Compound **2**) by Suzuki-Miyaura Coupling Reaction.

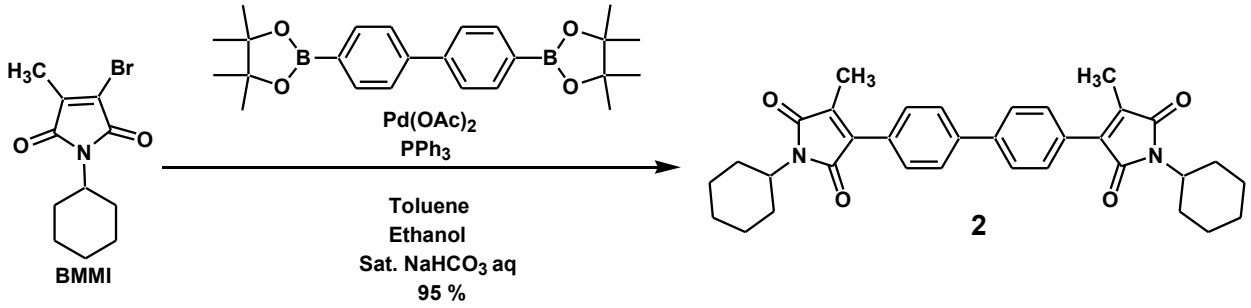

Scheme 4.3

A mixture of obtained 2-bromo-3-methyl-*N*-cyclohexylmaleimide (0.140 g, 0.520 mmol) and 4,4'-biphenyl-diboronic acid bis(pinacol) ester (0.100 g, 0.250 mmol) was added into the flask. Then, toluene (2 mL), ethanol (1 mL) and sat. $NaHCO_3$ aqueous solution (2 mL) was added, successively and the mixture was stirred at room temperature for 20 min. Added $Pd(OAc)_2$ (0.0110 g, 0.0600 mmol) and PPh_3 (0.0130 g, 0.0500 mmol) into the flask. The mixture was heated under reflux for 5 hrs under a nitrogen atmosphere. After that, the reaction mixture was extract with ethyl acetate. The residue was purified on a silica gel column using *n*-hexane / EtOAc (9/1: v/v) to obtain pale-yellow solid (m.p. 182 - 185 ºC, 0.11 g, 0.20 mmol, 95 %).

^{1}H-NMR (500 MHz, $CDCl_3$) δ (ppm from TMS): 7.68 - 7.74 (m, 8H), 3.96 - 4.02 (m, 2H), 2.23 (s, 6H), 2.05 - 2.18 (m, 4H), 1.85 - 1.88 (m, 4H), 1.57 - 1.74 (m, 6H),1.25 - 1.37 (m, 6H).

^{13}C-NMR (125 MHz, $CDCl_3$) δ (ppm from TMS): 157.6, 156.9, 133, 129.2, 129.0, 124.2, 123.1, 121.8, 60.9, 44.1, 40.9, 40.2, 28.1.

HRMS (TOF-ES+): calcd for $C_{34}H_{37}N_2O_4$ + 537.2753 [M+ H], found 537.2750.

4.2.4 Structure characterization

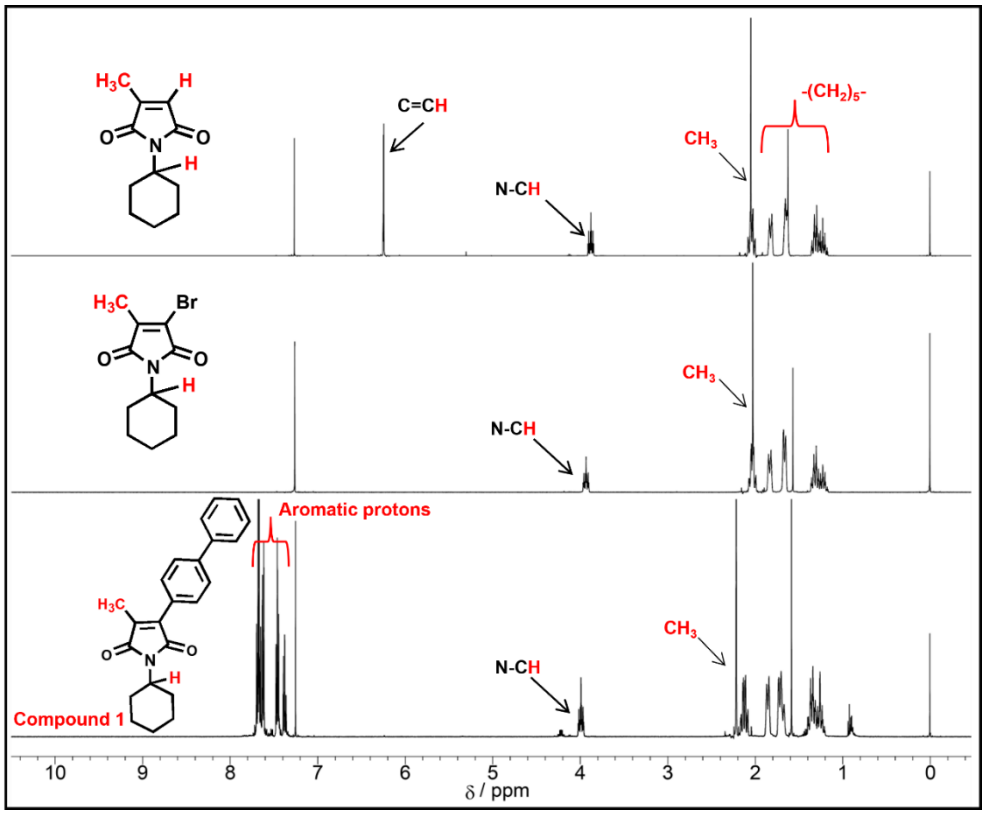

Figure 4.1. ^{1}H NMR Spectrum of compound **1** in $CDCl_3$.

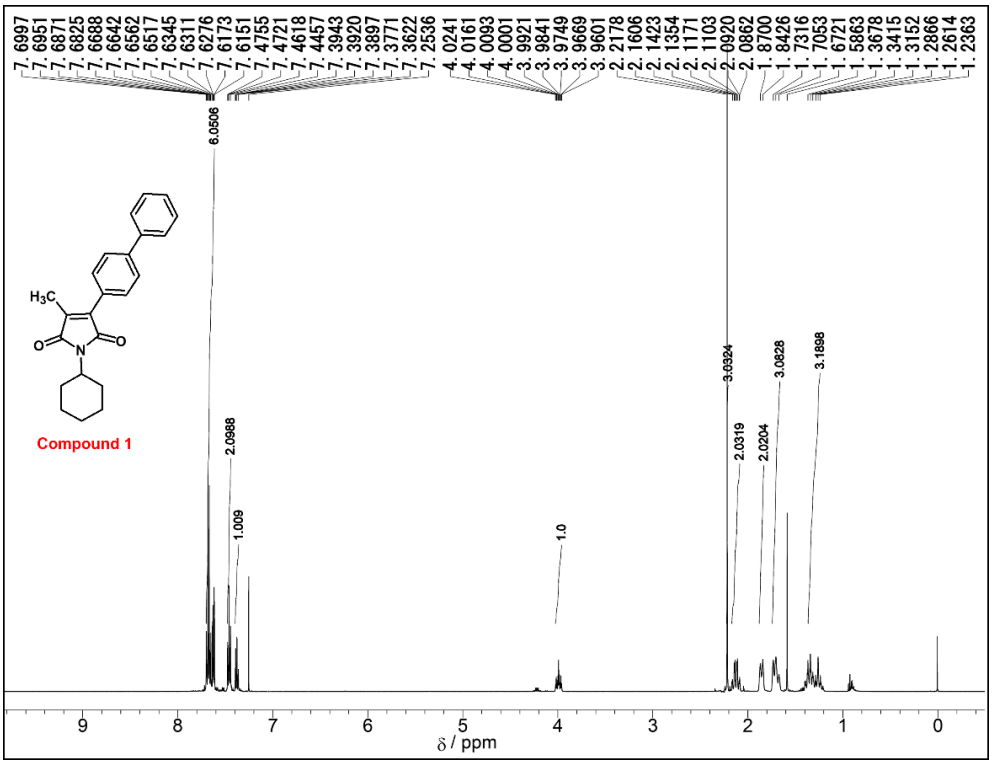

Figure 4.2. ^{13}C NMR Spectrum of compound **1** in $CDCl_3$.

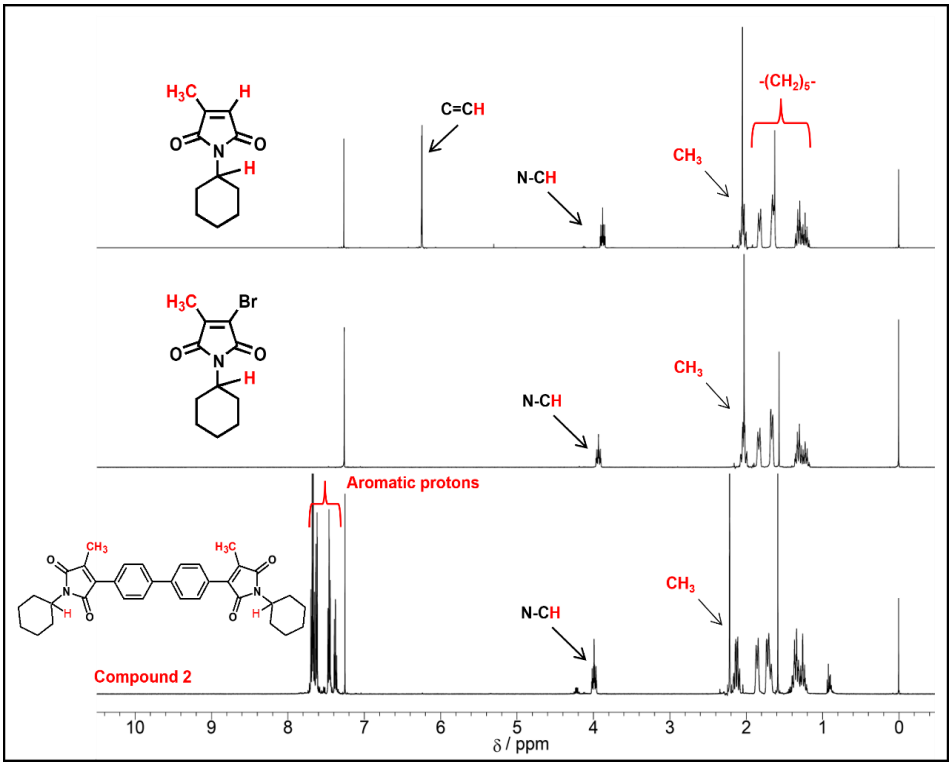

Figure 4.3. ^{1}H NMR Spectrum of compound **2** in $CDCl_3$.

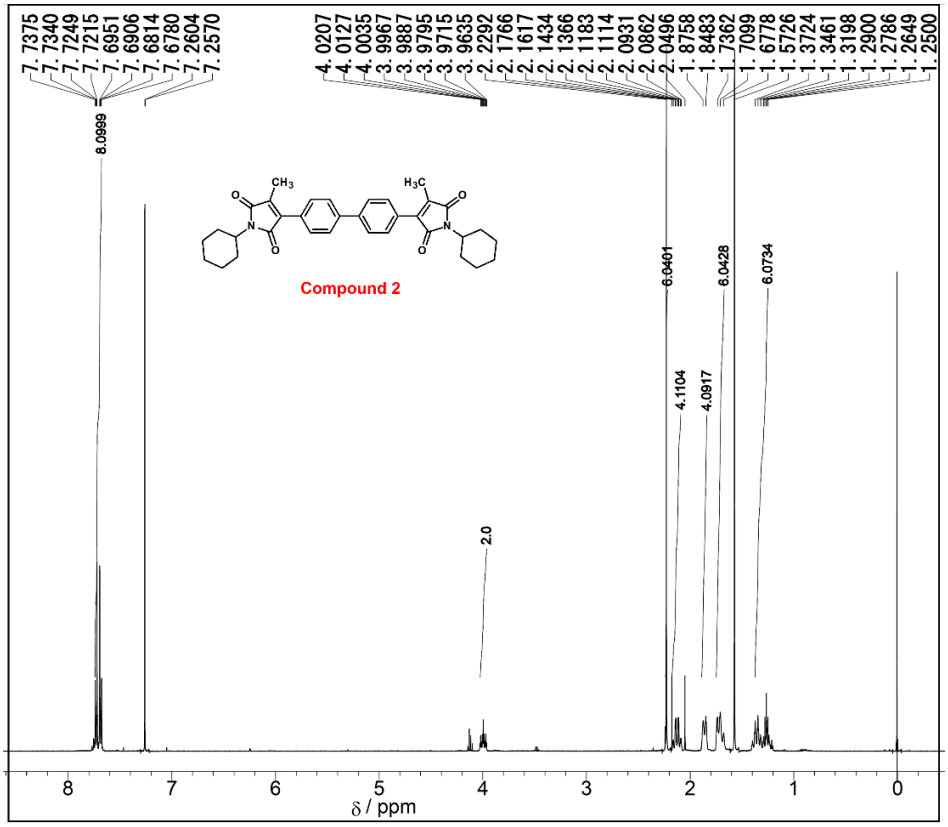

Figure 4.4. ^{13}C NMR Spectrum of compound **2** in $CDCl_3$.

4.3 Results and discussion

4.3.1 Syntheses and characterization

Two maleimide derivatives **1** and **2**, were designed as DSE fluorophores with high yields (> 90 %) and both emit in dilute THF solutions and in solid state. As shown in Scheme 1, we synthesized 2-bromo-3-methyl-*N*-cyclohexylmaleimide from citraconic anhydride and cyclohexylamine. The maleimide fluorophores **1** and **2** were then achieved from 2-bromo-3-methyl-*N*-cyclohexylmaleimide by reacting it with 4-biphenylboronic or 4,4'-biphenyldiboronic acid bis(pinacol) ester through the Suzuki-Miyaura coupling reaction, and their structures were confirmed by NMR (^{1}H and ^{13}C). The spectra characterization is described in Figure 4.1-Figure 4.4. The maleimide fluorophores are air-stable solids that are soluble in common organic solvents but insoluble in water.

The absorption spectra (Figure 4.5A) and fluorescence spectra (Figure 4.5B) of maleimide fluorophores **1** and **2** in dilute THF were examined, and all the photophysical data are summarized in Table 4.1. An absorption peak (λ max = 263 nm) of fluorophore **1** and two similar absorption peaks of fluorophore **2** (λ max = 241 nm, λ max = 281 nm), caused by the π-π* electron transition of the conjugated system of the maleimide ring, can be observed (Figure 4.5A). This is because fluorophores **1** and **2** differ in the number of maleimide rings they have. Moreover, a similar absorption peak of the two maleimide fluorophores can be observed, which is caused by biphenyl (Figure 4.5A). The absorption maximum wavelength of fluorophore **2** (λ max = 365 nm) was red-shifted relative to that of **1** (λ max = 349 nm). Furthermore, fluorophores **1** and **2** exhibit similar fluorescence emission at 461 nm with a large Stokes shift of 6961 cm^{-1} and 5705 cm^{-1} upon excitations at 349 nm and 365 nm, respectively (Figure 4.5B, Table 4.1). The large Stokes shift result in almost no spectral overlap between the absorption and emission peaks, creating good spectral separation. This can prevent the interference brought by the excitation light and scattered light, as well as the fluorescence intensity produced by self-absorption, thereby improving the response sensitivity of fluorescent molecules.[46-48]

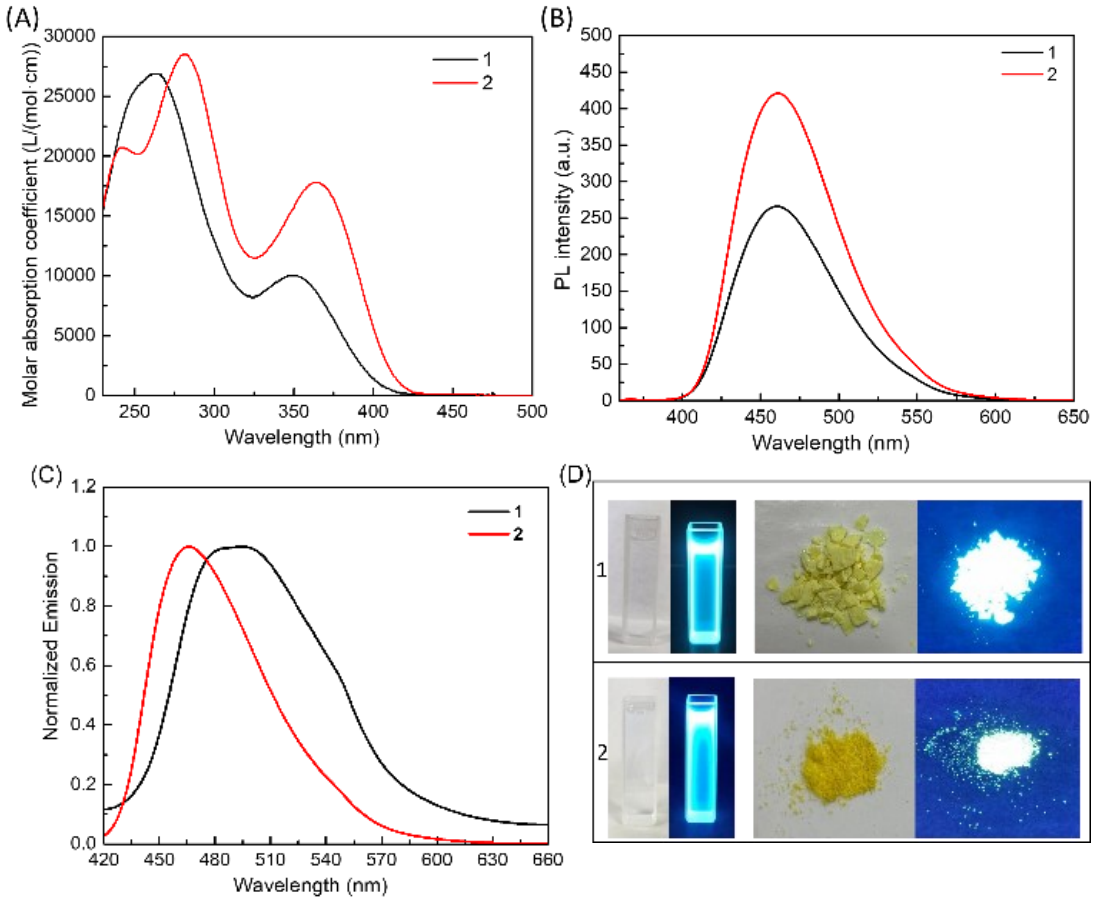

Figure 4.5. (A) UV spectra, (B) PL spectra at the excitation wavelength of 349 nm for fluorophore **1** and 365 nm for fluorophore **2** in THF (conc.: 1.0 x 10^{-5} mol/L), (C) PL spectra of fluorophores **1** and **2** in powder and (D) photographs under the visible and UV light (352 nm).

Table 4.1. Optical properties of fluorophores **1** and **2**

	λ_{abs} [a)] (nm)	ε [a] (L/(mol.cm))	λ_{em} [a] (nm)	Δs (cm^{-1})	CIE (x, y) [a)]	Φ (%) [b)] in solution	in powder
1	263, 349	$2.69x10^4$, $1.00x10^4$	461	6961	0.14, 0.15	81	81
2	241, 281, 365	$2.07x10^4$, $2.85x10^4$, $1.78x10^4$	461	5705	0.14, 0.15	77	22

a) 1.0 x 10^{-5} mol/L in THF. b) Φ is the fluorescence quantum yield.

4.3.2 Dual-State Emission (DSE) effects

Both fluorophore **1** and **2** exhibit strong blue emission in dilute THF, as shown in Figure 4.5D. Their CIE coordinates are (0.14, 0.15) and (0.14, 0.15), respectively. Specifically, as depicted in Figure 4.5D, the fluorophores also exhibit strong emission in the solid state. Their CIE coordinates are (0.20, 0.38) and (0.14, 0.21), respectively. In particular, fluorophore **1** exhibited high fluorescence quantum yields of 81 % both in THF solutions and in the solid state, revealing remarkable dual-state emission (DSE) effects (Table 4.1 and Figure 4.5D). Similarly, fluorophore **2** obtained high fluorescence quantum yields of 77 % in THF solutions and relatively lower fluorescence quantum yields of 22 % in the solid state. Despite this, it still exhibited the dual-state emission (DSE) effects (Table 4.1 and Figure 4.5D). The lower fluorescence quantum yields in the solid state may be caused by stronger intermolecular quenching effects, as fluorophore **2** contains a larger conjugated plane.

The fluorescence spectra of these maleimide fluorophores in the solid state were analyzed, as shown in Figure 4.5C. For fluorophore **1**, the fluorescence maximum wavelength at 495 nm has a 34 nm red shift relative to that in dilute THF. Similarly, for fluorophore **2**, the fluorescence maximum wavelength at 466 nm has a 5 nm red shift relative to that in dilute THF. These results indicate that fluorophores **1** and **2** overcome the limitation of emitting in only one state, (solution or solid), and exhibit fluorescence in both solution and the solid state. In solution, high conjugation can enhance the fluorescence performance of fluorescent molecules. In addition, although these molecules have freedom of motion in solution, their interactions with the solvent can restrict their vibrational and rotational motions to some extent, reducing nonradiative decay and increasing radiative decay, which enhances the emission efficiency of fluorescent molecules in solution. However, in the solid state, the emission of fluorophores occurs due to significantly restricted molecular motion, which reduces nonradiative decay and increases radiative decay, leading to fluorescence emission.[49-50] Furthermore, the biphenyl unit of fluorophore **1** is connected to a maleimide ring by a rotatable C-C single bond, which allows for free rotation in the single molecule state but is hindered in the aggregated state. In contrast, the biphenyl unit of fluorophore **2** is connected to two maleimide rings by a rotatable C-C single bond. Due to its more flexible molecular structure, fluorophore **2** exhibits weaker emission in the solid state compared to fluorophore **1**, which has a more restricted molecule motion.

Since the maleimide fluorophores **1** and **2** are soluble in common organic solvents but insoluble in water, we used water as a poor solvent in this solvent system to examine their fluorescent behaviours in a mixture of water and THF under different water volume fractions. Our aim was to further confirm their photoluminescence properties in aggregates. As shown in Figure 4.6- Figure 4.8, fluorophores **1** and **2** exhibit different levels of red shift and a similar trend in fluorescence intensity change with varying water volume fractions in the mixed solvent. When the water volume fraction ranges from 0% to 60%, the fluorescence spectra exhibit a red shift for fluorophore **1** (48 nm) and fluorophore **2** (39 nm), along with a change in color (Figure 4.8). The CIE coordinates of fluorophore **1** range from (0.14, 0.15) to (0.22, 0.48), and the CIE coordinates of fluorophore 2 range from (0.14, 0.15) to (0.19, 0.41). Additionally, the PL intensity also decreases. These results may be attributed to the change in polarity of the mixture of solvents with the addition of water, which results in a decrease in PL intensity by an intramolecular charge transfer (ICT).[36] However, when the water volume fraction is more than 60%, the PL intensity increases with an increase in the water volume fraction. This is because the aggregates gradually form with an increase in the water volume fraction, and the molecular motion is restricted, resulting in aggregates induced emission. The formation of aggregates can also be confirmed by the changes of absorption spectra of fluorophore **1** and fluorophore **2** in water-THF mixtures with varying water volume fractions (Figure 4.6, Figure 4.7). With an increase in the water volume fraction, a red shift of the absorption maximum wavelength occurred. And the level-off off tails of the absorption peaks appeared in the visible region, which can be attributed to light-scattering effects and indicate the formation of aggregates.[51-52]

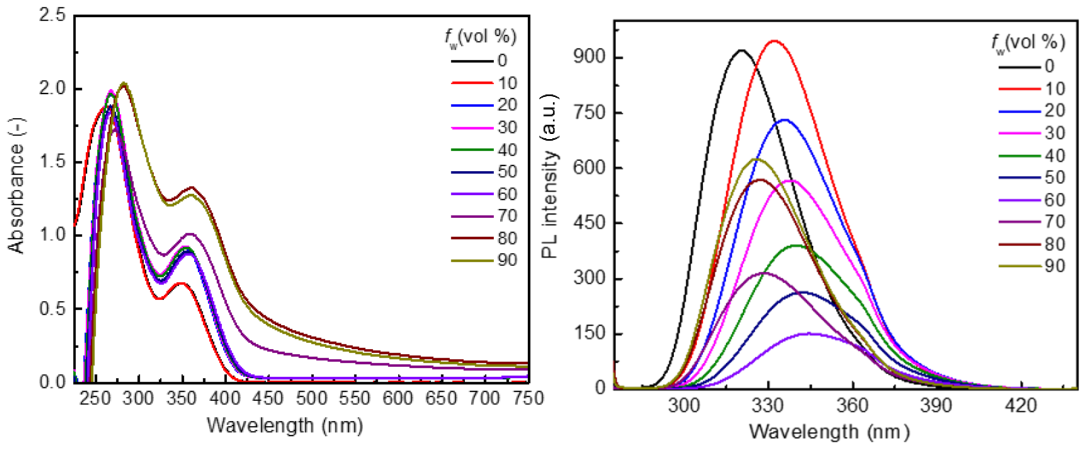

Figure 4.6. Absorption spectrum and emission spectrum of fluorophore **1** in a mixture of water-THF.

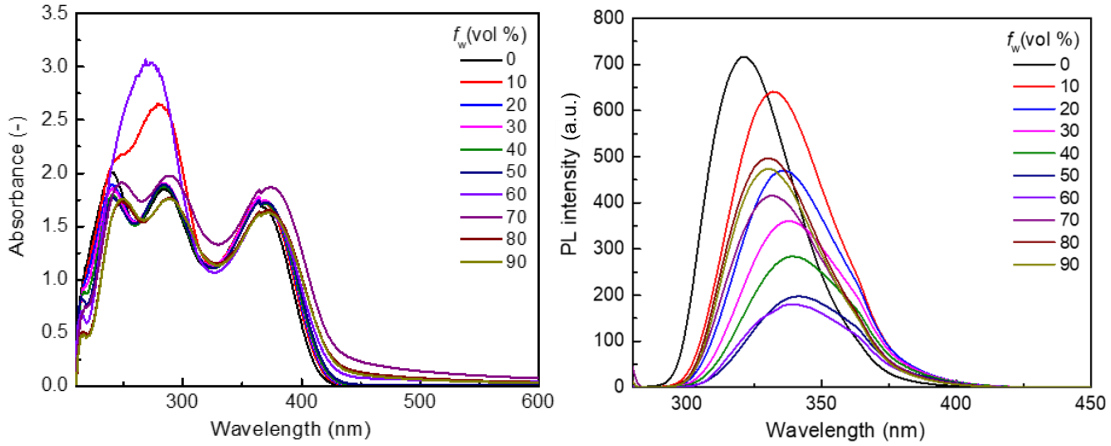

Figure 4.7. Absorption spectrum and emission spectrum of fluorophore **2** in a mixture of water-THF.

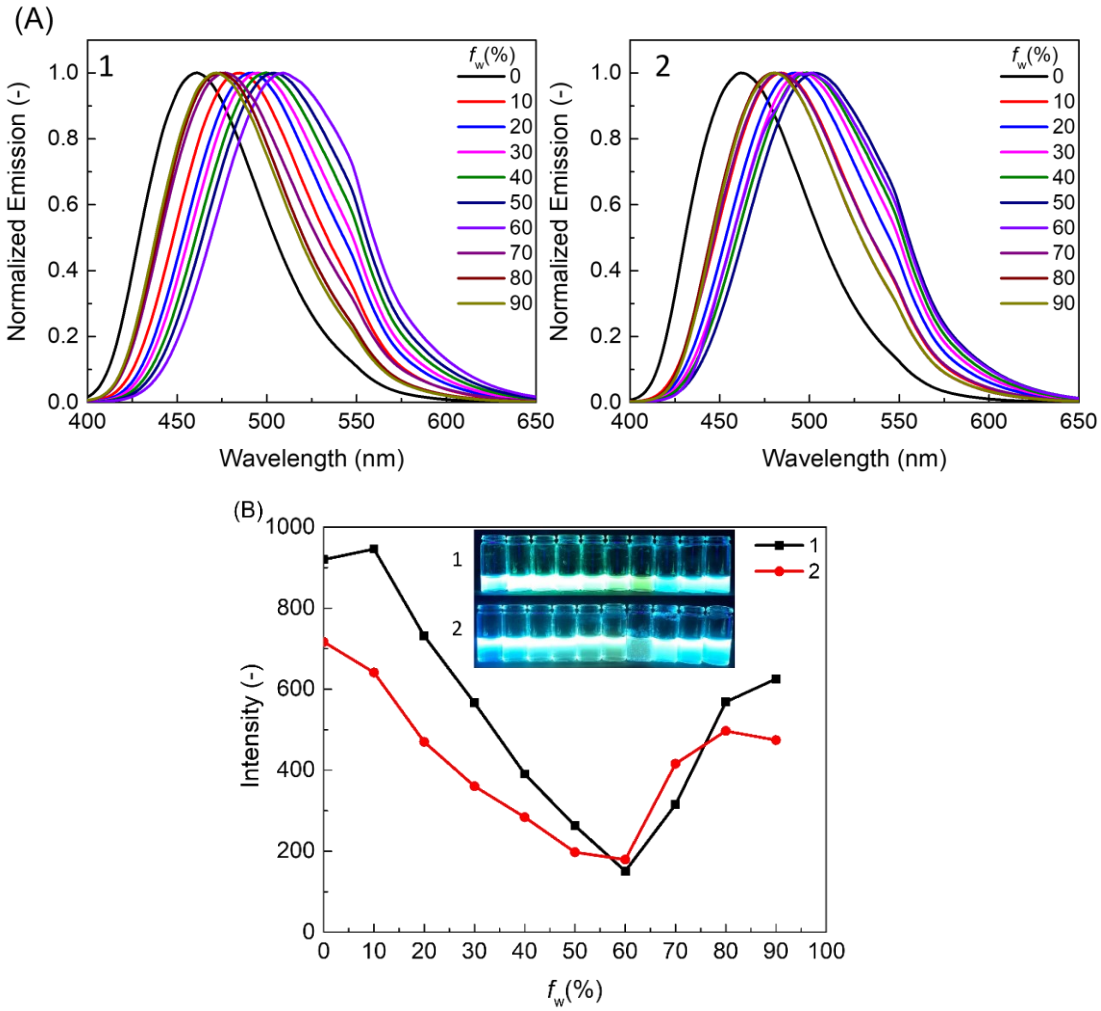

Figure 4.8. (A) PL spectra and (B) fluorescence intensity of PL spectra at the excitation wavelength of 349 nm for fluorophore **1** and 365 nm for fluorophore **2** in a mixture of water-THF (*conc.*: 1.0 x 10^{-5} mol/L).

In most synthetic reactions, the presence of water can cause many problems, such as the generation of by-products and a reduction in product yields.[53] In recent years, some organic fluorescent dyes have been developed as fluorescence sensors for detecting water in organic solvents.[54-58] Similarly, we believe that the fluorophores can provide some possibilities as fluorescent sensors for the water detection.

4.3.3 Density functional theory (DFT) quantum calculations

The photophysical properties of maleimide fluorophores **1** and **2** at the molecular level were investigated using density functional theory (DFT) at the B3LYP/6-31G (d) level of theory with the Gaussian 09 program. The highest occupied molecular orbital (HOMO), the lowest unoccupied molecular orbital (LUMO) and optimized conformation of fluorophores **1** and **2** were investigated. The computational results were visualized using Multiwfn software[39] and VMD - Visual Molecular Dynamics software. The results indicated that the HOMO → LUMO transitions were the dominant contributors for fluorophores **1** and **2**, accounting for 90% and 94% respectively. As shown in Figure 4.9A, the highest occupied molecular orbital (HOMO) of fluorophore **1** was primarily localized on the biphenyl unit (donor moiety), while the lowest unoccupied molecular orbital (LUMO) was mainly localized at the maleimide ring (acceptor moiety) to form the donor-acceptor (D-A) construct. The HOMO - LUMO gap for fluorophore **1** was 3.64 eV, with the HOMO at -6.04 eV and the LUMO at -2.40 eV. Similarly, the HOMO of fluorophore **2** was primarily localized on the biphenyl unit (donor moiety), while the LUMO was mainly localized at the two maleimide rings (acceptor moieties) to form the acceptor-donor-acceptor (A-D-A) construct. The HOMO - LUMO gap for fluorophore **2** was 3.47 eV, with the HOMO at -6.06 eV and the LUMO at -2.59 eV. The cyclohexane ring in the fluorophore molecule **1** and **2** makes little contribution to either the HOMO or the LUMO energy level. The spatial distribution between the HOMO and LUMO indicated a typical intramolecular charge transfer (ICT) between the donor and acceptor components.[6] In addition, the donor biphenyl is connected to the acceptor

maleimide ring by a rotatable carbon-carbon single bond. In the optimized conformation of **1**, the dihedral angle between the maleimide ring and its adjacent phenyl ring is 29°, while the dihedral angle between two phenyls of biphenyl is 37°. For fluorophore **2**, the dihedral angle between the maleimide ring and its adjacent phenyl ring is 31° and the dihedral angle between two phenyls of biphenyl is 34°. Furthermore, we also observed their non-planar structure through the optimized conformation of fluorophores (Figure 4.9B). These structures also contribute to the emission in the solid. Because the non-planar molecule structures can inhibit ACQ, which is caused by the intermolecular π-π stacking interaction in the solid state.

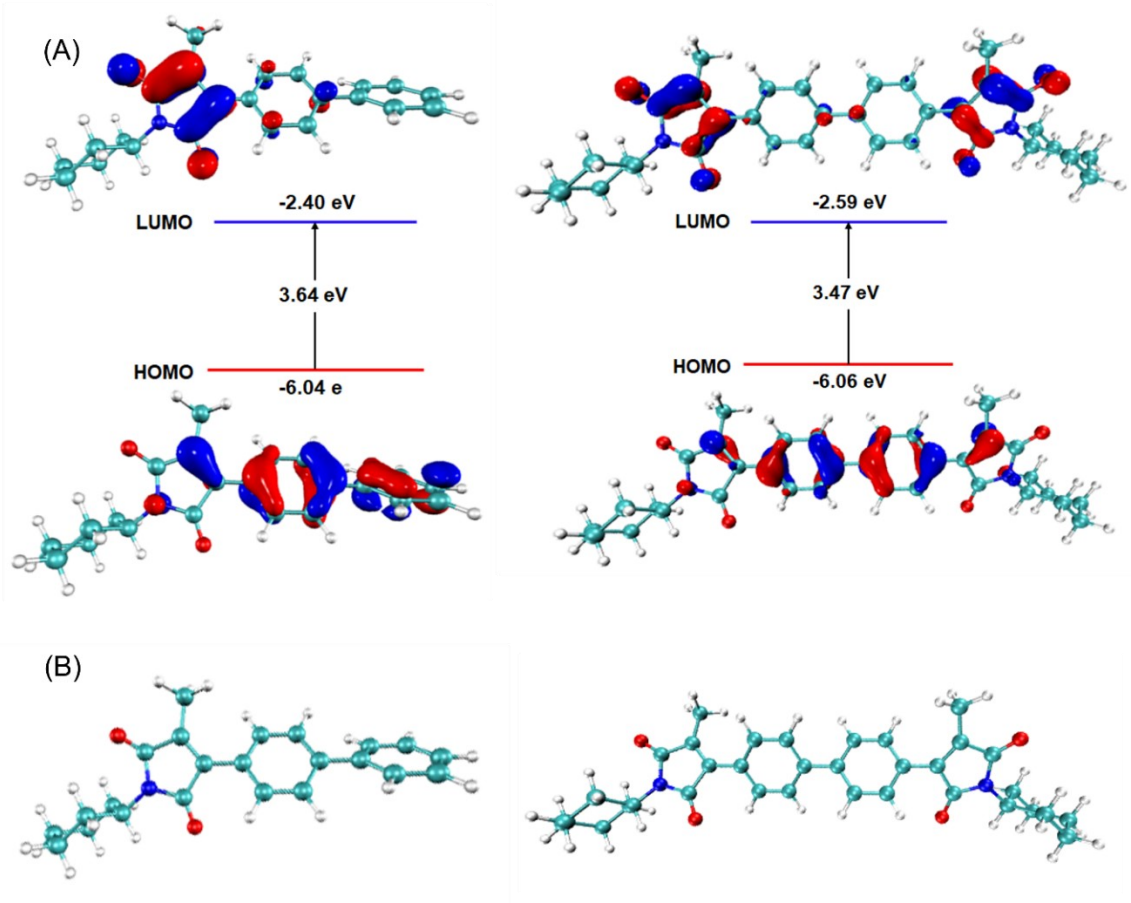

Figure 4.9. A) HOMO and LUMO distribution and (B) Optimized conformations of fluorophores **1** (left) and **2** (right)at the B3LYP/6-31G (d) level in Gaussian.

4.3.4 Solvatochromism

The ground state or excited state of the organic molecules may change when the compound is dissolved in a different solvent, which can further alter the absorption or fluorescence spectra. Therefore, we investigated the absorption spectra and fluorescence spectra of maleimide fluorophores **1** and **2** in solvent of different polarity such as toluene, THF, acetone, acetonitrile and DMF. As shown in Table 4.2, absorption spectra of these fluorophores exhibited little changes with varying solvent polarities, indicating that the ground state of the fluorophores is minimally influenced by solvent polarity. However, for fluorophore **1**, the emission maximum wavelength showed an 18 nm red shift when the solvent polarity was varied from toluene (460 nm) to DMF (478 nm). This shift was accompanied by a color change from purplish-blue (CIE coordinates: 0.14, 0.14) to blue (CIE coordinates: 0.15, 0.25) (Figure 4.10, Figure 4.11 and Table 4.2). A similar result was observed for fluorophore **2**, with the emission maximum wavelength showing a 26 nm red shift when the solvent polarities were varied from toluene (458 nm) to DMF (484 nm). This shift was accompanied by a color change from purplish blue (CIE coordinates: 0.14, 0.13) to greenish blue (CIE coordinates: 0.16, 0.30) (Figure 4.10, Figure 4.11 and Table 4.2). This phenomenon should be attributed to the effectiveness of the intramolecular charge transfer (ICT) mechanism, which was subsequently confirmed by the change of dipole moment obtained from the Lippert-Mataga equation.

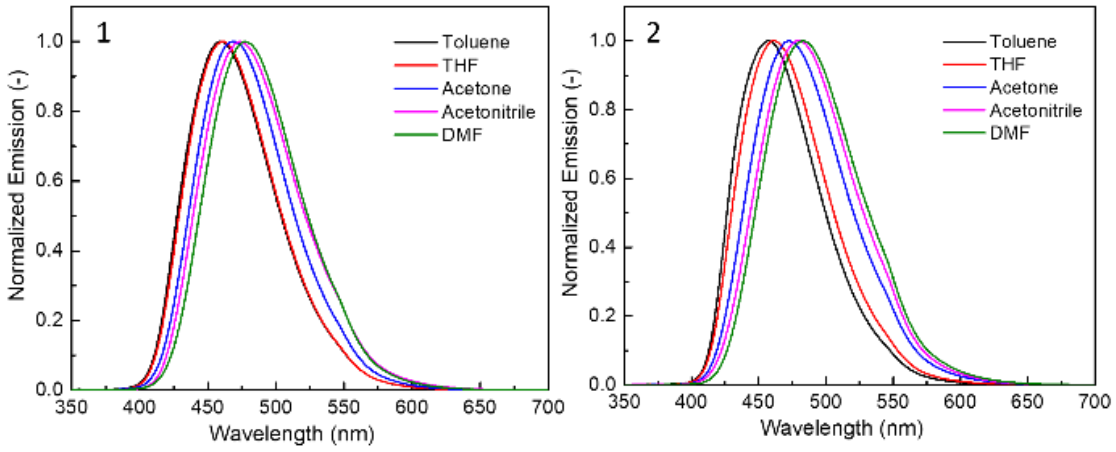

Figure 4.10. PL spectra at the excitation wavelength of 349 nm for fluorophore **1** and 365 nm for fluorophore **2** in solvent of different polarity (*conc.*: 1.0 x 10^{-5} mol/L).

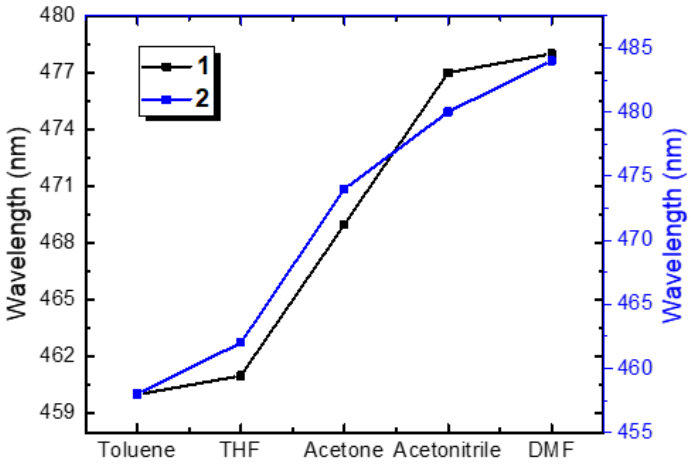

Figure 4.11. The change of the emission maximum wavelength of fluorophore **1** and **2** in solvent of different polarity (*conc*.: 1.0 x 10^{-5} mol/L).

Table 4.2. Optical properties of fluorophores in different solvent.

	1					**2**				
Solvent	λ_{abs} [a)] (nm)	λ_{em} [a] (nm)	Δs (cm^{-1})	CIE (x,y)	$\mu_e - \mu_g$ [b]	λ_{abs} [a)] (nm)	λ_{em} [a] (nm)	Δs (cm^{-1})	CIE (x,y)	$\mu_e - \mu_g$ [b]
Toluene	353	460	6590	0.14, 0.14	1.23 D	368	458	5340	0.14,0.13	2.09 D
THF	349	461	6961	0.14, 0.15	5.03 D	365	461	5705	0.15,0.16	8.62 D
Acetone	348	469	7414	0.14, 0.19	6.09 D	360.5	474	6642	0.15,0.23	10.9 D
Acetonitrile	349	472	7467	0.15, 0.24	6.36 D	359.5	480	6983	0.15,0.28	11.5 D
DMF	351	478	7569	0.15, 0.25	6.13 D	364.5	484	6774	0.16,0.30	11.1 D

a) 1.0 x 10^{-5} mol/L

b) μ_e and μ_g represents the Dipolar moments in the excited (*e*) and ground (*g*) states, respectively.

The Lippert-Mataga equation is a model that is used to study the influence of solvent polarity on the photophysical properties of fluorophores.[59-62] It is expressed by the following equation:

$$\Delta\upsilon = \upsilon_{ab} - \upsilon_{em} = \frac{2\Delta f}{hca^3}\left(\mu_e - \mu_g\right)^2 + const \qquad (1)$$

(Where Δυ represents the Stokes shift, *h* represents the Planck constant, c represents the Speed of light, a represents the Onsager cavity radius, μ_e and μ_g represents the Dipolar moments in the excited (*e*) and ground (*g*) states, respectively.)

$$\Delta f = \frac{(\varepsilon-1)}{(2\varepsilon+1)} - \frac{(n^2-1)}{(2n^2+1)} \qquad (2)$$

(Where ε and n represents the Permittivity and the refractivity of the solvent, respectively.)

The change in the position of absorption and emission spectra due to solvation is often explained based on the degree of stabilization of the ground state (S_0) or the first excited state (S_1), which is determined by their respective dipole moments.[63-65] We obtained the dipole moments difference of the S_0 and S_1 of fluorophores **1** and **2** in various solvents according the Lippert-Mataga equation, which are summarized in Table 4.2 (The Onsager cavity radius was obtained using Gaussian and Multiwfn[66]). The dipole moment of the excited state with respect to the ground state in solvent of different polarity all shows an increase. For example, the dipole moment difference (μ_e-μ_g) of fluorophores **1** and **2** in toluene is 1.23 D and 2.09 D, respectively, while in the polar solvent DMF, they are 6.13 D and 11.1 D, respectively. The significant increase in the dipole moment difference (μ_e-μ_g) observed in polar solvents compared to weakly polar solvents suggests the effectiveness of the ICT mechanism. Additionally, we further examined the effect of solvent polarity changes on the change in the position of absorption and emission spectra using the Lippert-Mataga equation. We studied the relationship of Stokes shift ($\Delta\upsilon$) and solvent orientation polarizability (Δf) in solvent of different polarity using the Lippert-Mataga equation. As shown in Figure 4.12, the Stokes shift of fluorophore **1** increased with the solvent orientation polarizability (Δf), exhibiting a linear correlation with a slope of 3239 cm^{-1}. The Stokes shift of fluorophore **2** also increased with the solvent orientation polarizability (Δf), exhibiting a linear correlation with a slope of 5364 cm^{-1}. Furthermore, the correlation between the Stokes shift and the empirical solvent polarity parameter $E_T(30)$ also helps to confirm the solvent-dependent effect.[67-68] The empirical polarity parameter $E_T(30)$ was proposed by Reichardt, which is an empirical parameter used to characterize solvent polarity with a specified compound as a standard.[69] It is applicable to various polar solvents. As shown in Figure 4.13, the dependence of the Stokes shift of the empirical polarity parameter $E_T(30)$ proceeds linearly for fluorophores **1** (R^2 = 0.92) and **2** (R^2 = 0.95). The observed linear changes in Stokes shift also provide evidence that the obtained maleimide fluorophores are sensitive to solvents and exhibit a positive solvatochromic fluorescence effect.

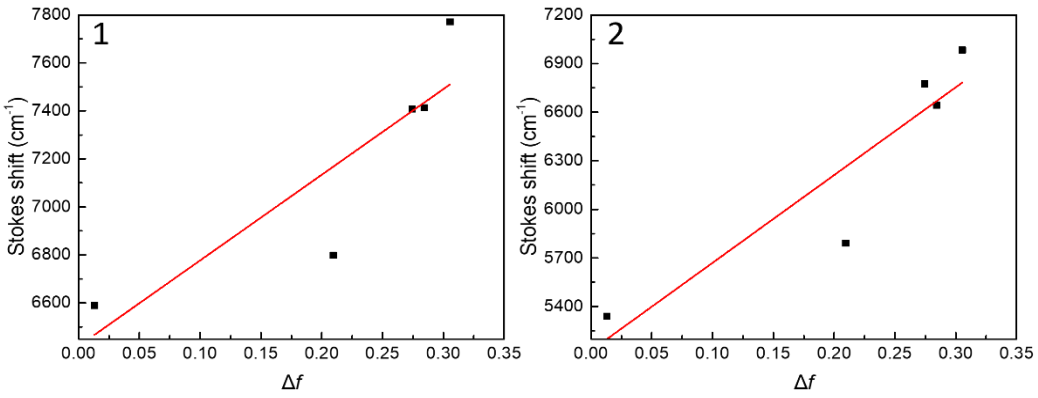

Figure 4.12. Lippert-Mataga plots showing Stokes shift as a function of solvent orientation polarizability (Δf).

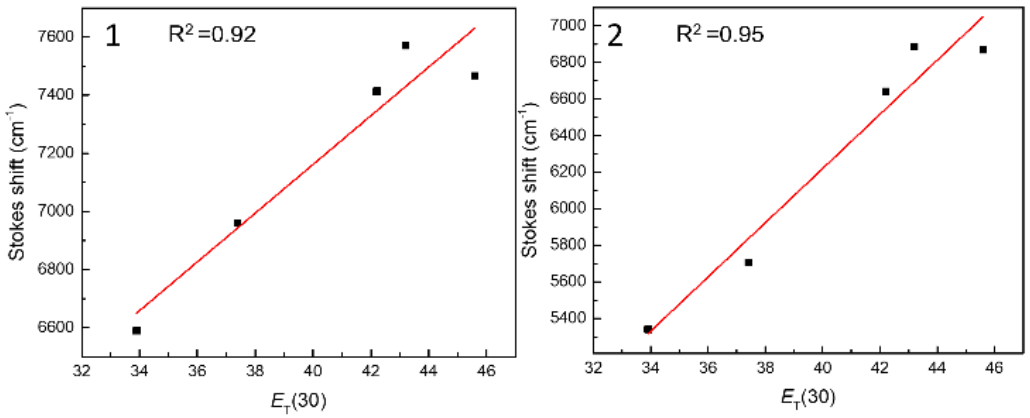

Figure 4.13. Correlation of Stokes shift with the empirical solventpolarity parameter E_T(30).

4.3.5 Acid/ alkali responsive properties

In order to confirm the acid/ alkali responsive properties of fluorophores, we have made the dilute THF solution of fluorophores **1** and **2**, and we also have drop casted the solution on a thin layer chromatography (TLC) plate and allowed the solvent to evaporate to form a film. As shown in Figure 4.14, both the solution and the film exhibit acidochromic behavior when they are stimulated by trifluoroacetic acid (TFA). And the color is recovered when the TFA mixture solution is subsequent stimulated by triethylamine (TEA).

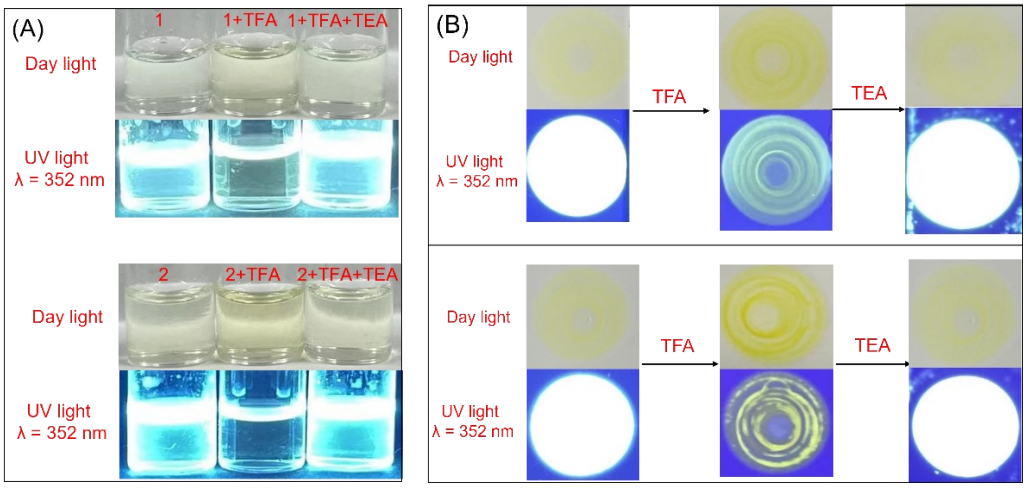

Figure 4.14. Photographs showing the response of the THF solution (A) and the film on a TLC plate (B) of fluorophores **1** (up) and **2** (down) on addition of TFA and then with TEA.

The UV-vis spectra and PL spectra were also obtained in a dilute THF solution with the addition of TFA and TEA to confirm this change. It showed the same response as the addition of TFA and TEA observed in the film. The PL intensity decreased with the addition of TFA, while it recovered with the subsequent addition of TEA, demonstrating reversible acidochromic behavior (Figure 4.15). The emission maximum wavelength of fluorophores **1** (λ max = 482 nm) and **2** (λ max = 473 nm) with the addition of TFA was red-shifted relative to their THF solution (λ max = 461 nm), respectively. These changes are probably due to the enhanced ICT between the biphenyl donor and protonated maleimide ring with the addition of TFA.[62,70-71] In the UV-vis spectra of fluorophores **1** and **2**, we observed that after adding TFA, the shape of the peak at the 247 nm caused by the π-π* electron transition of the maleimide conjugated system changed, becoming sharper, and the peak intensity increased significantly (Figure 4.15). At the same time, the position of the peak also shifted upon adding TFA: for fluorophore **1**, from λ_{abs} = 263 nm to λ_{abs} = 247 nm, and for fluorophore **2**, from λ_{abs} = 241 nm to λ_{abs} = 247 nm. These observations suggest that upon addition of TFA, protonation of the maleimide conjugated system occurs, leading to alterations in molecule's electronic structure and charge distribution. These changes affect the electronic energy levels and transitions within the molecule, consequently leading to modifications in its absorption spectrum.[72] Moreover, when the maleimide conjugated system becomes protonated, it causes a change in the electron density distribution of the molecule, which can alter the chemical environment and cause changes in the shifts of peaks in the ^{1}H NMR spectra. Therefore, based on the analysis of ^{1}H NMR spectra upon the addition of TFA for fluorophore **1** and **2**,

the shifts of peaks confirmed the protonation in the presence of acid (as shown in Figure 4.16 and Figure 4.17). In addition, we explored the practical application of **1** and **2** as potential acid / alkali fluorescent on/off sensors by smearing their respective THF solutions on filter paper. The filter paper exposed to TFA vapor exhibited a visual color change, which recovered when they were subsequently exposed to TEA vapor (Figure 4.18). Under UV light, these filter papers exhibited some fluorescence quenching with TFA vapors and recovered upon subsequent exposure to TEA vapors. The process can be repeated more than three times. Based on these characteristics, we can believe in the potential of fluorophores **1** and **2** as smart materials for acid / alkali switches.

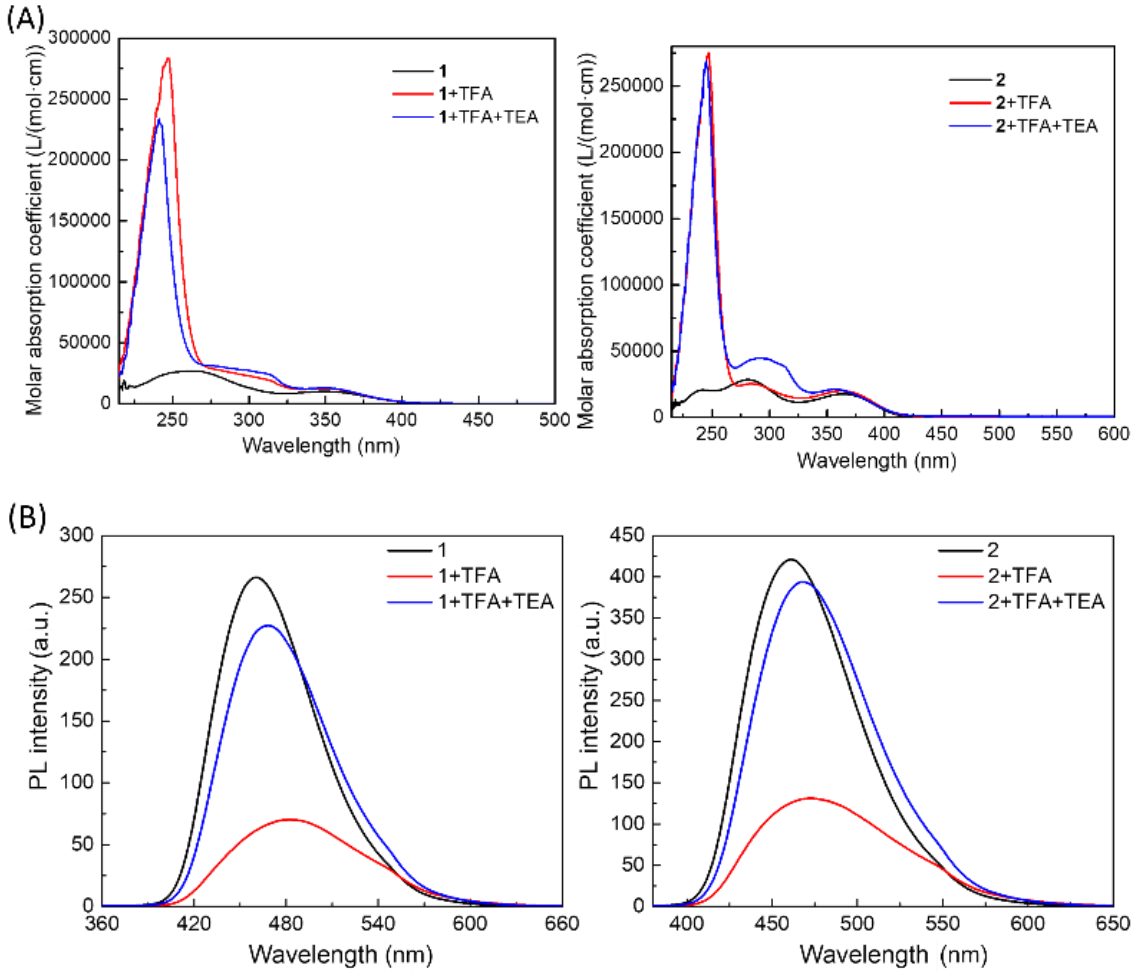

Figure 4.15. UV spectra, (B) PL spectra of fluorophores **1** and **2** in the presence of 0.1M TFA/TEA.

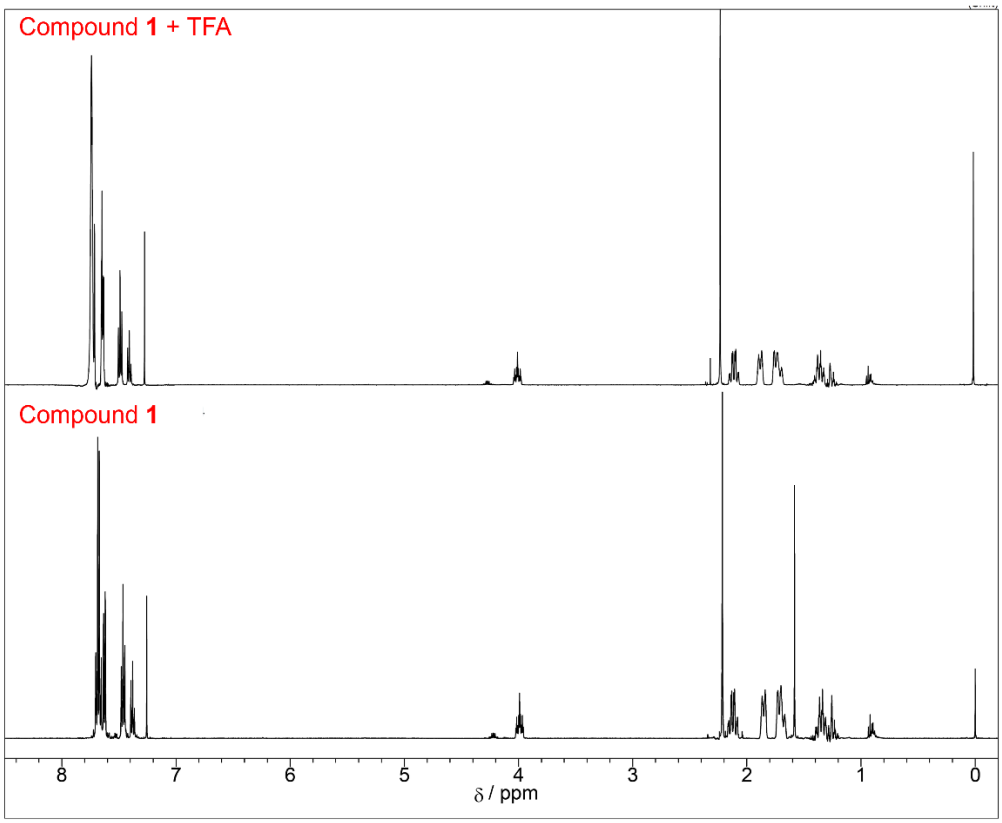

Figure 4.16. ^{1}H NMR Spectrum of compound **1** on addition of TFA in $CDCl_3$.

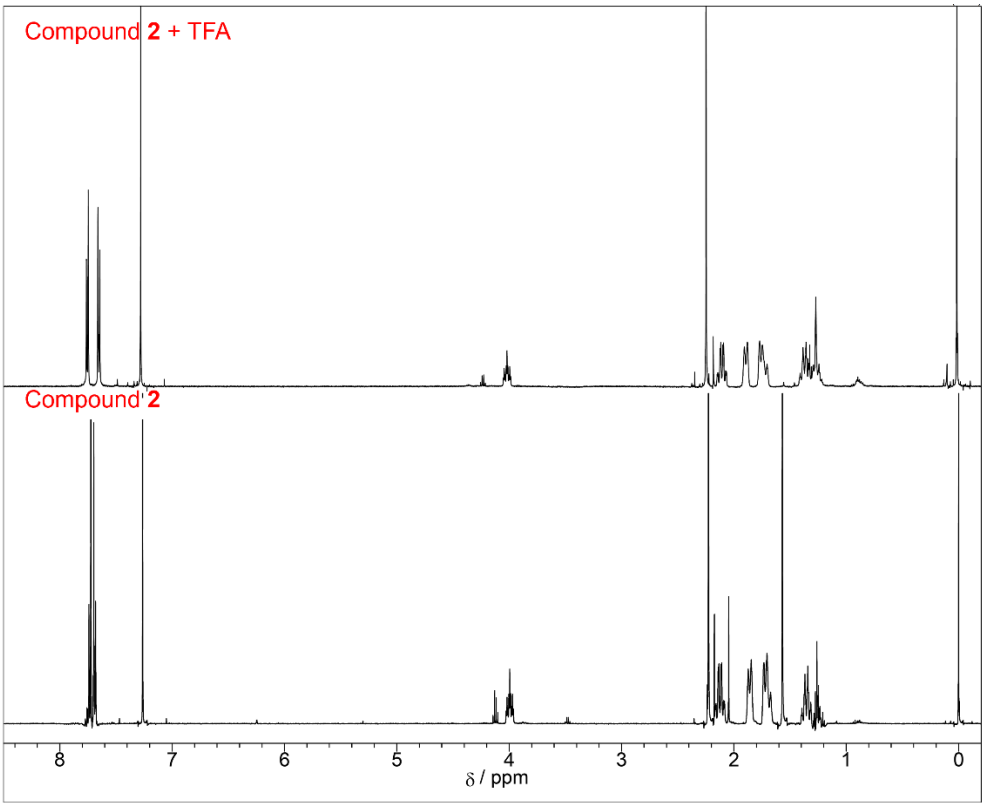

Figure 4.17. ^{1}H NMR Spectrum of compound **2** on addition of TFA in $CDCl_3$.

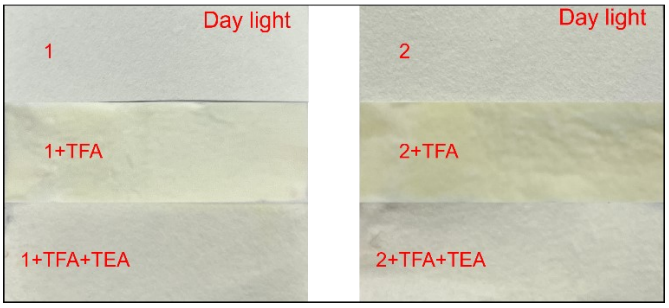

Figure 4.18. The filter paper of fluorophores **1** and **2** which exposed to TFA/TEA vapor under the visible.

4.4 Conclusions

We designed and synthesized two new maleimide molecules that display bright blue emission both in solution and in solid state, showing DSE effects. This overcomes the disadvantage of many molecules that only emit in a single state. As new type DSE molecules that possess simple structures, they can provide a strategy for the design of DSE molecules and serve as a basis for further development of DSE molecules. Moreover, fluorophore **1** exhibits a high fluorescence quantum yield in THF solution (Φ_{F1} = 81 %) and in the solid states (Φ_{F1} = 81 %). This is advantageous as blue-emitting materials for the emissive layer of organic light-emitting diodes (OLEDs). On the other hand, based on the fact that the fluorophores show a color change with the change of water content in THF-Water solution, they can be providing some ideas about fluorescence sensors for detecting water in organic solvents. The fluorophores also display a positive solvatochromic effect in solvent of different polarity, and they respond to the addition of trifluoro acetic acid (TFA) / triethyl amine (TEA), displaying reversible acidochromic behavior.

4.5 References

1 Z. Li, J. R. Askim and K. S. Suslick, *Chem. Rev*., 2019, **119**, 231-292.

2 M. Gao, F. Yu, C. Lv, J. Choo and L. Chen, *Chem. Soc. Rev*., 2017, **46**, 2237-2271.

3 J. Liu, W. Zhu, H. Chen, Y. Lin and X. Li, *Sci. Adv. Mater.*, 2020, **12**, 1361-1370.

4 Z. Ma, S. Qiu, H-C. Chen, D. Zhang, Y-L. Lu and X-L. Chen, *J. Asian Nat. Prod. Res*., 2021, 1-15.

5 Q. Li, S. Liu, J. Li, X. Pan, J. Zhu and X. Zhu, *Macromol Rapid Commun*., 2021,**42**, 2000517.

6 E. Lakay, S. Hermans, K. Koch and B. Klumperman, *Chem. Eng. J*., 2021, **414**, 128761.

7 N. Sharma, S. Kumar, Y. Chandrasekaran and S. Patil, *Org. Electron*., 2016, **38**, 180-185.

8 Y. Mise, K. Imato, T. Ogi, N. Tsunoji and Ooyama, *New J. Chem*., 2021, **45**, 4164-4173.

9 T. Förster and K. Kasper, *Z. Phys. Chem. (Muenchen, Ger.)*, 1954, **1**, 275-277.

10 S. A. Jenekhe and J. A. Osaheni, *Science*, 1994, **265**, 765-768.

11 R. Bakalova, Z. Zhelev, I. Aoki, H. Ohba, Y. Imai and I. Kanno, *Anal. Chem*., 2006, **78**, 5925-5932.

12 J. Mei, N. L. C. Leung, R. T. K. Kwok, J. W. Y. Lam and B. Z. Tang, *Chem. Rev.*, 2015, **115**, 11718-11940.

13 G. C. Schmidt, *Ann. Phys*., 1921, **370**, 247-256.

14 F. Wurthner, *Angew. Chem. Int. Ed*., 2020, **59**, 14192-14196.

15 J. Luo, Z. Xie, J. W. Y. Lam, L. Cheng, H. Chen, C. Qiu, H. S. Kwok, X. Zhan, Y. Liu, D. Zhu and B. Z. Tang, *Chem. Commun*., 2001, 1740-1741.

16 S. Xu, T. Liu, Y. Mu, Y. F. Wang, Z. Chi, C. C. Lo, S. Liu, Y. Zhang, A. Lien and J. Xu, *Angew. Chem., Int. Ed*., 2015, **54**, 874-878.

17 H. Qu, X. Tang, X. Wang, Z. Li, Z. Huang, H. Zhang, Z. Tian and X. Cao, *Chem. Sci*., 2018, **9**, 8814-8818.

18 E. P. J. Parrott, N. Y. Tan, R. Hu, J. A. Zeitler, B. Z. Tang and E. Pickwell-MacPherson, *Mater. Horiz*., 2014, **1**, 251-258.

19 J. Shi, N. Chang, C. Li, J. Mei, C. Deng, X. Luo, Z. Liu, Z. Bo, Q. Dong Yong and Z. Tang Ben, *Chem. Commun*., 2012, **48**, 10675-10677.

20 H. Nie, K. Hu, Y. Cai, Q. Peng, Z. Zhao, R. Hu, J. Chen, S.J. Su, A. Qin and B. Z. Tang, *Mater. Chem. Front*., 2017, **1**, 1125-1129.

21 Y. Hu, X. Liang, D. Wu, B. Yu, Y. Wang, Y. Mi, Z. Cao and Z. Zhao, *J. Mater. Chem. C*,

2020, **8**, 734-741.

22 H. Sun, X.X. Tang, R. Zhang, W.H. Sun, B.X. Miao, Y. Zhao, Z.H. Ni, *Dyes Pigm*., 2020, **174**, 108051.

23 M. Kaur, H. Kaur, M. Kumar and V. Bhalla, *Chem. Rec*., 2021, **21**, 240-256.

24 G. Chen, W.B. Li, T.R. Zhou, Q. Peng, D. Zhai, H.X. Li, W.Z. Yuan, Y.M. Zhang and B. Z. Tang, *Adv. Mater*., 2015, **27**, 4496-4501.

25 F. Yu, Q. Yan, K. Liang, Z. Cong, Q. Shao, Y. Wanga, L. Hong, L. Jiang, G. Ye, H. Wang, B. Chi, G. Xia, *J. Lumin*., 2021, **233**, 117882.

26 S. Kumar, P. Singh, P. Kumar, R. Srivastava, S.K. Pal and S. Ghosh, *J. Phys. Chem. C.,* 2016, **120**, 12723-12733.

27 Y. Li, Y. Lei, L. Dong, L. Zhang, J. Zhi, J. Shi, B. Tong and Y. Dong, *Chem. Eur. J*., 2019, **25**, 573-581.

28 M. N. Huang, R. N. Yu, K. Xu, S. X. Ye, S. Kuang, X. H. Zhu and Y. Q. Wan, *Chem. Sci*., 2016, **7**, 4485-4491.

29 Y. Y. Zhang, J. T. Pan, C. Y. Zhang, H. W. Wang, G. B. Zhang, L. Kong, Y. P. Tian and J. X. Yang, *Dyes Pigm*., 2015, **123**, 257-266.

30 T. T. Jing and L. F. Yan, *Sci China Chem*., 2018, **61**, 863-870.

31 W. J. Li, D. D. Liu, F. Z. Shen, D. G. Ma, Z. M. Wang, T. Feng, Y. X. Xu, B. Yang and Y. G. Ma, *Adv. Funct. Mater*., 2012, **22**, 2797-2803.

32 Q. Qiu, P. Xu, Y. Zhu, J. Yu, M. Wei, W. Xi, H. Feng, J. Chen and Z. Qian, *Chem. Eur. J*., 2019, **25**, 15983-15987.

33 J. L. Belmonte-Vázquez, Y. A. Amador-Sánchez, L. A. Rodríguez-Cortés and B.Rodríguez-Molina, *Chem. Mater*., 2021, **33**, 7160-7184.

34 F. Li, X. Li, Y. Wang and X. Zhang, *Angew.Chem.Int.Ed.*, 2019, **58**, 17994-18002.

35 H-C. Yeh, W-C. Wu and C-T. Chen, *Chem. Commun*., 2003, 404-405.

36 J. Wang, R. Zheng, H. Chen, H. Yao, L. Yan, J. Wei, Z. Lin and Q. Ling, *Org. Biomol. Chem*., 2018, **16**, 130-139.

37 M. Nakamura, K. Yamabuki and T. Oishi, K. Onimura, *J. Polym. Sci. Part A: Polym. Chem*., 2013, **51**, 4945-4956.

38 K. Onimura, M. Matsushima, M. Nakamura, T. Tominaga, K. Yamabuki and T. Oishi, *J. Polym. Sci. Part A: Polym. Chem*., 2011, **49**, 3550-3558.

39 A. Bisi, R. L. Arribas, M. Micucci, R. Budriesi, A. Feoli, S. Castellano, F. Belluti, S. Gobbi, C. Rios, A. Rampa, *Eur. J. Med. Chem*., 2019, **163**, 394-402.

40 Y. Wang, Q. Zhang, F. Li, J. Gong, X. Zhang, *Dyes Pigm*., 2020, **172**, 107823.

41 C. Zhai, G. Fang, W. Liu, T. Wu, L. Miao, L. Zhang, J. Ma, Y. Zhang, C. Zong, S. Zhang and C. Lu, *ACS Appl. Mater. Interfaces*., 2021, **13**, 42024-42034.

42 J. Qian, G. Zhang, J. Cui, L. Zhou, Z. Chen, Z. Zhang, W. Zhang, *Sens. Actuators B Chem.*, **311**, 127923.

43 M. Pervez, A. K. Pearce, J. T. Husband, L. Male, M. T. Sucarrat and R. K. O'Reilly, *Chem. Eur. J.,* 2022, **28**, e202201877.

44 H. Mu, K. Miki, T. Kubo, K. Otsuka and K. Ohe, *Chem. Commun*., 2021, **57**, 1818-1821.

45 X. D. Yang, K. Yamabuki and K. Onimura, *New J. Chem*., 2022, **46**, 1232-1237.

46 H. M. Fahmy, H. M. Kandel, H. A. S. Al-shamiri, N. A. Negm, A. H. M. Elwahy and M. T. H. A. Kana, *J. Fluoresc*., 2018, **28**, 1421-1430.

47 Z. E. Chen, Q. L. Qi and H. Zhang, *Spectrochim. Acta A Mol. Biomol. Spectrosc.,* 2020, **238**, 118384.

48 X. Wang, L. Zhang, Q. Li and Y. Gao, *Dyes Pigm*., 2020, **181**, 108614.

49 Y. Hong, J. W. Y. Lam and B. Z. Tang, *Chem. Soc. Rev*., 2011, **40**, 5361-5388.

50 Y. Hong, J. W. Y. Lam and B. Z. Tang, *Chem. Commun*., 2009, 4332-4353.

51 H. Li, Y. Guo, G. Li, H. Xiao, Y. Lei, X. Huang, J. Chen, H. Wu, J. Ding and Y. Cheng, *J. Phys. Chem. C*., 2015, **119**, 6737-6748.

52 Y. Kumar, N. K. Singh, S. Mukhopadhyay, D. S. Pandey, *Inorganica Chimica Acta*., 2023, **546**, 121294.

53 Y. Zhang, D. Li, Y. Li and J. Yu, *Chem. Sci*., 2014, **5**, 2710-2716.

54 S. Pawar, U. K. Togiti, A. Bhattacharya and A. Nag, *ACS Omega*, 2019, **4**, 11301-11311.

55 W. Cheng, Y. Xie, Z. Yang, Y. Sun, M-Z. Zhang, Y. Ding and W. Zhang, *Anal. Chem*., 2019, **91**, 5817-5823.

56 H. Sun, X. X. Tang, B. X. Miao, Y. Yang and Z. H. Ni, *Sens. Actuators B Chem*., 2018, **267**, 448-456.

57 Y. Ooyama, M. Sumomogi, T. Nagano, K. Kushimoto, K. Komaguchi, I. Imae and Y. Harima, *Org. Biomol. Chem*., 2011, **9**, 1314-1316.

58 C. Reichardt, *Chem. Rev*., 1994, **94**, 2319-2358.

59 R. M. Adhikari and D. C. Neckers, *J. Phys. Chem. A*., 2009, **113**, 417-422.

60 V. D. Singh, A. K. Kushwaha and R. S. Singh, *Dyes Pigm*., 2021,**187**, 109-117.

61 Y. Zhang, T. Zhang, X. Wang, L. Kong and J. Yang, *Dyes Pigm*., 2021, **188**, 109230.

62 T. Sachdeva and M. D. Milton, *J. Mol. Struct*., 2021, **1243**, 130768.

63 M. Mas-Montoya´, A. G. Alcaraz, A. E. Ferao, D. Bautista and D. Curiel, *Dyes Pigm.,* 2023, **209**, 110924.

64 Y. Han, T. Zhang, X. Chen, Q. Chen and P. Xue, *CrystEngComm.*, 2021, **23**, 202-209.

65 L. Di, J. Yang, W. Tang, L. Gai, Z. Zhou and H. Lu, *J. Org. Chem*., 2021, **86**, 601-608.

66 T. Lu, F. Chen, *J. Comput. Chem*., 2012, **33**, 580-592.

67 R. Nandy and S. Sankararaman, *Beilstein J. Org. Chem*., 2010, **6**, 992-1001.

68 E. S. Starnovskaya, D. S. Kopchuk, A. F. Khasanov, O. S. Taniya, I. L. Nikonov, M. I. Valieva, D. E. Pavlyuk, A. S. Novikov, G. V. Zyryanov and O. N. Chupakhin, *Molecules*., 2022, **27**(20), 6879.

69 C. Reichardt, *Angew. Chem. Int. Ed. Engl.*, 1979, **18**, 98-110.

70 V. K. Vishwakarmaa, V. Adupa, K. A. Reddy and A. A. Sudhakar, *J. Mol. Struct*., 2021, **1225**, 129120.

71 Y.Chen, B. Bai, Q. Chai, M. Zhang, J. Wei, H. Wang and M. Li, *Soft Matter*., 2019, **15**, 6690-6695.

72 S. Achelle, J. Rodríguez-López, F. Bureš and F. R. Guen, *Chem. Rec*., 2020, **20**, 440-451.

Chapter 5

Summary

In chapter 1, based on the background and overview of this research, the concept of AIE and DSE are introduced. In addition, the research purpose and significance of this research also been clarified.

In chapter 2, a series of AIEE conjugated maleimide molecules with simple structures containing different amino groups were synthesized and characterized. Because the intramolecular rotation is restricted in the solid state, which reduces the nonradiative decay, these molecules show AIEE characteristics. Additionally, their non-planar conformations are also helpful to inhibit intermolecular π-π stacking and enhance the emission. These AIEE molecules can solve the ACQ problems of some molecules in the solid state, and unlike common AIE molecules, they can also show emission in both solution and the solid state. In addition, the molecules respond to differences in the polarity of various solvents and show positive solvatochromism. Therefore, as new AIEE molecules, conjugated amino-maleimides can enrich the types of AIEE molecules, and they are expected to provide a new strategy for the development of the AIE field.

In chapter 3, based on the molecules that synthesized in chapter 2, a series of AIEE conjugated maleimide molecules with simple structures containing different amino groups were synthesized and characterized. Because the intramolecular rotation is restricted in the solid state, which reduces the nonradiative decay, these molecules show AIEE characteristics. Additionally, we speculate that the molecules that synthesized in this chapter also have non-planar conformations which can be helpful to inhibit intermolecular π-π stacking and enhance the emission in solid state. The highest occupied molecular orbital (HOMO), the lowest unoccupied molecular orbital (LUMO) and optimized conformation will be verified in future study by density functional theory (DFT) quantum calculations.

In chapter 4, we have designed and synthesized two new maleimide molecules displaying bright blue emission both in solution and solid state, show DSE effects. This is made up the

disadvantage of many AIE molecules only emission in a single state. As new type of DSE molecules they can provide a strategy for the design of DSE molecules and provide a basis for further development of DSE molecules. Moreover, the fluorophore **1** exhibit high fluorescence quantum yield in THF solution (Φ_{F1} = 81 %) and in solid states (Φ_{F1} = 81 %). This is advantageous for it as blue emission materials for the emissive layer of organic light-emitting diode (OLED). On the other hand, based on the fluorophores show a color change with the change of water content in THF-Water solution, they can be used as fluorescence sensors for the water detection in organic solvents. The fluorophores also display a positive solvatochromic effects in different polarity solvents and they in response to the addition of trifluoro acetic acid (TFA) / triethyl amine (TEA), display the reversible acidchromic behavior. Based on above properties, fluorophores **1** and **2** provide more possible for their potential applications as fluorescent sensors.

Acknowledgements

I would like to express my gratitude to all those who helped me during the writing of this thesis.

My deepest gratitude goes first and foremost to Professor Kenjiro Onimura, Polymer Chemistry Laboratory, Department of Chemistry, Graduate School of Science and Technology, Yamaguchi University, my supervisor, for his constant encouragement and guidance. He has walked me through all the stages of the writing of this thesis. Without his consistent and illuminating instruction, this thesis could not have reached its present form.

Second, I would like to express my heartfelt gratitude to Lecturer Kazuhiro Yamabuki, who gave me many opinions in carrying out this research.

Finally, I would like to express my sincere gratitude to everyone in the Polymer Chemistry Laboratory for their great help and cooperation in conducting research.